University of Cagliari

Ph.D. in Chemical Science and Technology

XXVIII cycle
Scientific sector **CHEM03**

Design and Synthesis of Photoactive Molecules based on Metal Dithiolenes

Ph.D. Thesis of

Attar Salahuddin Sayedshabbir

Supervisor:

Prof. Paola Deplano

Coordinator

Prof. Mariano Casu

Final exam 2014 - 2015

Dedicated to Prof. Paola Deplano and my parents

Nature and its Science are certainly spectacular and amazing but I often wonder why it is so...

Abstract

This work reports on the design, synthesis and characterization of some homoleptic and heteroleptic d^8 metal (Ni, Pd, Pt) dithiolene complexes.

Chapter 1 provides the background required to properly design metal dithiolenes exhibiting desired properties.

Chapter 2 describes the synthesis & characterization of homoleptic radical monoanionic complexes showing multi-properties. Among these, a platinum complex prepared using a ligand containing a quinoxaline moiety connected through a dithieno bridge to the dithiolene core, shows unusual anti-Kasha solution proton dependent luminescence. The interaction of protons with these complexes is described with a view to understand their photo/electrocatalytic behaviour in aqueous acidic systems. Photocatalytic preliminary experiments on noble metal free homoleptic Ni-complex for hydrogen production from aqueous acidic solutions are described.

Chapter 3 describes design, synthesis and characterization of chiral/achiral heteroleptic d^8 metal dithiolene complexes, suitable as donor-metal-acceptor chromophores for 2^{nd} order NLO applications. It describes how with the presence or absence of acid (protons) in solutions of complexes can afford two switchable chemical forms (having different electronic properties) which can possibly display contrast in their NLO response. It also describes, by inclusion of chirality in the acceptor ligand, a non-centrosymmetric arrangement of molecules in crystalline medium to preserve NLO response in the bulk. Moreover, the unusual proton dependent dual luminescent properties of some of these complexes are described.

Lastly Chapter 4 contains conclusions, perspectives and appendices for this work are mentioned.

Chart 1 Dithiones & Dithiolates

***Dithione Acceptors* (A)**

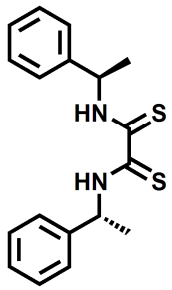

(R)-α-MBAdt
A1

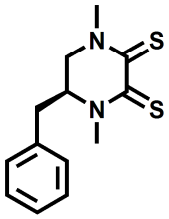

(S)-5-BnMe$_2$pipdt
A2

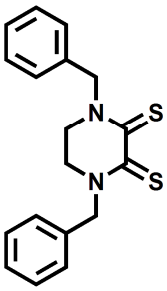

Bn$_2$pipdt
A3

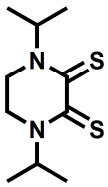

i-Pr$_2$pipdt
A4

***Dithiolate Donors* (D)**

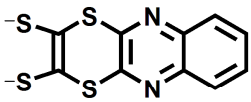

quinoxdt
D1

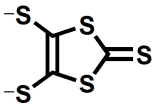

dmit
D2

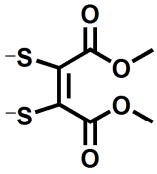

ddmedt
D3

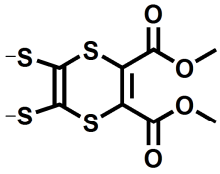

dddmedt
D4

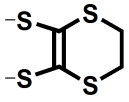

dddt
D5

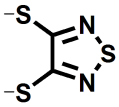

tdas
D6

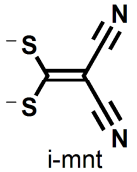

i-mnt
D7

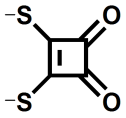

sqdt
D8

Chart 2 Homoleptic monoanionic complexes

***Metal Complexes* (M-C)**

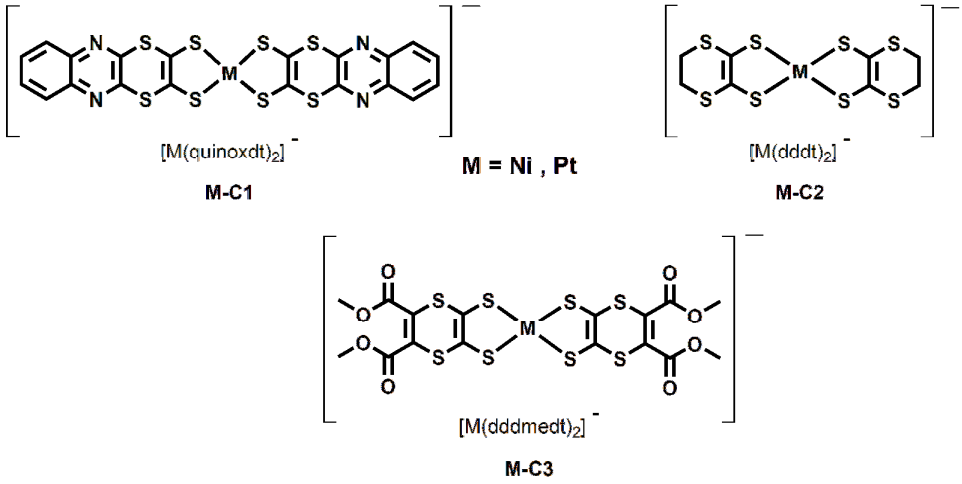

Chart 3 Heteroleptic monoanionic complexes

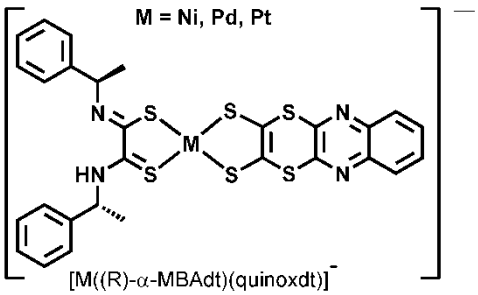

[M((R)-α-MBAdt)(quinoxdt)]$^-$

M-C4

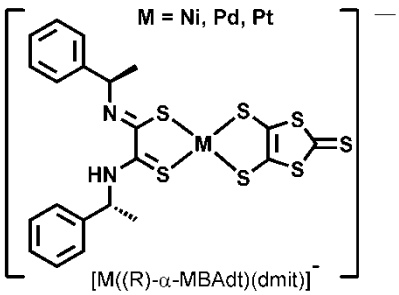

[M((R)-α-MBAdt)(dmit)]$^-$

M-C5

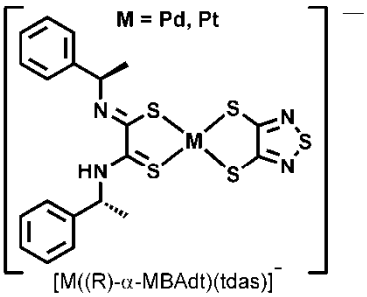

[M((R)-α-MBAdt)(tdas)]$^-$

M-C6

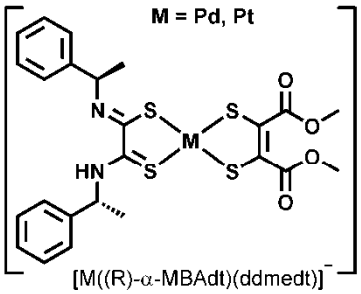

[M((R)-α-MBAdt)(ddmedt)]$^-$

M-C7

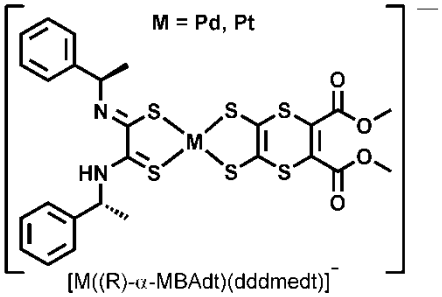

[M((R)-α-MBAdt)(dddmedt)]$^-$

M-C8

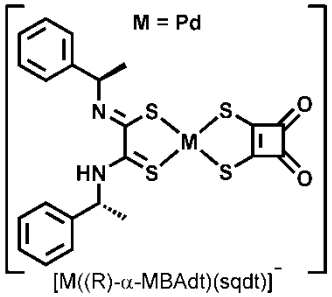

[M((R)-α-MBAdt)(sqdt)]$^-$

M-C9

Chart 4 Heteroleptic neutral complexes

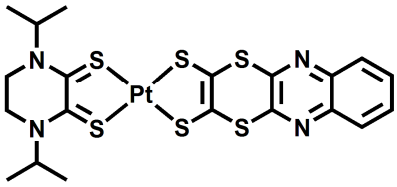

Pt(iPr$_2$pipdt)(quinoxdt)
Pt-C10

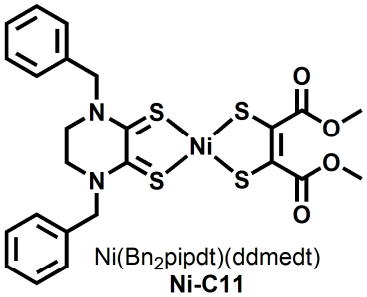

Ni(Bn$_2$pipdt)(ddmedt)
Ni-C11

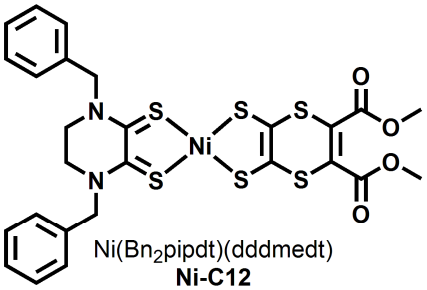

Ni(Bn$_2$pipdt)(dddmedt)
Ni-C12

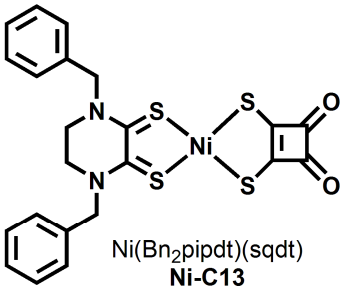

Ni(Bn$_2$pipdt)(sqdt)
Ni-C13

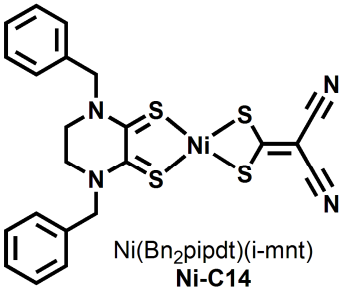

Ni(Bn$_2$pipdt)(i-mnt)
Ni-C14

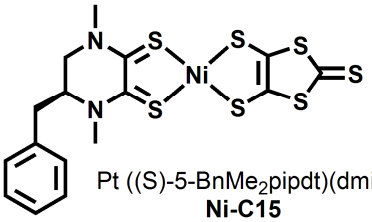

Pt ((S)-5-BnMe$_2$pipdt)(dmit)
Ni-C15

Table of contents

Chapter 3 Synthesis, characterization and properties of heteroleptic complexes $[ML_1L_2]^n$, n = 0, -1 M=Ni(II), Pd(II) and Pt (II), L_1=dithioxamide L_2=dithiolate

Chapter 4 Conclusion, Perspectives and Appendices

Chapter 1 Introduction and Background

1.1. Introduction

Functional materials based on metal complexes are of current interest in material science being their properties tunable with molecular precursors and the way they interact at supra-molecular level using low-cost and energy-saving chemical strategies. In particular, metal complexes are object of extensive investigation both for basic science, due their rich electronic[1], magnetic[2] and optical[3] properties, and for applications, due to their great potential in molecular photonics, and solar energy harnessing, where energy from the sun is converted into chemically stored energy to provide renewable energy needed for a sustainable development. In fact limited natural fossil fuels availability and environmental concerns related to CO_2 emissions are stimulating increasing use of clean and renewable energy and fuel sources[4]. Among the several approach to address these problems, the employment of photocatalytic systems, which harvest sunlight, the largest energy resource among the renewable energy sources, and split water, producing molecular oxygen and hydrogen, a transportable fuel, is strongly pursued[5]. By taking into account the proton reduction to hydrogen from aqueous solvents, in addition to the photocatalyst, a photosensitizer (PS) and a sacrificial electron-donor are required. In some instances these complexes may exhibit both photo-catalytic and electro-catalytic properties. Several attempts have been performed to try to obtain light and or electro-responsive molecular and supra-molecular materials capable to mimic or even to enhance naturally occurring systems but this goal is far from being reached. For example a radical monoanion Ni dithiolene complex $[Ni(ddmedt)_2]^{-\cdot}$ [1], shown in ***Figure 1.1a*** was proposed as functional model of hydrogenase.[6] This

complex showing redox activity is capable to catalyze the proton reduction of p-toluensolphonic acid (TsOH), while dianionic dithiolenes such as $[Ni(mnt)_2]^{2-}$ (mnt=maleonitrile dithiolato) do not. It was suggested that the activity may be relatable to the radical character and the reduction wave at E_0= -0.341 V at a value similar to that of Ni hydrogenase (Desulfovibrio gigas; E_0 = -0.34 V).

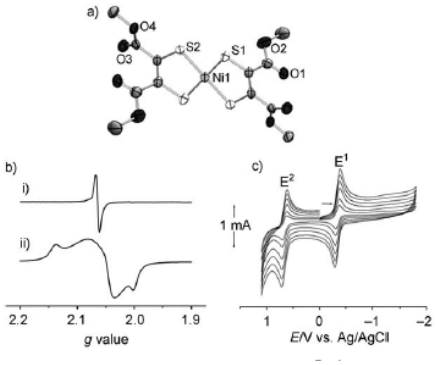

Figure 1.1

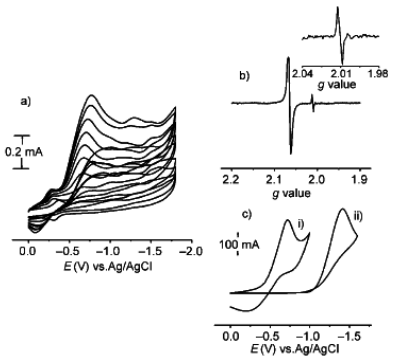

Figure 1.2

Figure 1.1, a) Perspective view of the monoanion $[NiII(L^{2-})(L^{\cdot-})]$, in crystals of $[Ni(ddmedt)_2]$. Hydrogen atoms and PPh_4^+ cation have been omitted for clarity. b) X-band EPR spectrum in DMF i) at 298 and ii) at 107 K. c) Cyclic voltammograms (2 mM) in CH_3CN/0.2M tetrabutylammonium perchlorate (TBAP) at various scan rates (50–500 mVs^{-1}). ***Figure 1.2,*** a) Cyclic voltammetric responses of [1] as a function of added TsOH of increasing concentrations (0.0017 g per addition) in CH3CN (glassy carbon working electrode (GCE), TBAP, 0.2M). b) EPR spectrum (2 mM/DMF) after the addition of TsOH at 298 K; inset: enlargement of the new signal that was observed after the addition of TsOH. c) Cyclic voltammograms of the reduction of TsOH in water (NaClO4, 0.2M); i) GCE surface coated with [1] (1 mm), ii) a polished GCE.

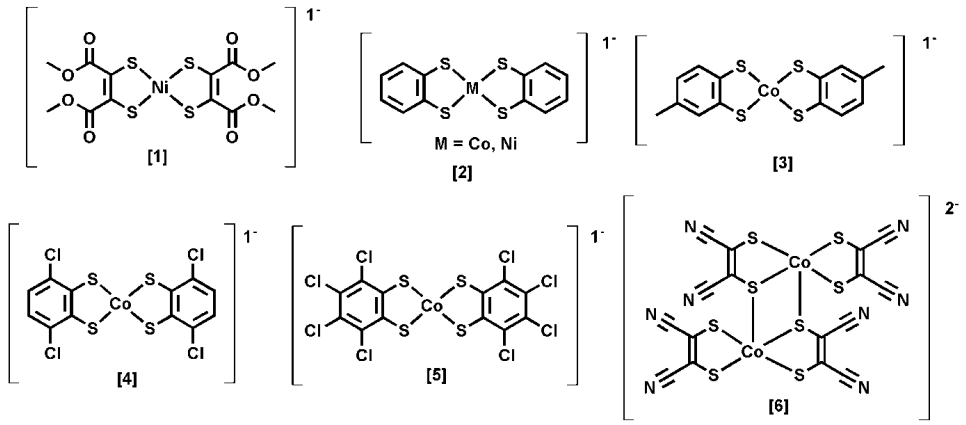

Figure 1.1, Structures of active catalysts for photo-electrochemical reduction of protons

Extensive theoretical [7] and experimental [8] studies have been addressed to cobalt complexes (***Figure 1.1*** [***1-6***]) [9] also with the view to employ noble-metal-free complexes. Some Nickel and molybdenum complexes[10] with dithiolene ligands have also been explored for light driven hydrogen generation. It was found that the complex $Bu_4N[Co(bdt)_2]$ [***2***] (bdt=1,2-benzenedithiolate) works well as catalyst for proton reduction in the presence of $[Ru(bpy)_3]^{2+}$ (PS=photosensitizer) and AA (ascorbic acid) at pH=4. Reductive quenching of PS* by AA and complexes seems to be dominant. It is suggested that during photolysis the generated $[Ru(bpy)_3]^{+}$ reduce cobalt complexes forming an intermediate (-2 complex) which undergoes rapid first protonation followed by subsequent second protonation over the central core (*syn* S-protonation) forming a neutral intermediate which undergoes reduction followed by a rearrangement forming proton bonded cobalt intermediate finally leading to hydrogen formation. (***Scheme 1.1***) Electrochemical experiments were performed to elucidate the reaction mechanism, and the shift at more negative potential of the 1-/2- process of the complexes was explained by

taking into account a first protonation and reduction of the complex and after that a second reduction and protonation to form H_2. It was shown that the TBA $[Ni(bdt)_2]$ shows poor catalytic activity, likely relatable to its highly cathodic electrocatalytic wave.

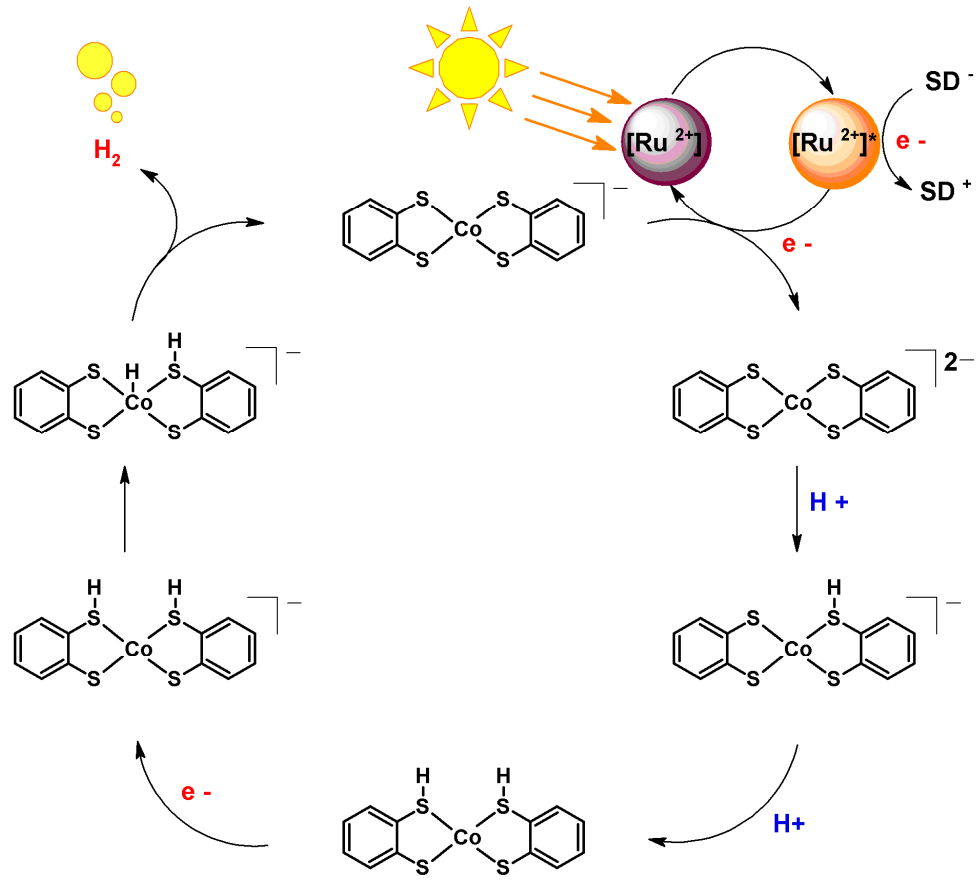

Scheme 1.1, proposed mechanism for photocatalytic hydrogen generation from aqueous solutions

The above mentioned complexes [***1-6***], showing photo-and/or electrocatalytic properties, belong to the class of homoleptic metal dithiolene complexes.

Another class of metal-dithiolene complexes: heteroleptic square-planar complexes of transition d^8 metals exhibits remarkable properties for photonic applications, being active at molecular level as second order NLO (non-linear-optical) chromophores. Nonlinear optics is the branch of optics that describes the behavior of light in media where the dielectric polarization responds nonlinearly to the light. Most often molecules with extensive π-delocalized system are required to promote NLO properties which are related to the polarizability of the electrons under the effect of the electric field of the light and are dependent on electronic transitions with high CT character. Accordingly, molecules containing electron-donor, and electron-acceptor groups connected by a π-bridge and giving rise to an asymmetric charge distribution in the ground state, are suitable to generate second-order NLO properties. This can be achieved by employing transition-metal coordination compounds, where d^n-metal orbitals work as suitable bridge between donor-acceptor ligands. The doubling of the frequency of the incident light, through the second harmonic generation process, is one example of nonlinear optical (NLO) phenomena that is currently exploited in lasers, optical communications, optical data processing and storage, and electro optical devices (second- harmonic generation: SHG, as well as to modulate the NLO response due to reversible redox- or proton-switching of the first hyperpolarizability. However, to be suitable for photonic applications (SHG) in the bulk, a non centro-symmetric crystal packing or thin films or sol-gel glasses incorporating the NLO chromophore under poling is required.

In this Introduction two classes of photo-active molecules based on transition metal dithiolene complexes: the homoleptic and heteroleptic ones have been cited.

My Thesis work has been addressed to design, synthesize and investigate the properties of new complexes belonging to these classes to better elucidate and optimize their properties, in particular attempt to point out:

1) the photo-electro-catalytic properties of homoleptic complexes in producing molecular hydrogen from acid solutions; whether or not this activity may be relatable to the radical character of complexes; whether or not this activity require complexes with ligands capable to interact with protons.
2) The capability of heteroleptic complexes to alternate (switch) between two chemical forms displaying contrast in their NLO response, as a result of external stimuli such as light irradiation, pH variation, and redox reaction; and the conditions to obtain noncentrosymmetric molecular materials, prerequisite to achieve second-order NLO phenomena in the bulk.

In order to make clearer the rational design of selected complexes, it seems worth to recall here the properties of metal-dithiolene complexes, restricted to the class of metal d^8 square-planar derivatives of interest here.

1.2. Background on Square-planar d^8 metal dithiolenes

1.2.1. Noninnocence of ligands and complexes

Molecular structures having 1,2-ene-dithiolate dianion, radical thiolate monoanion, 1,2-dithioketones and thione thiolate mono anion functionality are capable to coordinate with metals and their complexes are termed deliberately as dithiolenes irrespective of their oxidation states to retrospect the noninnocent character of such ligands.[11] (***Scheme 1.2***)

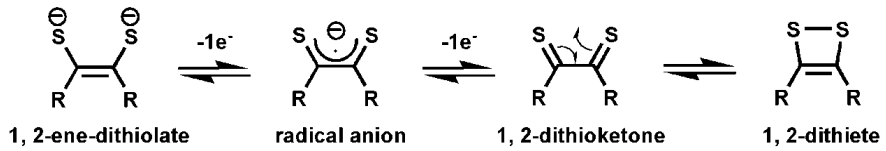

Scheme 1.2, Dithiolene ligands and their oxidation states

In the complexes of noninnocent ligands the oxidation state of the metal is not easily defined due to the uncertainty in oxidation state of ligands. In such complexes due to possibility of ligands to electrochemically undergo one electron redox process, uncertainties arise in assigning spin state of central metal.

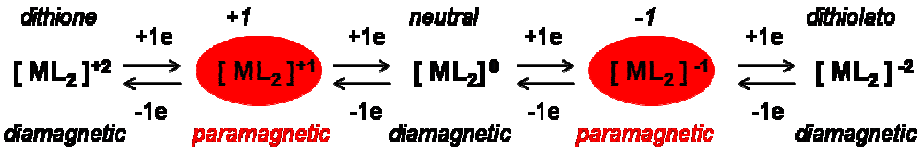

Scheme 1.3, Redox activity of metal dithiolenes where L = $R_2C_2S_4$

In square-planar d8-metal-dithiolenes [Ni(II), Pd(II), Pt(II)], and the members of the series may spread from the dianionic to the dicationic form with minor structural changes at molecular level.(***Scheme 1.3***)

Applying classical Lewis formalism, bonding in these systems can be interpreted as follows. Complexes having +2 oxidation state of metal with ligands as 1, 2-dithione and 1, 2-ene dithiolate form can be applied to only dimagnetic dicationic and dianionic members of the series. (***Scheme 1.4***) For neutral dimagnetic complexes can be rationalized in two ways, one involving resonance hybrid (a) among the limiting forms where the M(II) is coordinated to one neutral dithione molecule and one dithiolate anion, the other non classical Lewis description (b) involving the M(II) coordinated to two ligands in radical form where the spins are antiferromagnetically coupled. Similar non classical Lewis description are required to describe mono cationic (c) and mono anionic (d) complexes where the M(II) is

coordinated respectively to one thione ligand and one ligand in radical form, and to one dithiolato ligand plus one ligand in radical form with the spin (S =1/2) highly delocalized over the molecule.[12]

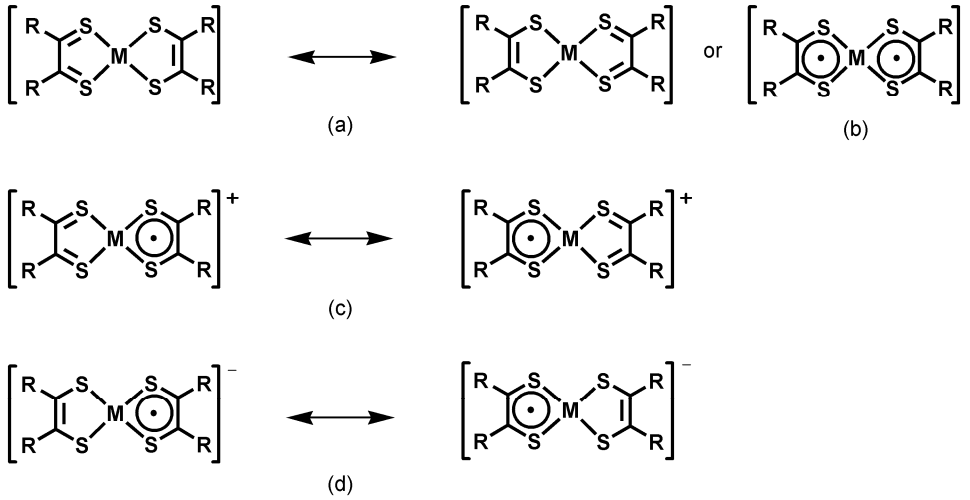

Scheme 1.4, Lewis classical structures and non classical resonance structures

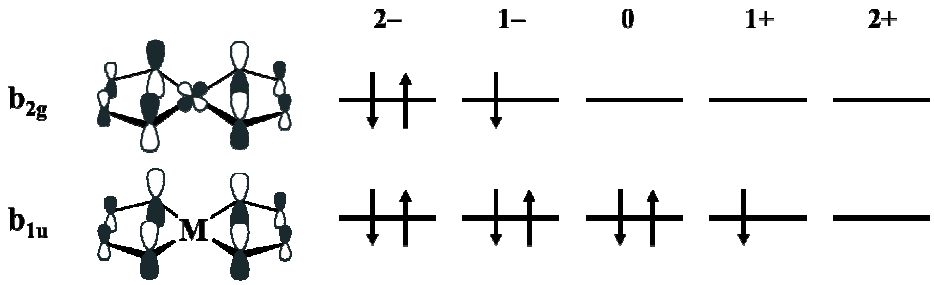

Figure1.3, Electronic configuration of redox states in central complexation core

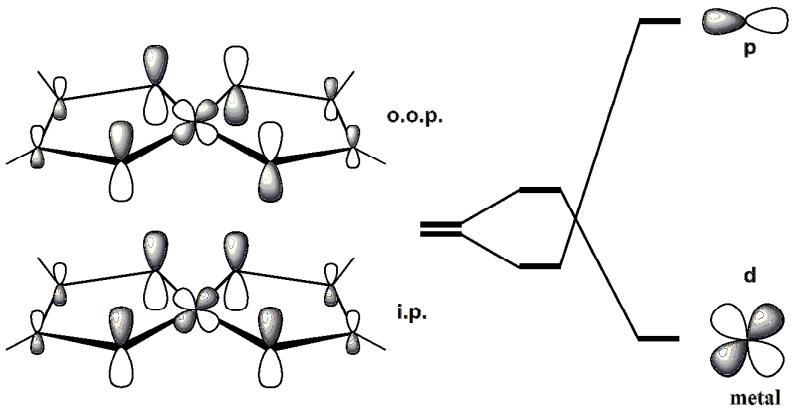

Figure 1.4, Inverted bonding scheme in d^8 metal dithiolenes

1.2.2. Electronic properties

The 2+ and 2− limits in oxidation states of the square planar d^8 metal (II) bis dithiolene complexes are due to the isolated frontier π-MOs, consisting of the in phase (HOMO) and out-of phase (LUMO) combinations of a C_2S_2 orbital (with π C-C and π^* C-S character) stabilized by one high lying p_π orbital and destabilized by a lower lying d_π orbital.[13] (***Figure 1.4***) The *d* metal orbitals are stabilized relative to ligand orbitals which induce "inverted bonding scheme", while in normal bonding scheme the *d*-orbitals are destabilized relative to the ligand orbitals.[14]

Moreover, electro-delocalization in ligands that are geometrically fixed in co-planarity with the dithiolene-core by metal coordination, decreases the frontier π-MOs gap and consequently lowers the oxidation and reduction potential of the related complexes. The ligands can be easily modified with various substituents and this allows tuning the nature of the most accessible redox status and related properties of these complexes. Different functional properties can be achieved depending on the redox status of complexes:

- the neutral diamagnetic complexes, where only the low lying orbital is populated, behave as a near infrared (NIR) dyes due to an intense electronic transition falling at low energies and relatable to the HOMO–LUMO dipole-allowed transition($b_{1u} \rightarrow b_{2g}$ in D_{2h} symmetry)
- Monoanionic derivatives are paramagnetic and preserve the properties as NIR dye, so that they exhibit both magnetic and optical properties. In these complexes the LUMO becomes a half-filled orbital (SOMO = singly occupied molecular orbital), and the related HOMO→SOMO transition undergoes a bathochromic shift and decrease in intensity relative to neutral complexes.
- Dianionic derivatives are diamagnetic and commonly do not absorb in the NIR, since a bleaching of the above mentioned peak is observed because the former LUMO becomes doubly occupied. For these reasons, electronic spectra, magnetic and electrochemical measurements provide suitable tools to assess the electronic structures in these complexes.

The electronic effect on the frontier orbitals of central C_2S_2 by various substituents (R) at the dithiolene core has also been evaluated.[15] Generally, π-acceptor substituents lower the energy of both these frontier MOs and favor the anionic state, while π-donor substituents raise the energy of both these orbitals so that the former HOMO can become depopulated (LUMO).

1.3. References

1. (a) M.L. Kirk, R.L. Mc Naughton and M.E. Helton in Dithiolene Chemistry: Synthesis, properties and applications, Progress in Inorganic Chemistry, Vol. 52 (Ed. E. I. Stiefel) (b) Tanaka, H. (2001). A Three-Dimensional Synthetic Metallic Crystal Composed of Single-Component Molecules. *Science, 291*(5502), 285-287.

2. (a) Coomber, A. T., Beljonne, D., Friend, R. H., Brédas, J. L., Charlton, A., Robertson, N., … Day, P. (1996). Intermolecular interactions in the molecular ferromagnetic NH4Ni(mnt)$_2$. H_2O. *Nature, 380*(6570), 144-146. (b) Lieffrig, J., Jeannin, O., Auban-Senzier, P., & Fourmigué, M. (2012). Chiral Conducting Salts of Nickel Dithiolene Complexes. *Inorganic Chemistry, 51*(13), 7144-7152.

3. (a) U. T. Mueller-Westerhoff, in Comprehensive Coordination Chemistry Vol. 9, (Ed. G. Wilkinson) Pergamon, Oxford, 1987, 595-631 (b) B. J. Coe, in Comprehensive Coordination Chemistry II, Vol. 9, (Eds J. A. Mc Cleverty and T. J. Meyer) Elsevier-Pergamon, Oxford, 2004, 621-687

4. (a) Lewis, N. S., & Nocera, D. G. (2006). Powering the planet: Chemical challenges in solar energy utilization. *Proceedings of the National Academy of Sciences, 103*(43), 15729-15735. (b) Youngblood, W. J., Lee, S. A., Maeda, K., & Mallouk, T. E. (2009). Visible Light Water Splitting Using Dye-Sensitized Oxide Semiconductors. Accounts of *Chemical Research, 42*(12), 1966-1973. (c) Tran, P. D., Wong, L. H., Barber, J., & Loo, J. S. (2012). Recent advances in hybrid photocatalysts for solar fuel production. *Energy & Environmental Science, 5*(3), 5902. (d) Wang, M., & Sun, L. (2010). Hydrogen Production by Noble-Metal-Free Molecular Catalysts and Related Nanomaterials. *ChemSusChem, 3*(5), 551-554. (e) Luo, S., Mejía, E., Friedrich, A., Pazidis, A., Junge, H., Surkus, A., … Beller, M. (2012). Photocatalytic Water Reduction with Copper-Based Photosensitizers: A Noble-Metal-Free System. *Angewandte Chemie, 125*(1), 437-441. (f) Vrubel, H., & Hu, X. (2012). Molybdenum

Boride and Carbide Catalyze Hydrogen Evolution in both Acidic and Basic Solutions. *Angewandte Chemie International Edition, 51*(51), 12703-12706. (g) Wang, X., Xu, Q., Li, M., Shen, S., Wang, X., Wang, Y., … Li, C. (2012). Photocatalytic Overall Water Splitting Promoted by an α-β phase Junction on Ga_2O_3. *Angewandte Chemie International Edition, 51*(52), 13089-13092.

5. (a) Barber, J. (2009). Photosynthetic energy conversion: natural and artificial. *Chem. Soc. Rev, 38*(1), 185-196. (b) Tachibana, Y., Vayssieres, L., & Durrant, J. R. (2012). Artificial photosynthesis for solar water-splitting. *Nature Photonics, 6*(8), 511-518. (c) Pinaud, B. A., Benck, J. D., Seitz, L. C., Forman, A. J., Chen, Z., Deutsch, T. G., … Jaramillo, T. F. (2013). Technical and economic feasibility of centralized facilities for solar hydrogen production via photocatalysis and photoelectrochemistry. *Energy & Environmental Science, 6*(7), 1983

6. Begum, A., Moula, G., & Sarkar, S. (2010). A Nickel(II)-Sulfur-Based Radical-Ligand Complex as a Functional Model of Hydrogenase. *Chemistry - A European Journal, 16*(41), 12324-12327.

7. Solis, B. H., & Hammes-Schiffer, S. (2012). Computational Study of Anomalous Reduction Potentials for Hydrogen Evolution Catalyzed by Cobalt Dithiolene Complexes. *J. Am. Chem. Soc, 134*(37), 15253-15256.

8. McNamara, W. R., Han, Z., Alperin, P. J., Brennessel, W. W., Holland, P. L., & Eisenberg, R. (2011). A Cobalt–Dithiolene Complex for the Photocatalytic and Electrocatalytic Reduction of Protons. *J. Am. Chem. Soc, 133*(39), 15368-15371.

9. McNamara, W. R., Han, Z., Yin, C., Brennessel, W. W., Holland, P. L., & Eisenberg, R. (2012). Cobalt-dithiolene complexes for the photocatalytic and electrocatalytic reduction of protons in aqueous solutions. *Proceedings of the National Academy of Sciences, 109*(39), 15594-15599.

10. (a) Das, A., Han, Z., Brennessel, W. W., Holland, P. L., & Eisenberg, R. (2015). Nickel Complexes for Robust Light-Driven and Electrocatalytic Hydrogen Production from

Water. *ACS Catal, 5*(3), 1397-1406. (b) Eckenhoff, W. T., Brennessel, W. W., & Eisenberg, R. (2014). Light-Driven Hydrogen Production from Aqueous Protons using Molybdenum Catalysts. *Inorganic Chemistry, 53*(18), 9860-9869.

11. (a) Periyasamy, G., Burton, N. A., Hillier, I. H., Vincent, M. A., Disley, H., McMaster, J., & Garner, C. D. (2007). The dithioleneligand—'innocent' or 'non-innocent'? A theoretical and experimental study of some cobalt–dithiolene complexes. *Faraday Discuss, 135,* 469-488. (b) M.L. Kirk, R.L. Mc Naughton and M.E. Helton in Dithiolene Chemistry: Synthesis, properties and applications, Progress in Inorganic Chemistry, Vol. 52 (Ed. E. I. Stiefel (c) Eisenberg, R., & Gray, H. B. (2011). Noninnocence in Metal Complexes: A Dithiolene Dawn. *Inorganic Chemistry, 50*(20), 9741-9751.

12. (a) Paola deplano, M. Laura Mercuri, Angela Serpe and Luca Pilia, *chapter 16*, The chemistry of metal Enolates part 2, 879-925 (Patai series Editor: Jacob Zabicky) (b) Lim, B. S., Fomitchev, D. V., & Holm, R. H. (2001). Nickel Dithiolenes Revisited: Structures and Electron Distribution from Density Functional Theory for the Three-Member Electron-Transfer Series $[Ni(S_2C_2Me_2)_2]^{0,1-,2-}$. *Inorganic Chemistry, 40*(17), 4257-4262.

13. Curreli, S., Deplano, P., Faulmann, C., Ienco, A., Mealli, C., Mercuri, M. L., … Trogu, E. F. (2004). Electronic Factors Affecting Second-Order NLO Properties: Case Study of Four Different Push-Pull Bis-Dithiolene Nickel Complexes. *Inorganic Chemistry, 43*(16), 5069-5079.

14. Balch, A. L., & Holm, R. H. (1966). Complete Electron-Transfer Series of the $[M\text{-}N_4]$ Type. *J. Am. Chem. Soc, 88*(22), 5201-5209.

15. (a) Lauterbach, C., & Fabian, J. (1999). Density Functional Derived Structures and Molecular Properties of Nickel Dithiolenes and Related Complexes. Eur. J. Inorg. Chem, 1999(11), 1995-2004. (b) Aragoni, M. C., Arca, M., Demartin, F., Devillanova, F. A., Garau, A., Isaia, F., … Verani, G. (1999). New $[M(R,R'timdt)_2]$ Metal-

Dithiolenes and Related Compounds (M = Ni, Pd, Pt; R,R‘timdt = Monoanion of Disubstituted Imidazolidine-2,4,5-trithiones): An Experimental and Theoretical Investigation. *J. Am. Chem. Soc, 121*(30), 7098-7107. (c) Jacques, W., Daul, C., Van Zelewsky, A., Goursot, A., & Penigault, E. (1982). The electronic structure of bis(o-phenylenediamido)nickel, $Ni[C_6H_4(NH)_2]_2$. *Chemical Physics Letters, 88*(1), 78-83.

Chapter 2
Synthesis and characterization of photoactive Homoleptic radical anionic metal dithiolenes

2.1. Design and synthesis

As pointed out earlier in Chapter 1, the proper design of ligands allows tuning the nature of the most accessible redox status and related properties of these complexes at molecular level. Moreover, it has been pointed out that dithiolenes fused with suitable heterocycles promote intermolecular interactions in solid as well as in solution states.[1] In this chapter, I have reported case of d^8 metal dithiolenes where the ligands contain a 1,4-dithiino heterocycles fused with the dithiolene core with a view to obtain stable monoanionic radical complexes. Moreover additional functionality (quinoxaline, diester) was introduced fused with 1,4-dithieno ring (***Figure 2.1***) because of their ability to interact with protons (through N and/or S -protonation), Ligand ***D1*** have emitting properties and the dithieno bridge which interrupts the π-communication between electrons of dithiolate and the quinoxaline ring. The electronic features of the ligand allow to obtain d^8 metal complexes in the radical monoanionic form.

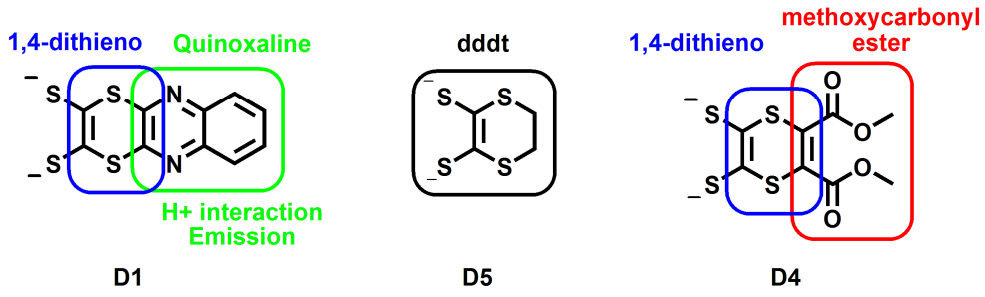

Figure 2.1, features of (a) [1,4]dithiino[2,3-b]quinoxaline-2,3-bis(thiolate) ligand (quinoxdt, ***D1***) (b) 5,6-dihydro-1,4-dithiine-2,3-bis(thiolate) ligand (dddt, ***D5***) and (c) 5,6-bis(methoxycarbonyl)-1,4-dithiine-2,3-bis(thiolate) ligand (dddmedt, ***D4***)

These complexes should be suitable to point out the capability of N or S atoms to interact with protons and their potential as photocatalyst for H_2 generation in

aqueous solutions. In addition, the investigation of the quinoxdt derivative were performed in order to check for the potential of ligand in providing photoluminescence properties to metal complexes.

The synthesis of complexes involve single step reaction between the dithiolate ligand (***D1, D4*** and ***D5***) and corresponding Ni(II), Pt(II) metal salt. The protected dithiolene ligands precursors [**1**] were synthesized by previously reported procedures.[1] All the radical anionic dithiolene metal complexes with ***Ni-C1, C2 or C3*** and ***Pt-C1, C2 or C3*** were synthesized in a similar manner (***Scheme 2.1***).

Scheme 2.1, General synthesis of radical anionic metal dithiolenes and structures

Ene-1,2-dithiolate dianion was obtained by the deprotection of [**1**] in with sodium methoxide in methanol chloroform mixture followed by treatment with Ni or Pt salts. The complexes with quinoxdt ligands were precipitated with chiral counterion (R)-N, N, N-trimethyl-1-phenylethanaminium [(R)-Ph(Me)HC*-NMe_3] while dddt and dddmedt complexes with tetra butyl ammonium bromide (Bu_4N). All the reactions were carried out with degassed solvents and under argon followed by precipitation with counterion in presence of air. The **Pt-C1** complex is selected for detailed representation of results for most instances in this chapter.

2.2. Characterization

2.2.1. Crystal Structures

Crystals suitable for X-ray diffractometric characterization for (R)-Ph(Me)HC*-NMe_3[M(quinoxdt)$_2$] were grown by slow diffusion of diethyl ether into a concentrated solution of complexes in DMF. Both the ***M-C1*** complexes crystallize in triclinic system with chiral *P1* space group due to the presence of the enantiopure cation (*R*)-Ph(Me)HC*-NMe_3^+. In the lattice, a DMF molecule of crystallization is also present per each complex anion entity. A summary of data collection and structure refinement for ***M-C1*** and are reported in ***Table 2.1.***

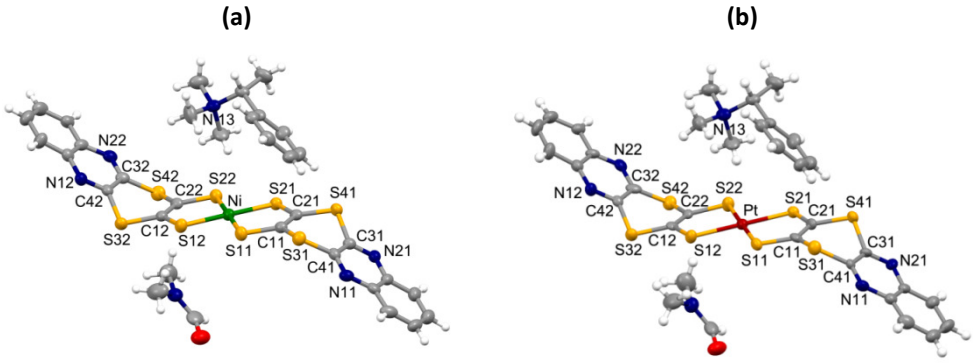

Figure 2.2, Molecular structure of a) (*R*)-Ph(Me)HC*-NMe_3[Ni(quinoxdt)$_2$]·DMF (***Ni-C1***) and b) (*R*)-Ph(Me)HC*-NMe_3[Pt(quinoxdt)$_2$]·DMF (***Pt-C1***) with thermal ellipsoids drawn at the 30% probability level.

Table 2.1, Summary of X-ray crystallographic data for ***M-C1***

	Ni-C1	***Pt-C1***
Empirical formula	$C_{34}H_{33}N_6NiOS_8$	$C_{34}H_{33}N_6OPtS_8$
Formula weight	856.85	993.23
Colour, habit	Brown, plate	Red, plate
Crystal size, mm	0.32 x 0.25 x 0.12 mm	0.32x0.27x0.13
Crystal system	Triclinic	Triclinic
Space group	*P*1	*P*1
***a*, Å**	7.8870(10)	7.917(3)
***b*, Å**	9.521(2)	9.545(4)
***c*, Å**	13.704(2)	13.778(5)
α, deg.	76.019(3)	75.536(6)
β, deg.	75.252(3)	74.930(5)
γ, deg.	75.761(3)	76.395(5)
***V*, Å^3**	946.8(3)	957.2(6)
Z	1	1
***T*, K**	293(2)	293(2)
ρ (calc), Mg/m^3	1.503	1.723
μ, mm^{-1}	0.991	4.139
θ range, deg.	1.56 to 26.56	1.56 to 26.54
No.of rflcn/obsv	11192 / 7742	11445 / 7838
GooF	1.001	1.010
***R*1**	0.0414	0.0533
***wR*2**	0.0685	0.1351

$R1 = \Sigma||F_O|-|F_C||/\Sigma|F_O|$, $wR2 = [\Sigma[w(F_O^2-F_C^2)^2]/\Sigma[w(F_O^2)^2]]^{½}$, $w = 1/[\sigma^2(F_O^2) + (aP)^2 + bP]$, where $P = [\max(F_O^2,0) + 2F_C^2]/3$

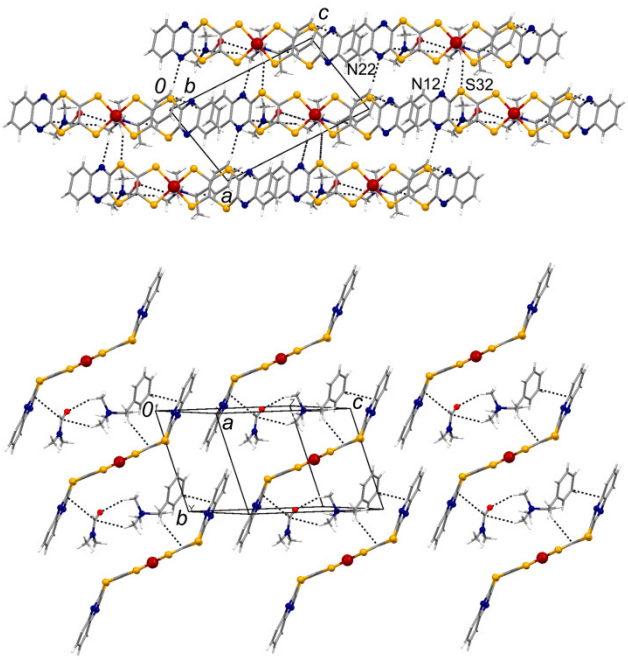

Figure 2.3, Crystal packing of (*R*)-Ph(Me)HC*-$NMe_3[PtL_2]$·DMF. Above, projection along the *b*-axis. Below, projection approximately along the *a*-axis. A portion of a Supramolecular layers is shown. Dashed lines represent shortest contacts between the anion complex, DMF and the chiral cation.

The structure of ***M-C1*** consists of a square planar metal bound by four sulfur atoms from two bidentate S, S dithiolate ligands. The Pt-S bond distances are in the relatively narrow range of 2.267(6)-2.288(6) Å, while Ni-S bond distances are from 2.148(3) - 2.161(3) Å. whereas in the S-C-C-S fragments that comprise the formal dithiolate moieties, there is a greater variability in the bond distances. In particular, for ***Pt-C1*** the fragment S(11)-C(11)-C(21)-S(21) of the first ligand presents C-S bond distances that are, on average, 0.06 Å shorter than the S(12)-C(12)-C(22)-S(22) system of the second ligand while for ***Ni-C1*** complex the

difference is low 0.01 Å partly because of smaller metal radius, ***(Table 2.2,)*** Consistently the C-S bond distances within the bent hexaatomic ring are longer for the first ligand [1.78(2) and 1.82(2) Å] with respect those of the second ligand [1.75(2) and 1.77(2) Å] while similar characteristic is displayed for Ni complex. The C-C bond distances of the two dithiolate moieties are in agreement with the presence of a double bond between the both the C(11)-C(21) and C(21)-C(22) systems though these distances decrease from ***Ni-C1*** to ***Pt-C1*** complex. These type of systems were previously extensively investigated and different bonding schemes can be proposed and they take into account both the metal oxidation state and the overall charge on the dithiolate system, which can be formulated as a radical anion ligand $L^{-\bullet}$ or as a dianionic ligand L^{2-}, respectively, ***Scheme 2.2.***[2-4]

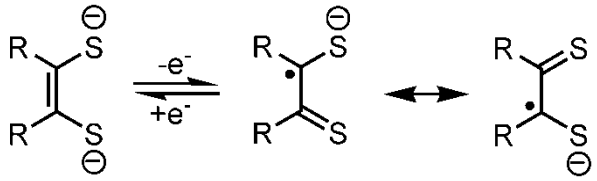

Scheme 2.2, Depiction of the formal electronic structure of the ligand, pure dithiolate L^{2-} (left) and the radical anion $L^{-\bullet}$ (right).

From a structural point of view, longer C-S distances are associated with a L^{2-} description, whereas shorter C-S distances point to a radical anion description. Even though the uncertainty on the bond distances are approximately 0.02 Å, it can be tentatively speculated that one of the ligand may be formulated as a radical and the second as a dianion, so that the molecular structure of the complex may be depicted as $[M^{II}(L^{-\bullet})(L^{2-})]^{-}$, instead of being represented as the

average structure of the resonance forms: $[M^{II}(L^{-\bullet})(L^{2-})]^{-} \leftrightarrow [M^{III}(L^{2-})(L^{2-})] \leftrightarrow [M^{II}(L^{2-})(L^{-\bullet})]^{-}$.

However, it has to be noted that the small variation in the bond distances in the two ligand systems may be a consequence of the different interactions exchanged by the two ligands with the surrounding molecules in the crystal lattice. The molecular structure exhibits a bent shape due to the presence of the two thioether groups in the hexaatomic ring close to the dithiolate moiety.

Table 2.2, Selected bond lengths (Å) and angles (°) for ***M-C1*** complexes, together with the optimized geometries of the complex anion $[ML_2]^{-}$.

Bonds	**Experimental by XRD**		**Calculated**		**Bonds**	**Experimental by XRD**		**Calculated**	
	Ni	**Pt**	**Ni**	**Pt**		**Ni**	**Pt**	**Ni**	**Pt**
M-S(11)	2.159(3)	2.267(6)	--	2.336	C(31)-C(41)	1.778(8)	1.44(2)	--	1.449
M-S(21)	2.148(3)	2.268(6)			C(32)-C(42)	1.437(10)	1.45(2)		
M-S(12)	2.149(3)	2.267(6)			C(11)-C(21)	1.358(10)	1.31(3)	--	1.366
M-S(22)	2.161(3)	2.288(6)			C(12)-C(22)	1.350(10)	1.33(3)		
C(11)-S(11)	1.737(9)	1.71(2)	--	1.745	C(41)-S(31)	1.765(9)	1.77(2)	--	1.775
C(21)-S(21)	1.716(9)	1.72(2)			C(31)-S(41)	1.778(8)	1.79(3)		
C(12)-S(12)	1.724(9)	1.75(2)			C(42)-S(32)	1.763(8)	1.73(2)		
C(22)-S(22)	1.719(9)	1.77(2)			C(32)-S(42)	1.763(9)	1.74(2)		
C(11)-S(31)	1.766(9)	1.82(2)	--	1.789					
C(21)-S(41)	1.749(9)	1.78(2)							
C(12)-S(32)	1.772(9)	1.77(2)							
C(22)-S(42)	1.759(9)	1.75(2)							
					Angles				

M-S(11)-C(11)	103.0(3)	101.9(8)	--	102.8	S(11)-C(11)-C(21)	120.4(7)	124(2)	--	122.8
M-S(21)-C(21)	104.0(3)	102.1(6)			S(21)-C(21)-C(11)	120.3(7)	123(0)		
M-S(12)-C(12)	103.1(3)	103.1(7)			S(12)-C(12)-C(22)	121.1(7)	123(2)		
M-S(22)-C(22)	103.4(3)	102.0(6)			S(22)-C(22)-C(12)	120.0(8)	122.4(1)		
S(11)-M-S(21)	92.2(11)	89.3(2)	--	88.4					
S(12)-M-S(22)	92.1(11)	89.7(2)							

The peripheral aromatic systems of the two ligands are approximately parallel (the dihedral angle between the two mean planes formed by the aromatic groups is ~ 2°), whereas the dihedral angle between the mean coordination plane and these peripheral aromatic systems is approximately 40°. The crystal packing and relevant intermolecular interactions are reported in ***Figures 2.3*** and ***2.4*** In particular, the assembly (*R*)-Ph(Me)HC*-$NMe_3[ML_2]$·DMF (L = Quinoxdt) forms Supramolecular layers that run parallel to the *b* crystallographic axis. Each layers interacts with adjacent ones by means of CH_{methyl}···N(12), CH_{methyl}···S(32), and CH_{phenyl}···N(22) contacts (***Figure 2.3***).

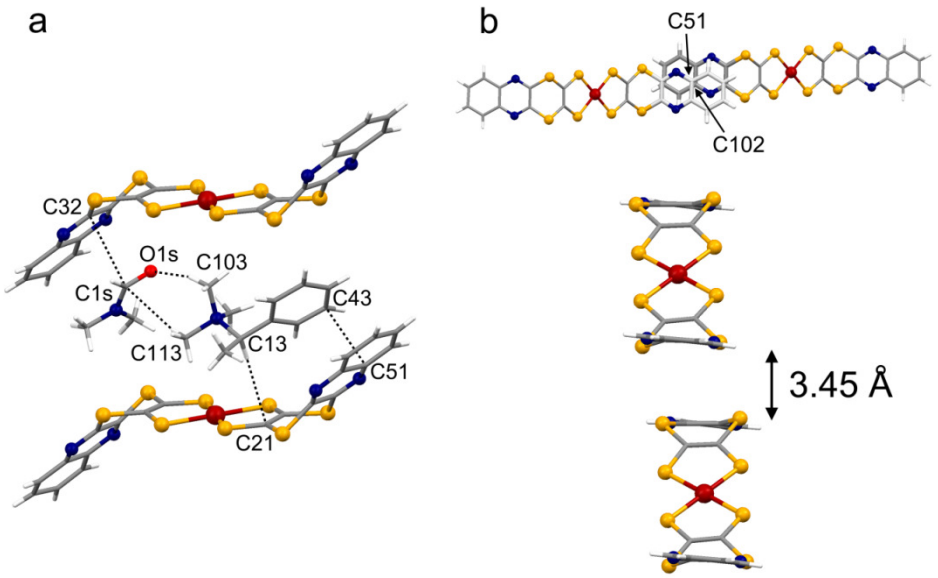

Figure 2.4, Highlight on the interaction occurring within one supramolecular layer. Short intermolecular interaction are depicted as dashed lines. a) DMF and cation sandwiched between two anions. b) Depiction of the partial π stack occurring between the peripheral fragment of the ligands.

These contacts occur between the nitrogen and sulphur atoms of the ligand and the methyl and phenyl groups of the chiral cation. Within the layers the cation and the DMF molecules are sandwiched between two complex anions (***Figure 2.4a***) with which they exchange different interactions. In particular, the cation interacts with the peripheral part of one ligand by means of a partial π stack (C(43)-C(51) = 3.33(3) Å), and by means of a C-H··· π contact (C(13)-C(21) = 3.77(3) Å), whereas the DMF molecule interacts with one of the ligands by means of a partial π stack [C(1s)-C(32) = 3.31(4) Å]. The DMF molecule and the cation interacts by means of CH_{methyl}···O(1s) and CH_{methyl}···C(1s) contacts. Moreover, the complex anions give rise to a partial π stack through the peripheral aromatic

fragment of the ligands, and the minimum distance within this stack is exhibited by the C(51) and C(102) atoms [3.45(4) Å, ***Figure 2.4b***].

2.2.2. Computational studies

Theoretical calculations were performed by Dr. Luciano Marchiö at University of Parma and are reported here to provide better understanding of nature of bonding and related properties. The complexes ***M-C1*** (M = Ni, Pd, Pt) exhibit a S=1/2 ground state and the calculations were performed with the spin unrestricted formalism. The ***M-C1*** experimental geometry was known from X-ray structural characterization. A good agreement between the calculated and experimental geometries even though the metal-sulphur distances is slightly overestimated by the calculations (≈0.6 Å). Another important difference can be noted by inspecting the bond distances of the dithiolate ligands. In fact, in the experimental geometry the two ligands show some differences within the framework of the dithiolate system involved into the metal coordination. On the opposite the optimized structure is highly symmetric with the two ligand fragments having identical geometries. By comparing the optimized geometries of the three complexes, it can be observed that the ligand structure is almost invariant. The main difference is due to the M-S bond distances, which are very similar for the ***Pt*** and ***Pd-C1*** complexes (~ 2.33 Å) and are, as expected, significantly shorter for the ***Ni-C1*** complex (~2.20Å).

The composition of selected molecular orbitals and their energy levels for the three complexes are depicted in ***Figures 2.5.*** It can be appreciated that in both cases the SOMO is the out of plane antibonding combination between the d_{xz} metal orbital and a π* ligand centred (LC) orbital, having more than 55% 3pz-

sulphur character (***Table 2.4.***). According to the fragmental composition of the SOMO, the MS_4 moiety increases the contribution to the SOMO along the Ni, Pd, Pt series at the expenses of the remaining part of the ligands, ***Figure 2.6.*** Consistently, the contribution of the metals to the SOMO increases from 6 to 11% on going from the ***Ni*** to ***Pt-C1*** complex. Interestingly, the LUMO in these complexes is represented by the π* orbital localized on the peripheral aromatic fragments of the ligands, at variance with similar metal dithiolate systems, in which the LUMO is mainly represented by an in-plane σ-antibonding interaction between the metal d_{xy} or $d_{x^2-y^2}$ and S 3pσ orbitals.[3,5-7] This type of orbital is the LUMO+2 in the case of the ***Ni*** and ***Pd-C1*** complexes whereas it is found at higher energies in the case of ***Pt-C1*** (LUMO+4). This molecular orbital is composed by a decreasing d_{xy} contribution and a slight increasing contribution of the sulphur 3pσ orbitals, respectively, along the Ni, Pd, Pt series, ***Tables 2.4 and 2.5***. A similar MO sequence was found for the dianion [Ni(pdt)2]2- (pdt= bis(pyrazine-2,3-dithiolate)).[8]

Table 2.3, Population analysis and spin density of ***M-C1*** (M= Ni, Pd, Pt) in the gas-phase (B3LYP/6-311+G(d)-def2-TZVP). Contribution of the metal center and of the coordinated sulphur atoms[a] are reported.

		***3s* el.**	***3p* el.**	***n*d el.**	**(*n*+1)s el.**	**Mulliken atomic charges**	**NPA charges**	**NPA atomic spin density**	**Mulliken atomic spin density**	$\langle S^2 \rangle$
Ni-C1	**Ni**	core	core	8.94	0.42	0.058	0.536	0.170	0.146	0.756
	S	1.74	4.29	-	-	-0.877	-0.072	0.168	0.141	
Pd-C1	**Pd**	core	core	9.12	0.48	-0.579	0.345	0.093	0.000	0.755
	S	1.75	4.24	-	-	-0.655	-0.025	0.182	0.202	
Pt-C1	**Pt**	core	core	8.95	0.66	0.340	0.336	0.154	0.100	0.755
	S	1.74	4.24	-	-	-0.853	-0.019	0.180	0.150	

[a] = for symmetry reasons only the values of one sulphur is reported

Table 2.4, Percentage composition of selected molecular orbitals of ***M-C1*** (M= Ni, Pd, Pt) in the gas-phase (B3LYP/6-311+G(d)-def2-TZVP). Alpha spin orbitals are described.

	MO	$M(nd_{xy})$	$M(nd_{xz})$	$S_{coord}(3p_z)$	$S_{coord}(3p_{x,y})$	$C(2p_z)$	$S_{ring}(3p_z)$
$[Ni(L)_2]^-$	LUMO+2	34.5	-	-	45.6	-	-
	SOMO	-	6.1	56.1	1.9	22.7	8.2
$[Pd(L)_2]^-$	LUMO+2	27.6	-	-	46.1	-	-
	SOMO	-	8.0	57.3	2.6	20.8	6.4
$[Pt(L)_2]^-$	LUMO+4	23.2	-	-	48.2	-	-
	SOMO	-	11.0	57.9	2.9	18.6	5.2

Table 2.5, Contribution of metal and the two quinoxdt ligand fragments (L1 and L2) to the frontier molecular orbital for ***M-C1*** (M= Ni, Pd, Pt) in the gas-phase (B3LYP/6-311+G(d)-def2-TZVP). Alpha spin orbitals are described.

		α H-3	α H-2	α H-1	αSOMO	αLUMO	α L+1	α L+2	α L+3	α L+4
$[Ni(L)_2]^-$	Ni	50.83	39.96	2.39	6.10	0.27	0.07	36.00	0.08	4.33
	L1	24.59	30.02	48.80	46.95	49.86	49.97	32.00	49.96	47.83
	L2	24.59	30.02	48.80	46.95	49.86	49.97	32.00	49.96	47.83
$[Pd(L)_2]^-$	Pd	28.17	31.44	1.46	8.00	0.00	0.79	27.73	2.10	5.33
	L1	35.2	34.28	49.27	46.00	50.05	49.63	36.13	48.95	47.34
	L2	35.91	24.28	49.27	46.00	49.95	49.58	36.14	48.95	47.34
$[Pt(L)_2]^-$	Pt	21.62	37.80	2.58	11.34	0.36	0.00	6.64	0.63	24.83
	L1	39.19	31.10	48.71	44.33	49.76	50.08	46.68	49.68	37.58
	L2	39.19	31.10	48.71	44.33	49.76	49.92	46.68	49.69	37.58

In ***Figures 2.7*** is depicted the spin density for the two complexes, in agreement with the S=1/2 ground state. According to the Natural Population Analysis (NPA) the spin density is mainly localized on the sulphur atoms comprising the coordination environment, and it is also partially localized on the metal centers:

0.17 for Ni, 0.09 for Pd and 0.18 on Pt atoms, respectively. The population of the nd and (n+1)s orbitals for the three metals is reported in ***Table 2.3.*** The nd orbitals have an occupation of 8.94 for Ni, 9.12 for Pd and 8.95 for Pt, these values are in lines with those obtained for strictly related systems and the metal oxidation state for the three complexes can be considered as +2. The nd orbital occupation greater than eight electrons derives by the population of the nd_{xy} orbital as a consequence of the interaction with an antisymmetric sulphur based orbital of the ligands.[2, 9]

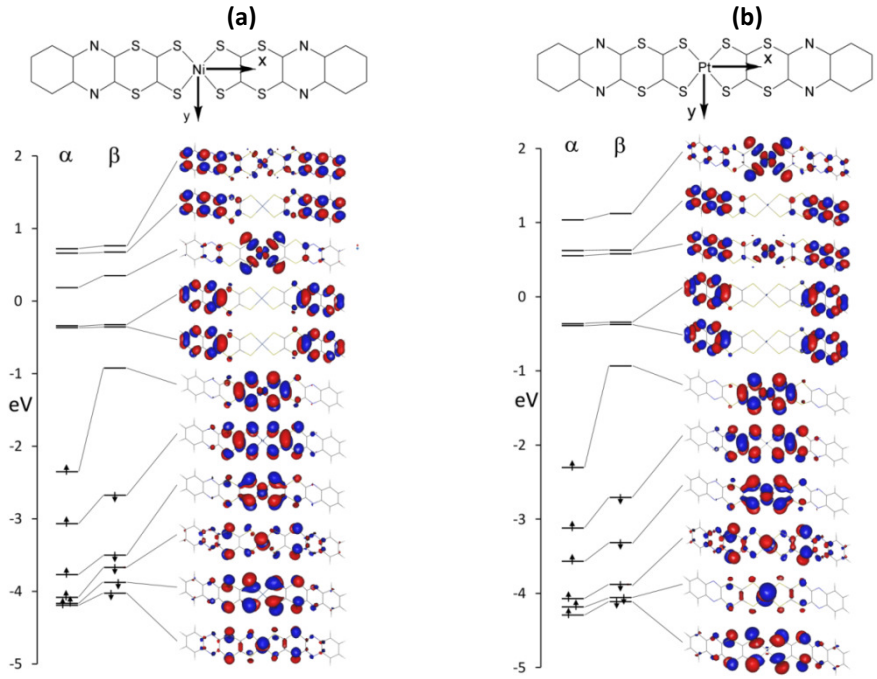

Figure 2.5, Energy levels and Kohn-Sham molecular orbitals for ***M-C1,*** as $[M(L)_2]^-$ from a spin unrestricted calculation (B3LYP/def2-TZVP_6-311+G(d)).

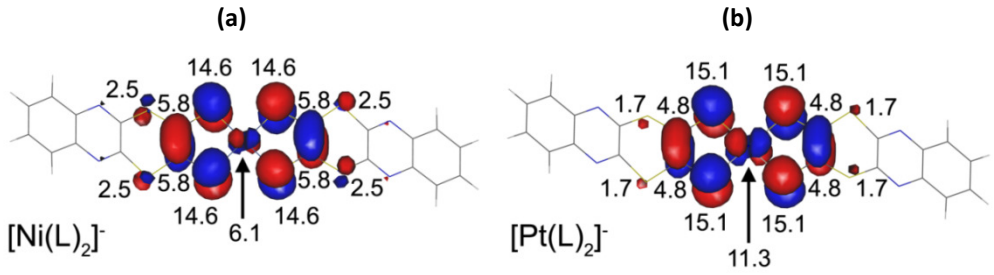

Figure 2.6, Percentage contributions of different atoms to the alpha SOMO of $[M(L)_2]^-$. (B3LYP/def2-TZVP_6-311+G(d)).

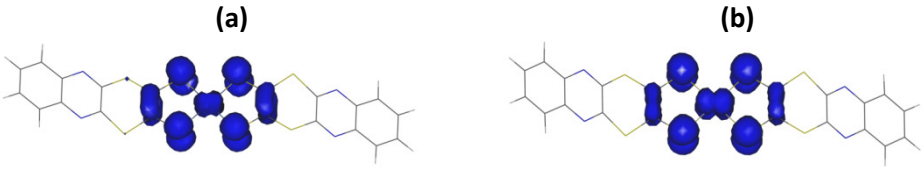

Figure 2.7, Depiction of the spin density distribution of $[M(L)_2]^-$ (B3LYP/def2-TZVP_6-311+G(d)), isosurface plot at 0.001 esu $Å^{-3}$.

2.3. Magnetic properties

DC magnetic susceptibility measurements on a polycrystalline sample of ***Pt-C1*** complex was performed with a Quantum Design MPMS-XL-5 SQUID magnetometer in the temperature range 8–350 K. The molar magnetic susceptibility (CGS units) vs. temperature is shown in ***Figure 2.8.*** The temperature dependence of the susceptibility is well described by the Curie law:

$$\chi_m = \frac{N\, p^2\, \mu_B^2}{3kT}$$

where *N* is the number of magnetic ions in a mole, $p = g[S(S+1)]^{1/2}$ is the effective Bohr magneton number, μ_B is the Bohr magneton and *k* is the Boltzmann

constant. The fit gives an effective Bohr magneton number p = 2.0 ± 0.1; the closest theoretical value is p = 1.73, corresponding to S=1/2.[10] The good fit with a simple Curie law and the value of p suggest a magnetic behaviour typical of an uncoupled S=1/2 ground state species.

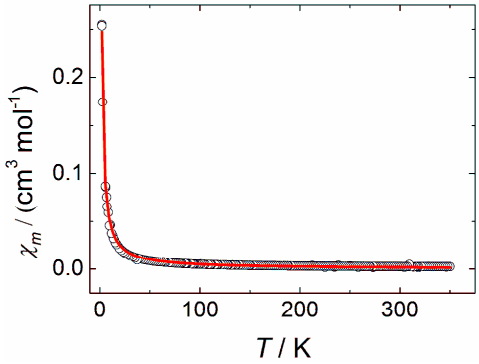

Figure 2.8, Molar magnetic susceptibility (CGS units) vs temperature for ***Pt-C1***. Experimental data (open circles) and the fit curve (solid line) are shown.

According to the structural analysis, the presence of a partial π-stack through the peripheral aromatic fragment of the ligands (3.45(4) Å) may result in magnetic interactions, as observed in d^8-monoanionic bisdithiolene complexes. For example, it was found that a separation of 3.45(4) Å between neighbouring fragments in a nickel-bisdithiolene system causes strong antiferromagnetic interactions.[10] In the present case, stacking motifs are not favourable to induce magnetic interactions, and this can be easily explained by considering that the stacking occurs through the periphery of the ligand (***Figure 2.4a***). In fact, the presence of a dithiino ring interposed between the aromatic moieties interrupts the communication with the metal-thiolate systems experiencing a spin density accumulation at the central complexation core $M(C_2S_2)_2$ (***Figure 2.4b***).

2.4. Electrochemical properties

Cyclic voltammograms (CV) of the complex were performed on anhydrous and argon-degassed DMF solutions, ***Figure 2.9,*** The CV exhibits two different waves: the reversible wave at $E_{1/2}$ = −0.292 V (vs Ag/AgCl) (see the inset in ***Figure 2.9***) is relatable to the reduction from $[PtL_2]^{1-}$ to the $[PtL_2]^{2-}$ species; an additional irreversible process can be associated to the formation of the neutral species after oxidation at +0.356 V and reduction process at +0.208 V restores the monoanionic species. The irreversibility of this last process is likely due to the poor solubility of the neutral derivative in the used solvent.

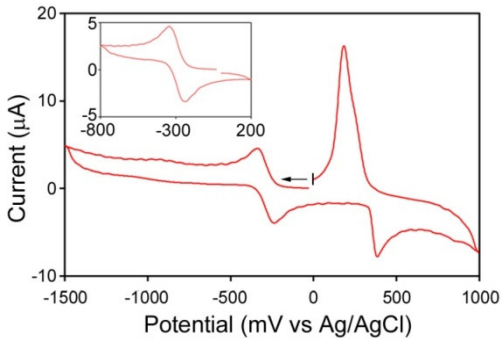

Figure 2.9, CV of ***Pt-C1*=[PtL_2]** c= 0.5×10^{-3} M in the presence of $TBAClO_4$ 0.2 M in DMF, WE: Pt; CE: Pt; RE: Ag^+/Ag (saturated KCl), scan rate: 100 mV/s.

2.4.1. Electrocatalytic proton reduction:

Cyclic voltammograms of ***Pt-C1*** in CH_3CN solution acquired upon successive additions of p-toluene-sulfonic acid (tosylic acid, TsOH) are reported in ***Figure 2.10.***The reduction wave relatable to the redox couple $[PtL_2]^{-1}/[PtL_2]^{-2}$ is still observed and new peaks of increasing current on increasing acid concentration and falling at more negative potentials, appear. These peaks are assigned to proton reduction. The cyclic voltammetric responses as a

function of added tosylic acid are similar to what observed in analogous nickel radical dithiolenes studied as electrocatalysts for proton reduction.[3]

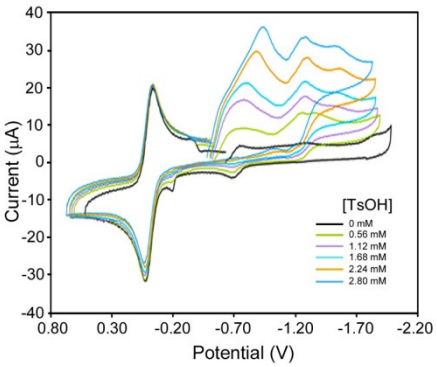

Figure.2.10. Cyclic voltammograms of ***Pt-C1*** [0,65 mM] in CH_3CN solution upon successive additions of TsOH. Working electrode: glassy carbon, GC; Counter electrode: Pt; Reference electrode: Ag; scan rate: 100 mV/s, $TBAClO_4$ 0,2 M, E1/2(Fc+/Fc) = 0V. All solutions were freshly prepared. Argon was used to purge all samples.

2.5. Optical properties

Complex TMEBA [$Pt(Quinoxdt)_2$] is characterized in the near infrared region by a broad absorption at 1085 nm in DMF with medium-high molar absorption coefficient [18.9×10^3 M^{-1} cm^{-1}] and weaker absorptions in the visible region, as shown in ***Figure 2.11a.***

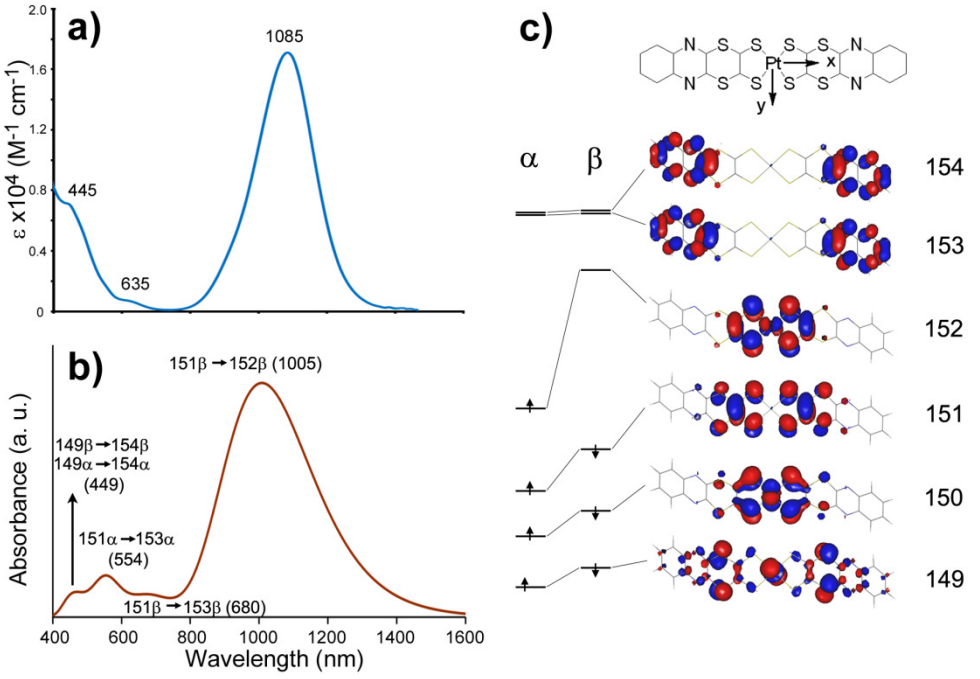

Figure 2.11, **(a)** Absorption spectrum of ***Pt-C1*** in DMF solution in the 400-1600 nm range. (**b)** TD-DFT, (B3LYP/def2-TZVP_6-311+G(d) calculated spectra of the ***Pt-C1*** anionic complex. In the inset the calculated MOs involved in the absorption transitions are shown in enlarged view. (**c)** Calculated MOs involved in the absorption transitions.

As already cited, the ***Ni-C1*** a salt with tetrabutyl ammonium counterion containing corresponding monoanion,[1] which shows similar spectral features to ***Pt-C1***, was previously reported and proposed as a dye for applications in Q-switching of Nd-YAG and Nd-YAP lasers more appealing with respect to [Ni(Pr^i_2timdt)$_2$], which is so far one of the near infrared dyes with highest absorptivity in the 1000 nm range.[11] The invoked superiority of the proposed Ni-candidate has been ascribed to its better matching with operating wavelengths of these lasers (1064 and 1079 nm respectively), despite [Ni(Pr^i_2timdt)$_2$] exhibits

much higher absorptivity (approximately five times higher than the case under discussion) as well as solubility.

On increasing addition of I_2 as oxidizing reagent to ***Pt-C1***, the NIR peak at 1085 nm, typical of the monoanion decreases and a new one increases at 854 nm. A well defined Isosbestic point at 942 nm is observed (***Figure 2.12a***) this reflects equilibrium between the monoanion and the neutral derivative.

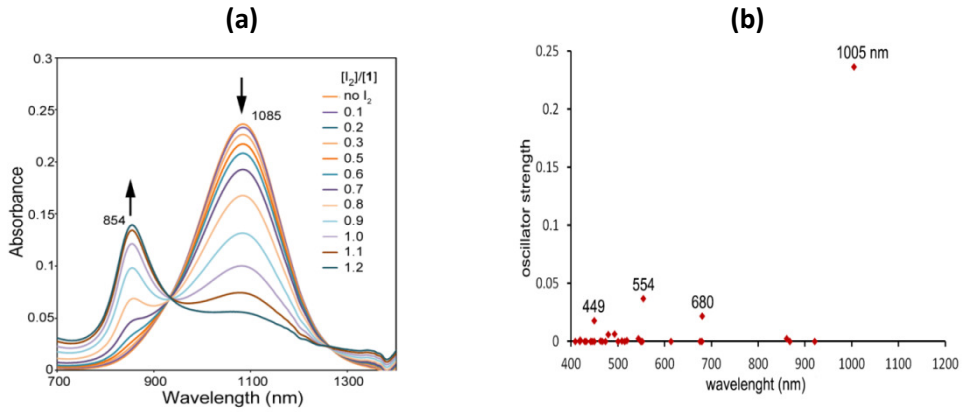

Figure 2.12, (a) Changes of absorption spectra for ***Pt-C1*** in DMF (c = 1.25 $\times 10^{-5}$M) on increasing concentrations of I_2. The new peak at 854 nm is ascribed to the formation of the neutral derivative. It should be remarked that the absorbance increase of the neutral species exhibits deviations from Beer's law which can be consistent with auto-association of the formed species. (b) Oscillator strengths of the 30 excitations for ***Pt-C1*** resulting from TD-DFT calculations.

With the help of TD-DFT calculations, the observed absorption bands in ***Pt-C1*** were assigned as shown in ***Figure 2.11b.*** These assignments only in part support those tentatively proposed in earlier.[1] The TD-DFT calculations were performed for 30 excitations, which are reported in ***Figure 2.12b.*** Most of these excitations have negligible intensity, and in the visible region three bands can be identified at 449, 554 and 680 nm, whereas the most intense band falls in the Near-IR region at 1005 nm. The experimental UV-vis spectrum shows a good agreement with the

simulated one. In fact, the near-IR band falls at 1085 nm, whereas in the visible region, there can be easily identified two bands at 445 and 635 nm. A third band can be identified as a shoulder around 550 nm, ***Figure 2.11a***. As for other analogous monoanionic derivatives[2] the peak falling in the near-IR is associated to a HOMO−1→SOMO transition. As previously described (see ***Figures 2.5b, 2.6b and 2.11***.), the HOMO−1 consists of π–orbitals formed by in phase combination of the $S_2C_2S_2$ moieties (with antibonding features) and the SOMO consists of an antibonding combination of the metal [$5d_{xz}$ Pt orbital] and π-orbitals of the $S_2C_2S_2$ system. It is noteworthy that no significant contribution of quinoxaline ring orbitals is provided to these orbitals. The two bands in the visible region at 680 and 554 nm were assigned as a HOMO−1→LUMO transitions. As previously described, the LUMO and LUMO+1 consist of π–orbitals of the quinoxaline and benzene-like moieties with no significant contribution of orbitals from dithiolene core. Thus HOMO−1→LUMO transitions have charge transfer character from dithiolene core (the $S_2C_2S_2$ ligand moieties) to the periphery of the ligand (the quinoxaline moieties). The band at 449 nm is mainly associated to a HOMO−3→LUMO+1 transition and in this case the excitation requires a charge transfer from the metal and thioether sulfur atoms towards the peripheral quinoxaline ring.

The photoluminescence spectra of ***Pt-C1*** were recorded in DMF and acetone solution as well as in the solid state. When excited at 420 nm and room temperature, these solutions showed emission at 572 nm. (***Figure 2.13a***) Instead, in the same experimental condition, no emission was displayed in the solid state.

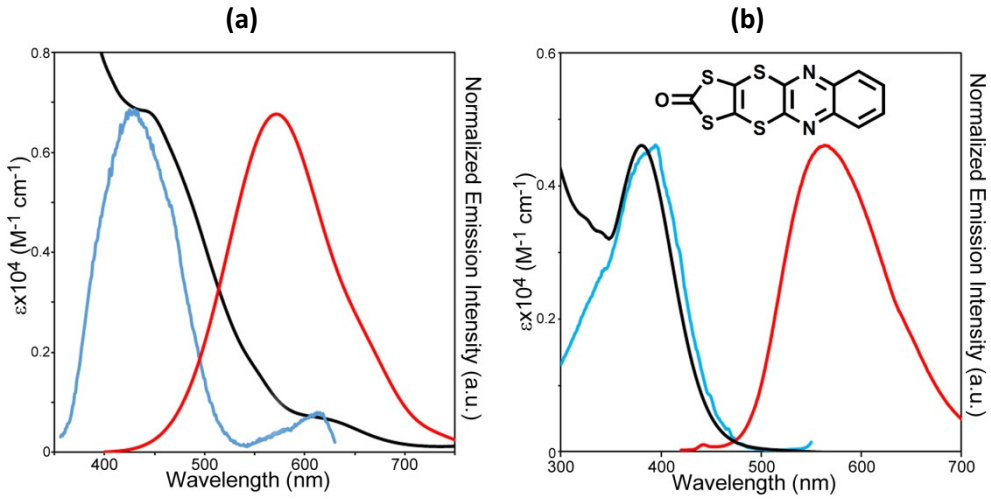

Figure 2.13, (a) Emission (red), excitation (blue) and absorption (black) spectra of ***Pt-C1*** in DMF solution. Excitation wavelength was 420 nm. The excitation spectrum was acquired by monitoring emission at 680 nm. (b) Absorption (black), emission (red) and excitation (blue) spectra of quinoxdt ligand (in the inset) in DMF solution. Excitation wavelength was 390nm. Excitation spectrum was acquired by monitoring emission at 560 nm.

The emission quantum yields, 0.11 % in acetone and 0.19 % in DMF were evaluated using the relative method by employing $[Ru(bpy)_3]Cl_2$ as suitable reference,[12] given the similarity of its absorption/emission spectral ranges with respect to ***Pt-C1***.

Table 2.6, Luminescence parameters for **Pt-C1** in DMF or acetone solutions

	λ_{ex}	λ_{em}	Solvent	Φ
Pt-C1	420	566	acetone	0.001145
	420	572	DMF	0.001928

Pt-C1 apparently violate the Kasha's rule for emission since emission at 572 nm (Excitation 420nm) observed, is at higher frequency than the lowest absorption band at 1085nm corresponding to HOMO−1→SOMO transition. Kasha's rule

violation regarding emission of higher excited states by organic molecules and metal complexes (metalloporphyrins) are recently reviewed[13] Metalloporphyrins exhibit characteristic absorption bands, called Q and Soret bands in the visible (500-700nm) and near-UV (400-500nm) regions corresponding to the $S_0 \rightarrow S_1$ (π, π^*) and $S_0 \rightarrow S_2$ (π, π^*) transitions. In addition to T_1 phosphorescence, these complexes exhibit both S_2 and S_1 fluorescence, with quantum yields and life times of S_2 fluorescence ranging from 10^{-3} – 10^{-5} and 0.1 to 5ps. The S_2 fluorescence yields were found essentially the same for complexes with different metals (including paramagnetic heavy atoms such as lanthanide ions) while the T_1 phosphorescence properties were affected by the nature of the metal ion. It was concluded that the main non-radiative process from S_2 is the internal conversion to S_1.

Regarding the system under discussion here, the emission is likely relatable to HOMO-1→LUMO transitions to the high excited state. As shown the LUMO consists of π-orbitals of quinoxaline and benzene-like moieties with no significant contribution of orbitals from dithiolene core. Thus the HOMO-1→LUMO transitions have charge transfer character from dithiolene core (the $S_2C_2S_2$ ligand moiety) to the periphery of the ligand (the quinoxaline moiety). The excitation spectrum confirms that the apparent anomalous emission actually originates from the molecule itself. (***Figure 2.13***) The location of the absorption and emission maximum of the free ligand similar to the one in ***Pt-C1***, the lack of emission in the solid state, relatable to the π-stacking through the peripheral quinoxaline part of the ligands, provide further support to the assignments.

The quantum yield (in the order 10^{-3}) and the evaluated lifetime of the observed emission (in the order of tens of ps) may be in agreement with an internal conversion to an emission state but this should give rise to an emission band falling at wavelength higher of the lowest energy band (>1100nm). Unfortunately this value is out of the wavelength range covered by our spectro-fluorimeter. Experimental (photophysical studies also based on transient absorption measurements) and theoretical studies involving researchers with additional instrumentation and skills are planned. The described behaviour may be then ascribed to a poor wave functions' overlap between the upper excited states (D_2 and D_1) of the complex so that the rate of internal conversion from the superior excited state (D_2) to the lowest one (D_1) is somewhat slowed down and radiative emission in the visible region becomes competitive. This may help to explain the unusual anti-kasha behaviour of this complex, showing emission at a lower wavelength than the lowest absorption band in the NIR region. Moreover the luminescence properties of ***Pt-C1*** are similar (quantum yield, life times) to those observed in analogous compounds where quinoxaline moiety can be considered as an ancillary ligand as in heterocyclic substituted platinum-1,2-enedithiolato [(dppe)Pt{S_2C_2(heterocycle)(R)}](dppe= diphenyl phosphino ethane, heterocycle = 2-qionox, R=Me, H) complexes which exhibit a lower lying transition falling near 450nm. This peak has been assigned to an intra-ligand 1,2-enedithiolate $\pi \rightarrow$ quinoxaline π^* transition (ILCT) responsible of two emissive states: ^{1}ILCT*(Φ~ 1x 10^{-3};life time ~0.1ns) and ^{3}ILCT* (720ns under Ar), this last quenched by acid addition. Flash photolysis experiments on [(dppe)Pt{S_2C_2(2-quinox)(H)}] in presence of benzoic acid, a proton source insufficient to protonate the ground state but an effective quencher, show a transient absorption spectrum

assignable to ^{3}ILCT* state, whose lifetime was shortened. The failure to generate ^{3}ILCT* state of the protonated form by direct excitation or proton quenching, was explained by taking into account that the protonation of quinoxaline leads to a rapid non-radiative decay.[14] More recently the luminescence properties showing emission in 600-800nm region[15] of dimetallic molybdenum(V) compounds containing bifunctional dithiolene ligands (BpyDTS$_2$= 2-bis(2-pyridyl)methylene-1,3-dithiolene) have been interpreted associating luminescence with an ILCT* state. The coincident of shape and position of emission spectrum of the dimetallic complex with that of mononuclear tin compound $(CH_3)_2Sn(BPyDTS_2)$, and theoretical calculations support the description of the ILCT* state as dithiolene $\rightarrow$ bis (2-pyridyl), while the metal seems to have a role in connecting the dithiolene ligands to improve emission efficiency. Similarly to these complexes, ***Pt-C1*** the emissive state is assigned to an intra-ligand dithiolene—$\pi\rightarrow$ quinoxaline (2-pyridyl)-π^* transition (ILCT) where the quinoxaline (2-pyridyl ring) is not in π-communication with the dithiolene core. The difference in lifetimes (tens vs one hundred ps) may be relatable to the different communication between the molecular fragments involved in the transition in the two cases. Instead in apparently similar cases such as $[Pt(qdt)]^{2-}$; qdt = quinoxaline-2,3-dithiolato, [Pt(phen)(qdt)]; phen = 1,10-phenanthroline[16] and [Pt(ppdt)2]2-; ppdt = pyrido(2,3-b)pyrazine-2,3-dithiolato,[17] the q and pp rings are in π-communication with the dithiolene core.

A rough estimation of emission lifetime of ***Pt-C1*** (through quantum yield and spectral data, ***Table 2.6***) yields a value of the order of tens of ps. This value is actually comparable to those evaluated for internal conversion processes in

similar dithione/ditholate systems.[18] Investigation on a series of analogous complexes where the quinoxaline moiety is pushed at higher distances from the metal centre though ligand design is planned in our laboratories to help clarify these points. In addition to these considerations, it is also known that when the energy gap between the upper excited states is sufficiently large, as in this case, exceptions to Kasha's rule may be expected.[19] However a thorough photophysical study, including transient absorption experiments, will be crucial to correctly assess the photocycle in this complex.

The emission is proton dependent, as shown in ***Figure 2.14a*** and ***2.14b*** for HCl addition to ***Pt-C1*** in acetone and DMF respectively in the 1:0 to 1:10 molar ratio, and the related quenching rate constants are of the same order of magnitude, though slightly higher for the acetone solution. On the other hand, the visible-NIR absorption spectra of the corresponding solutions show small changes, if any, as shown in ***Figure 2.15***. Similar behavior has been reported for the nickel complex $Et_4N[Ni(4\text{-pedt})_2]$ (4-pedt =1-(pyridine-4-yl)ethylene-1,2-dithiolate, where no shift of the Near-IR peak was observed when $HClO_4$ is added in the 1:0 to 1:4 concentration ratio range.[20]

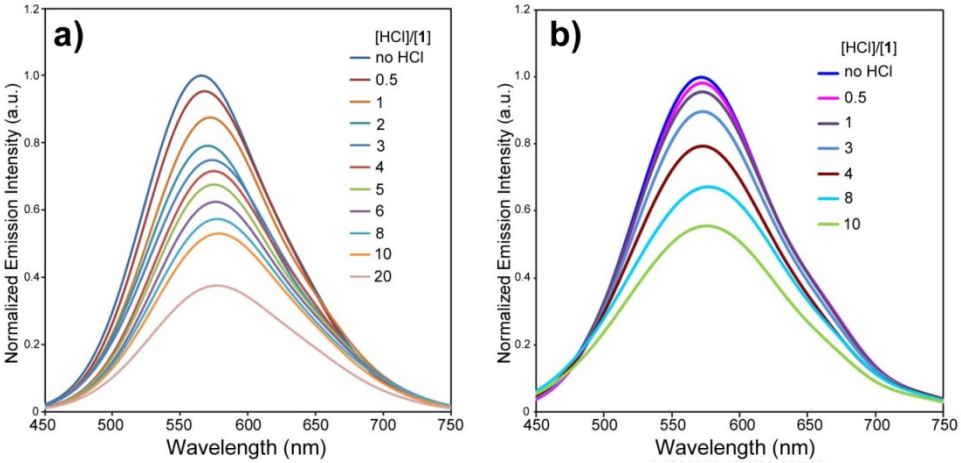

Figure 2.14, Variation of the emission spectrum of ***Pt-C1*** in acetone solution (a) and DMF solution (b) on increasing HCl concentration. Excitation wavelength was 420 nm.

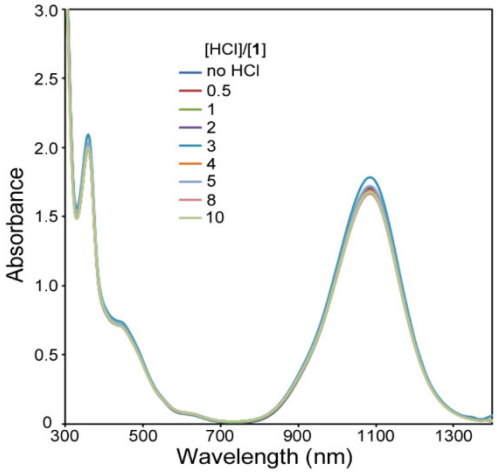

Figure 2.15, Absorption spectra for **Pt-C1** in DMF solution on addition of increasing amount of HCl.

Being the near-IR excitation mainly relevant to HOMO−1→SOMO transition, it seems reasonable to propose that the energy gap is not affected observably by the protonation of the quinoxaline moiety, which does not provide significant contribution to these orbitals. The quenching process after excitation at 420 nm,

depends on the proton source, and this process is less effective with TFA (trifluoroacetic acid) than with HCl, with a quenching rate constant more than one order of magnitude lower (***Figure 2.16***).

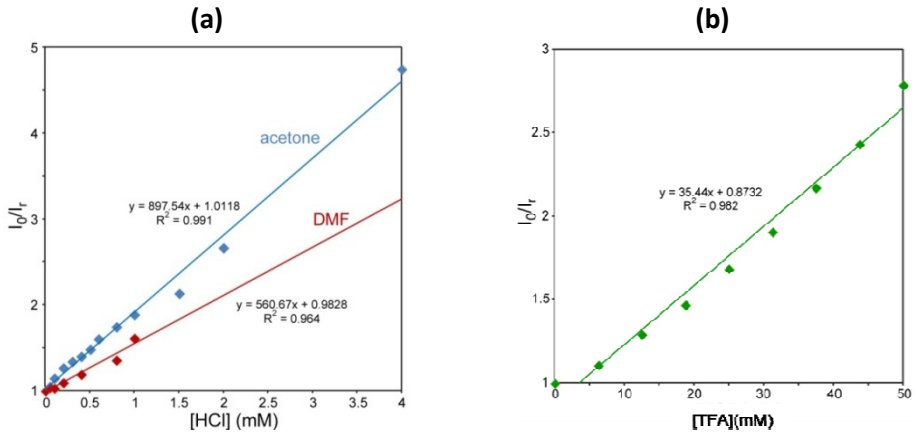

Figure 2.16, (a) Stern-Volmer plot for the emission quenching of ***Pt-C1*** by HCl addition in acetone (blue) and DMF (red). (b) Quenching by TFA in DMF (green) Dots represents experimental I_0/I_r values, solid lines represent linear fit to data. $k\tau_0$= 898 and 561 in acetone and DMF solution, respectively.

It has been previously observed that the quenching process depends on the acid strength of the proton quenchers, and high concentrations of mild acid quenchers are required to suppress the emission.[21] By using TFA in very strong excess with respect to ***Pt-C1,*** both a quenching of the luminescence, which undergoes a blue-shift on increasing TFA excess, and a change in the absorbance spectra is observed, as shown in ***Figure 2.17.***

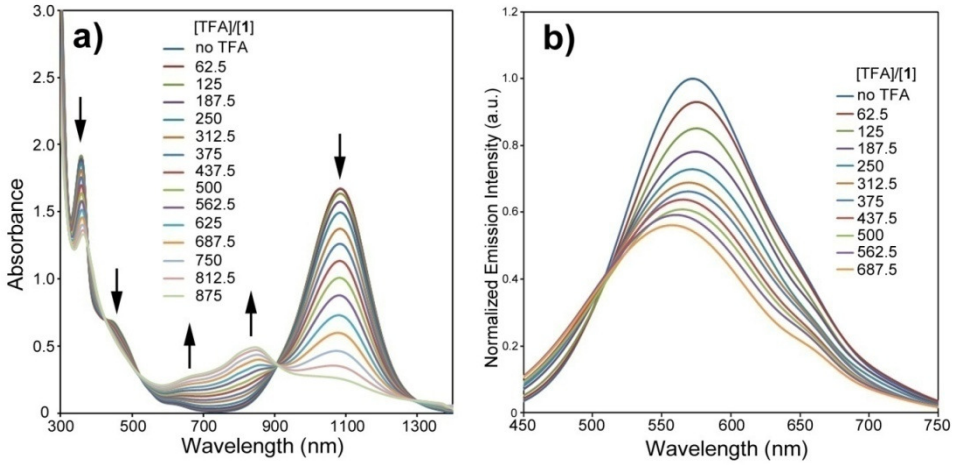

Figure 2.17, (a) Absorption spectra for ***Pt-C1*** in DMF solution (1×10^{-4} M) on variation of TFA concentration. (b) Variation of emission intensity of ***Pt-C1*** in DMF solution on increasing TFA concentration. Excitation wavelength was 420 nm.

In particular, in the absorption spectrum, a decrease of the intensity of the peak at 1085 nm typical of the monoanion, and the appearance of a peak at 854 nm is observed. This latter wavelength is predictable for the neutral species, and the presence of an Isosbestic point connecting the two bands may suggest equilibrium between these two species. However the intensity of the peak at 854 nm is much lower than predictable for the neutral derivative (***Figure 2.12a***). It is unclear whether this peak was relatable to the known neutral complex which may be auto-associated or to a new neutral form resulting from the protonation of the ligand. Apparently the solution seemed clear, but on standing the formation of a solid was observed, and this would tentatively justify the decrease in intensity of the new band at 854 nm and related to the neutral auto-associated $[PtL_2]^0$ that precipitates out of the solution. As far as the visible bands are concerned, the modification of the absorption spectrum upon acid addition (red shift of the visible bands) is fully justified by considering the nature of the electronic

transitions. In fact these excitations require a charge transfer from the central core of the complex towards the peripheral quinoxaline ring (LUMO and LUMO+1), the nitrogen of which is also the preferable protonation site of the complex. In fact, the charge distribution in **Pt-C1**, (see ***Table 2.3*** and ***Figure 2.18b***) obtained by the natural population analysis is also substantiated by the electrostatic potential (EP). As shown in ***Figure 2.18a***, the isodensity surface mapped with the electrostatic potential shows that the nitrogen atoms accumulate greater negative charge followed by the sulfur atoms of dithiolene core. Moreover, there is a moderate negative charge accumulation on the platinum and sulphur atoms of the dithiolenic core.

Thus the first protonation site of ***Pt-C1*** upon acid addition involves N atoms in agreement with quenching of emission experiments by HCl addition. No shift in emission signal is observed and this should be consistent with the dynamic quenching process. Instead using TFA in very strong excess with respect to ***Pt-C1***, both a quenching of luminescence accompanied by a blue-shift and a change in absorption spectra is observed in which both N-protonation and possibly proton transfer to the dithiolenic core may occur.

Noteworthy, no emission is observed by exciting the salt as solid with a wavelength near 440. In conclusion the employed ligand, where thioether groups adjacent to dithiolene core interrupt the π-communication of quinoxaline ring with the dithiolene core, has been shown to be able to favor the 1− as the most accessible status for the complex, while the incorporation of the heteroaromatic group like quinoxaline provides both luminescent properties as well as the

supramolecular architectures through π-π interactions and of H-bonding. It is noteworthy that given the ligand design above described, the observed short π-π contacts in ***Pt-C1***, while seem to be responsible for the loss of luminescence of the solid sample, do not affect its magnetic properties.

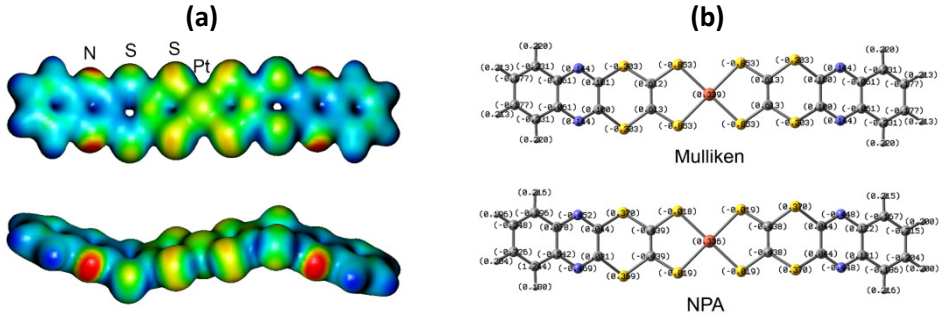

Figure 2.18, (a) Electrostatic potential for $[PtL_2]^-$·mapped on the isodensity surface. Color codes thresholds: red -0.15, yellow -0.1, green -0.05, light blue -0.0, blue 0.2. analysis (b) The charge distribution in ***Pt-C1***, (see Table 3) obtained by the natural population analysis

A similar behaviour was also seen by other complexes for example, ***Pt-C3*** where treatment of DMF solutions radical anionic species was converted into a neutral species on treatment with excess of HCl/TFA (***Figure 2.19a***). In particular, in the absorption spectrum, a decrease of the intensity of the peak at 1170 nm typical of the monoanion, and the appearance of a peak at 1003 nm is observed. This latter wavelength is confirmed for the neutral species on recording the absorbance spectrum of the complex obtained by oxidation with molecular Iodine, the presence of an Isosbestic point connecting the two bands may suggest equilibrium between these two species. However comparatively to the ***Pt-C1*** the intensity of the neutral peak in ***Pt-C2*** is much higher, may suggest auto-association of the neutral derivative.

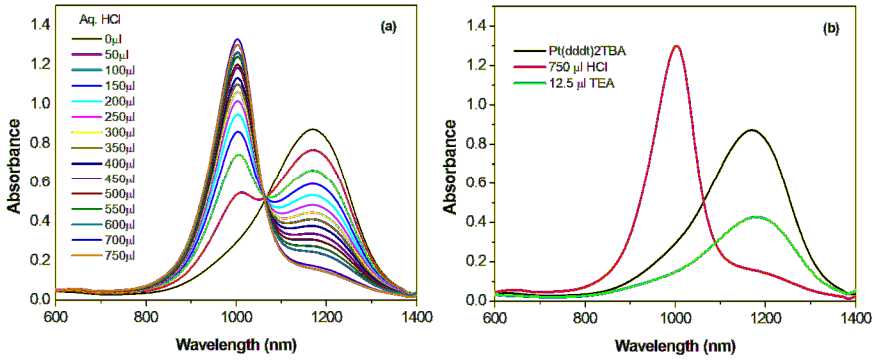

Figure 2.19, (a) Absorption spectra for ***Pt-C2*** in DMF solution (5×10^{-5} M) on variation of Aq.HCl (1×10^{-2} M) concentration. b) Reversible changes in absorption spectra on treatment with Aq. HCl and triethyl amine (TEA)

The possible conversion of $\mathbf{[ML_2]^-}$ to $\mathbf{[ML_2]^0}$ on treatment with excess of acid, the formation of peculiar peak assignable to neutral species required further experimental support. In order to support this redox reaction and identify the reaction products an experiment was performed in air tight scintillation vials where known concentrations of complexes (***M-C1, C2,*** and ***C3***) were treated with known amounts of conc. HCl till the alleged neutral species was formed (precipitation overnight). Hydrogen was detected in the headspace of scintillation vials when analyzed using gas chromatography (***Figure 2.20***). This redox reaction can be represented as shown in (***Scheme 2.3***). With all the complexes the molar ratio of hydrogen generated is higher with respect to complexes. Back reduction of the neutral complex (0 to -1) is possible within the solution making a redox cycle complete with proton reduction. Till date it is confirmed that within the solutions the alleged neutral species in solution can be reduced to -1 either by dilution or by treatment with sacrificial electron donor molecule (***Figure 2.19b***).

However this reaction needs further investigation by treatment with acids in presence of suitable sacrificial electron donating source.

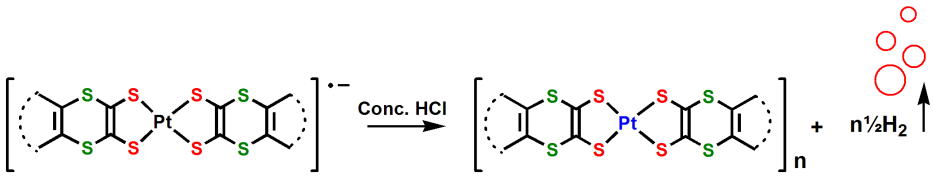

Scheme 2.3, Hydrogen generation using concentrated HCl by redox reaction

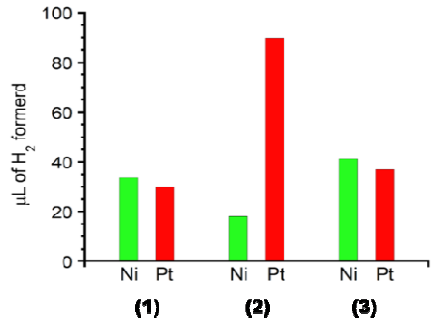

Figure 2.20, Quantity (µl) of Hydrogen generated by GC by solutions of (1) $(Bu_4N)[M(dddt)_2]$ c = 454.5µM in 10mL 10% DMF/ACN (2) $(Bu_4N)[M(dddmedt)_2]$ c = 454.5µM in ACN (3) $[M(quinoxdt)_2](TMEBA)$ c = 454.5µM in ACN

The features of radical anionic complexes (***M-C1, C2*** and ***C3***) mentioned above seemed also promising to further investigate this or similar complexes as photo- and/or electro-catalyst for proton reduction in acidic aqueous solutions.

2.6. Photocatalytic Hydrogen generation (HER)

All light-promoted photocatalytic hydrogen generation reactions begin with absorption of a photon by the photosensitizer (PS) to generate a high energy excited state *PS which can interact with quenchers or catalysts by redox processes. $[Ru(bpy)_3]Cl_2$ is among most studied, commonly used photosensitizer which has MLCT(Metal to Ligand Charge Transfer) absorption maxima at 452 nm. In this process $[Ru(bpy)_3]^{2+}$ absorbs visible light and gets converted to excited state $*[Ru(bpy)_3]^{2+}$, Excited state loses energy by fluorescence (emission) at (603nm) and returns to ground state. This is basic process by which using visible light one can transfer energy absorbed to other molecules through quenching the excited states of $[Ru(bpy)_3]^{2+}$ and in general other PS. Quenching refers to any process that decreases the fluorescence intensity of a given substance. The fluorescence is reduced through a nonradiating process. For a complex to act as a photocatalyst it is necessary that complex is able to quench the excited state of PS by various quenching processes involved such as oxidative, reductive quenching and energy transfer[22] (***Scheme 2.4***).

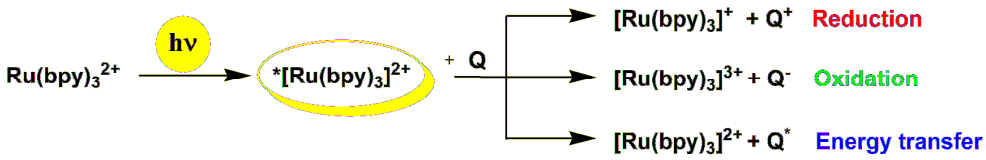

Scheme 2.4, Quenching pathways for excited state of $[Ru(bpy)_3]^{2+}$ where Q represents any quencher.

All the radical anionic complexes (***M-C1, C2*** and ***C3***) were able to quench the excited states of $[Ru(bpy)_3]^{2+}$ following a regular (linear) Stern Volmer behaviour,

an example of photoluminescence quenching of excited state of $[Ru(bpy)_3]^{2+}$ by ***Pt-C1*** is mentioned below (***Figure 2.21a***)

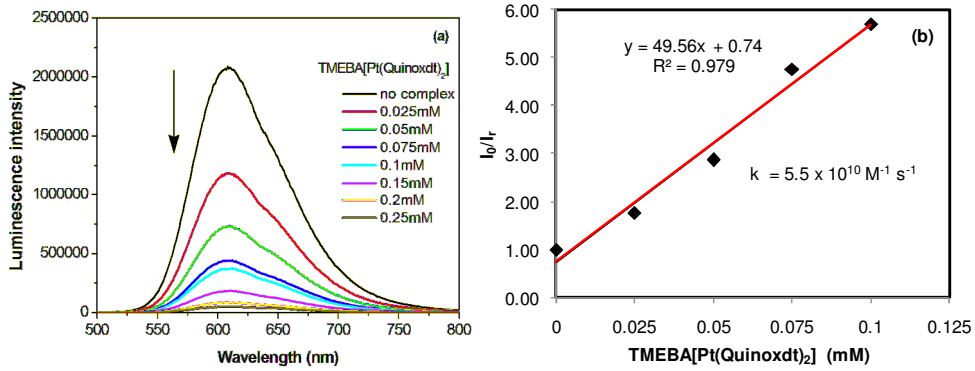

Figure 2.21, (a) Photoluminescence quenching of $Ru(bpy)_3^{2+}$ (10^{-4}M in H_2O) by increasing amount of ***Pt-C1*** complex. (b) Stern volmer plot for photoluminescence quenching.

For the photocatalytic reactions it is very important to remove the dissolved oxygen from the solutions as the excited states of photosensitizer may get quenched by oxygen. Complexes were evaluated for photocatalytic hydrogen generation using $[Ru(bpy)_3]Cl_2$ as a photosensitizer and ascorbic acid as a sacrificial electron donor. For this purpose the samples were degassed, individual solutions of catalyst, PS or AA were freezed under argon and the oxygen was removed from the system using continuous Argon-vacuum freeze-thaw method. The process was repeated 3 times to ensure traces of oxygen are removed from the solution. Further the samples were mixed in 4mL scintillation vial kept in Schlenk flask with sample holder, under positive flow of argon. The scintillation vials were then placed sealed under argon and transferred to the photo reactor.(***Figure 2.22d***) The solutions were irradiated with 520nm LEDs emitting light frequency at which the $[Ru(bpy)_3]^{2+}$ gets excited and the excited state can be

quenched by catalyst or a Ascorbic acid. The hydrogen gas formed in 1ml head space was analyzed by gas chromatography by manually injecting 250µl of gas. The area of negative peak shown by hydrogen is calculated by the Agilent GC software. The method is calibrated in similar concentrations as of hydrogen produced and then quantity of hydrogen evolved is calculated.

M-C1 and ***Ni-C3*** were screened for photocatalytic reactions. All the photocatalysis experiments were performed at Institute of Physical Chemistry, Friedrich Schiller University of Jena in the laboratory of Prof. Benjamin Dietzek and Dr. Martin Schulz under COST 1202 Short term scientific mission (STSM) programme. Except ***Ni-C3***, other complexes (***M-C1***) did not show any hydrogen evolution even after investigating in a variety of conditions. A lot of effort was employed to find right operating conditions at which maximum TONs of hydrogen is obtained. Experiments were performed by variation of concentrations or ratio of PS/Donor/catalyst to obtain highest area of negative peak shown by hydrogen evolution detected by gas chromatography. Among the different conditions employed, salient results are mentioned (***Figure 2.22a, b*** and ***c***). The pH of AA as well as the concentration plays an important role in quantity of hydrogen generation, earlier methods reported for dithiolene metal catalysts utilized an optimum pH value of 4.3, but the title ***Ni-C2*** works well with pH = 1.8. The conditions in which maximum hydrogen generation observed was selected for large scale experiment on a 40mL scale photoreactor (***Figure 2.23b***). TONs of hydrogen evolved was improved from 11 to 29 on switching from small scale (3mL) to large scale HER reaction (40ml) (***Figure 2.23a***). The turnover frequency

(TOF) for HER is very low but the stability of the catalytic system is high as the HER is observed even after a 5-6 days of irradiation.

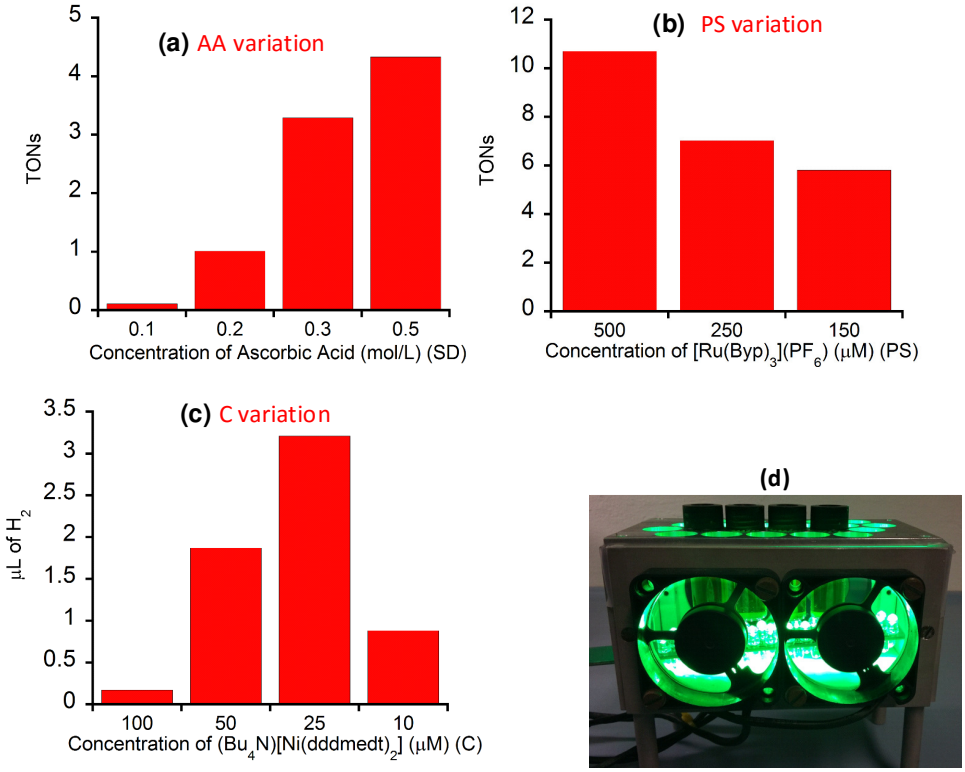

Figure 2.22, Photocatalytic hydrogen generation (PCHG) for ***Ni-C3*** in different conditions (a) $Ru(bpy)_3Cl_2$ = 500μM in 40% ACN in MeOH - C = 25 μM in ACN (b) A.A. = 0.5M - C = 50 μM in ACN (c) $Ru(bpy)_3Cl_2$ = 500μM in AC, A.A. = Aq. 0.1M pH = 4.3 (d) Small scale (3ml) photoreactor with 4ml scintillation reaction vials

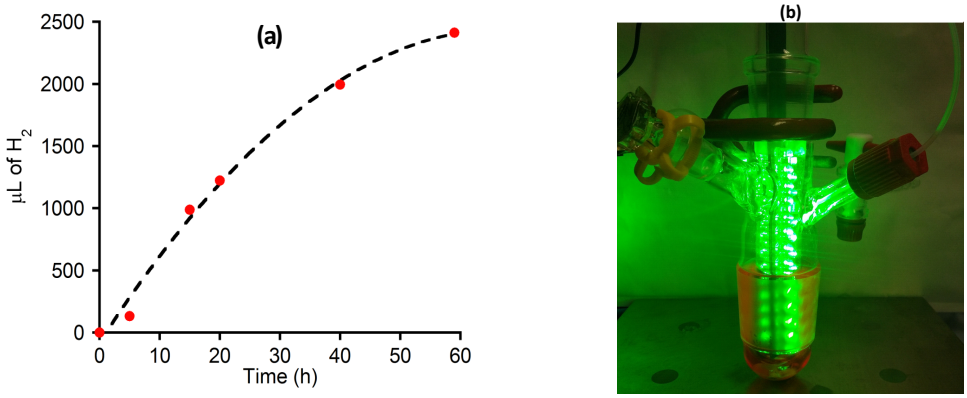

Figure 2.23, (a) Time dependent measurements (HER) for Ni-C3 C = 50 µM in ACN, $Ru(bpy)_3Cl_2$ = 500µM, A.A. = Aq. 0.5M pH = 1.8 (b) large scale (40mL) photoreactor. (image is without outer cooling water jacket-condenser)

2.7. Experimental

2.7.1. Synthetic procedures and analytical measurements

2.7.1.1. [(R)-Ph(Me)HC*-NMe_3][M(quinoxdt)$_2$]·DMF (*M-C1*).

48 mg (2.08 mmol) of Na in 60 mL of MeOH were added drop-wise to a stirred suspension of the ligand precursor (292 mg, 0.95 mmol) in the same solvent (50 mL). The mixture was stirred for 15 min at room temperature and the solution turned from yellow to dark brown. To this solution, $[Pt(DMSO)_2Cl_2]$ (200 mg, 0.47 mmol)/$NiCl_2.6H_2O$ dissolved in chloroform/Methanol (120 mL) was added drop wise. The reaction mixture was then refluxed for 180 min under argon atmosphere, cooled under air, filtered, and the solvent evaporated to a 1/4th of the initial volume. By addition of [(R)-Ph(Me)HC*-NMe_3]I (275 mg, 0.95 mmol) the precipitation of a brown solid was obtained. After 60 min of stirring, this crude

precipitate was collected by centrifugation and washed with diethyl ether (three times) and dried. Dark brown crystals (325 mg, 0.33 mmol; yield 79.0%) were obtained by recrystallization in DMF/diethyl ether. Analytical results are in accordance with the formula

[(R)-Ph(Me)HC*-NMe$_3$][Pt(quinoxdt)$_2$]·DMF (***Pt-C1***) Elemental Analysis: calculated for $C_{34}H_{33}N_6OPtS_8$ (993.23): C 41.11, H 3.35, N 8.46, S 25.83; found: C 41.3, H 3.5, N 8.5, S 25.2. UV-vis (in DMF solution): λ/nm (ε/molcm^{-1}dm^{-3}) 354 (2.04×10^4); 455 (7.01×10^3); 635sh (0.66×10^3); 1085 (1.89×·10^4). FT–IR (KBr): ν_{max}/cm^{-1} 3056 (vw); 3034 (vw); 1554 (w); 1479(w); 1455 (m); 1388 (vs); 1332 (m); 1255(vs); 1177 (vs); 1112 (vs); 954 (w); 866 (w); 841 (w); 759 (m); 708 (m); 598 (m); 465 (vw).

[(R)-Ph(Me)HC*-NMe$_3$][Ni(quinoxdt)$_2$]·DMF. (*Ni-C1*)

Elemental Analysis: calculated for $C_{34}H_{33}N_6NiOS_8$ (856.85): C 47.66, H 3.88, N 9.81, S 29.94 found: C 47.8, H 3.76, N 9.88, S 29.95 UV-vis (in DMF solution): λ/nm (ε/molcm^{-1}dm^{-3}) 318 (3.77×10^4); 461sh (6.77×10^3); 588 sh (1.2×10^3); 1087 (1.09× 10^4). FT–IR (KBr): ν_{max}/cm^{-1} 3059 (vw); 3032 (vw); 2921 (w); 1505(w); 1450 (m); 1383 (vs); 1252(s); 1174 (s); 1110 (s); 827 (m); 753 (m); 705 (w); 595 (m); 465 (vw).

2.7.1.2. Bu$_4$N[M(dddt)$_2$] (*M-C2*)

These complexes were prepared using literature already published.[23]

2.7.1.3. $Bu_4N[M(dddmedt)_2]$ (*M-C3*)

To a stirred solution of dimethyl 2-oxo[1,3]dithiolo[4,5-*b*][1,4]dithiine-5,6-dicarboxylate (0.15 g, 0.46 mmol) in 20 mL of Methanol was added drop wise a solution of sodium (23.5 mg, 1.02 mmol) in 10mL methanol and stirred for 30min. The reaction mixture was then diluted with 50mL Chloroform. A solution of $Pt(dmso)_2Cl_2$ (98 mg, 0.23 mmol) in 30mL $CHCl_3$ / $NiCl_2.6H_2O$ (55 mg, 0.23 mmol) in 20mL Methanol was added in small portions and then refluxed for overnight. The dark brown reaction mixture was concentrated to 1/4th volume and a solution, filtered through cotton plug and a solution of tetrabutyl ammonium bromide (0.3 g, 0.93 mmol) in 5mL Methanol was added. Brown colour precipitate formed was isolated by centrifuging and washing 20 ml X 3 times with diethyl ether to give ***M-C3*** as reddish-brown powders in quantitative yields.

$Bu_4N[Pt(dddmedt)_2]$ (***Pt-C3***) Elemental Analysis: calculated for $C_{32}H_{48}NO_8PtS_8$ (1026.32): C 37.45, H 4.71, N 1.36, S 24.99 found: C 37.49, H 4.76, N 1.34, S 25.01. UV-vis (in DMF solution): λ/nm (ε/molcm^{-1}dm^{-3}) 491sh (1.4 x 10^3); 1071 (9.65 x 10^3). FT–IR (KBr): ν_{max}/cm^{-1} 2957 (m); 2872 (w); 1723 (s); 1569(m); 1479 (w); 1433 (m); 1389 (s); 1246(vs); 1073 (w); 1012 (m); 871 (w); 753 (w); 685 (vw); 454 (vw).

$Bu_4N[Ni(dddmedt)_2]$ (***Ni-C3***) Elemental Analysis: calculated for $C_{32}H_{48}NNiO_8S_8$ (889.94): C 43.19, H 5.44, N 1.57, S 28.82, found: C 43.23, H 5.49, N 1.58, S 28.89, UV-vis (in DMF solution): λ/nm (ε/molcm^{-1}dm^{-3}) 542sh (1.11 x 10^3); 1062 (7.85×·10^3). FT–IR (KBr): ν_{max}/cm^{-1} 2957 (m); 2870 (w); 1720 (s); 1570(m); 1479 (w); 1434 (m); 1399 (s); 1248(vs); 1072 (w); 1006 (m); 879 (w); 752 (w); 681 (vw); 450 (vw).

2.7.2. Photophysical parameters evaluation

2.7.2.1. Quantum yield

Emission quantum yield was evaluated using the relative method8 though the following equation

$$\Phi = \Phi_R \frac{a_R}{a} \frac{I}{I_R} \frac{n^2}{n_R^2}$$

where the R index refers to the photoluminescence standard. Φ R= reference quantum yield; $a_R=1-10^{-AR}$, absorption factor of the reference at excitation wavelength; $a=1-10^{-A}$, absorption factor of the sample at excitation wavelength; AR=absorbance of the reference at excitation wavelength; A=absorbance of the sample at excitation wavelength; I=sample integrated emission; IR=reference integrated emission; n = refractive index of the medium.

2.7.2.2. Estimated emission lifetime

The emission lifetime ($\tau_{obs} = 1/\kappa_{obs}$) of ***Pt-C1*** was roughly estimated through the equation:

$$\Phi = \frac{\kappa_{rad}}{\kappa_{obs}}$$

Where κ_{rad} is the rate constant for spontaneous emission, which in turn was estimated through the Strickler-Berg equation23[24]

$$\kappa_{\mathrm{rad}} = \tau_{\mathrm{rad}}^{-1} = 8\pi n^2 c \frac{1}{\langle \lambda^3 \rangle} \frac{g}{g'} \int \frac{\sigma(\lambda)}{\lambda} d\lambda$$

Where *n* is the refractive index of the medium (1.43 for DMF), *c* is the speed of light in vacuum and *g, g'* refer to the degeneration of the ground and excited state respectively. $\langle\lambda^3\rangle$refers to the mean value of emission wavelength. σ(λ) is the absorption cross-section of ***Pt-C1***, which was estimated through the excitation spectrum normalized to absorption. The estimated value of emission lifetime is 45 ps.

2.7.2.3. Proton quenching

The emission quenching of ***Pt-C1*** upon proton addition was evaluated through the following equation:

$$\frac{I_0}{I_r} = 1 + K[\mathbf{H}^+]$$

where I_0, I_r represent the emission intensity in the absence and in the presence of the quencher (H+), respectively, while K is the constant of the quenching process.

2.7.3. Hydrogen Evolution Studies.

In all the experiments $(PF_6)_2[Ru(bpy)_3]$, Ascorbic acid and ***M-C1,C2*** or ***Ni-C3*** were used as Photosensitizer (PS), Sacrificial electron donor (SED) and catalyst (Cat.) respectively.

2.7.3.1. Small scale experiments:

Stock solutions of PS, 1mM in CH_3CN; SED, 1.2M in water pH ~1.8, (specific pH can be adjusted at this stage by adding Aq.NaOH measuring with a pH meter); catalysts, Cat. 0.5 mM solution in CH_3CN; were prepared in volumetric flask and then transferred in schlenk flask. All the solutions were degassed using freez-thaw

(liquid Nitrogen) method under argon atmosphere. A varying amount of PS, SED, and Cat. Were added to 4mL scintillation vial (kept under positive flow of argon) to obtain a total volume of 3 mL and desired concentrations. The sample vial was then capped under argon and were irradiated from below with green (520 nm) LEDs light arrays in small scale photocatalysis reactor fitted with cooling fans (***Figure 2.22d***). After 20 h photolysis time, the amount of hydrogen produced was measured by gas chromatography using gas tight syringe (250μl) from the headspace of the vials.

2.7.3.2. Large scale experiment:

After degassing the solutions, varying amount of PS, SED, and Cat. (above mentioned concentrations) were added to make up total volume of 40 mL and desired concentrations/ratios of each component in 4 neck photocatalytisis reactor (***Figure 2.23b***) having a total volume of 85mL. The hydrogen evolved was measured either directly using GC through helium carrier gas bubbeled in solution or by taking headspace aliquots of fully packed system and measuring with CP-3800 Gas Chromatograph equipped with a 5 Å molecular sieves column and polymer supported silica column purchased from Varian Inc. (UK) using ultra-high purity helium as the carrier gas. The signals were amplified with a Varian Star Workstation Chromatography Data system.

2.7.3.3. TON calculations

To calculate the number of moles of H_2 produced the ideal gas law is applied (PV= nRT):

$$TON = \frac{No.\,of\ moles\ of\ hydrogen\ produced}{number\ of\ moles\ of\ catalyst\ used}$$

The system method was calibrated for hydrogen signal sensitivity by hydrogen standard measurements (within in the range of negative peak maximum GC area of hydrogen displayed by the catalyst). The total amount of hydrogen produced in a photolysis experiment was obtained by the sum of hydrogen found in the gas phase (hydrogen found in the solution phase was assumed to be negligible).

2.8. References:

1. (a) Paola deplano, M. Laura Mercuri, Angela Serpe and Luca Pilia, chapter 16, The chemistry of metal Enolates part 2, 879-925 (Patai series Editor: Jacob Zabicky) (b) Hu, L., Qin, J., Zhou, N., Meng, Y., Xu, Y., Zuo, J., & You, X. (2012). Synthesis, characterization, and optical properties of new metal complexes with the multi-sulfur 1,2-dithiolene ligand. *Dyes and Pigments, 92*(3), 1223-1230.

2. Ray, K., Weyhermüller, T., Neese, F., & Wieghardt, K. (2005). Electronic Structure of Square Planar Bis(benzene-1,2-dithiolato)metal Complexes $[M(L)_2]$ z (z = 2−, 1−, 0; M = Ni, Pd, Pt, Cu, Au): An Experimental, Density Functional, and Correlated ab Initio Study. *Inorganic Chemistry, 44*(15), 5345-5360.

3. Begum, A., Moula, G., & Sarkar, S. (2010). A Nickel(II)-Sulfur-Based Radical-Ligand Complex as a Functional Model of Hydrogenase. *Chemistry - A European Journal, 16*(41), 12324-12327.

4. Ray, K., DeBeer George, S., Solomon, E. I., Wieghardt, K., & Neese, F. (2007). Description of the Ground-State Covalencies of the Bis(dithiolato) Transition-Metal Complexes from X-ray Absorption Spectroscopy and Time-Dependent Density-Functional Calculations. *Chemistry - A European Journal, 13*(10), 2783-2797.

5. Sproules, S., & Wieghardt, K. (2011). Dithiolene radicals: Sulfur K-edge X-ray absorption spectroscopy and Harry's intuition. *Coordination Chemistry Reviews, 255*(7-8), 837-860.

6. Szilagyi, R. K., Lim, B. S., Glaser, T., Holm, R. H., Hedman, B., Hodgson, K. O., & Solomon, E. I. (2003). Description of the Ground State Wave Functions of Ni Dithiolenes Using Sulfur K-edge X-ray Absorption Spectroscopy. J. Am. Chem. Soc, 125(30), 9158-9169.

7. Sarangi, R., DeBeer George, S., Rudd, D. J., Szilagyi, R. K., Ribas, X., Rovira, C., … Solomon, E. I. (2007). Sulfur K-Edge X-ray Absorption Spectroscopy as a Probe of Ligand−Metal Bond Covalency: Metal vs Ligand Oxidation in Copper and Nickel Dithiolene Complexes. *J. Am. Chem. Soc, 129*(8), 2316-2326.

8. Bruno, G., Almeida, M., Artizzu, F., Dias, J. C., Mercuri, M. L., Pilia, L., … Deplano, P. (2010). Innocence and noninnocence of the ligands in bis(pyrazine-2,3-dithiolate and -diselonate) d8-metal complexes. A theoretical and experimental study for the Cu(iii), Au(iii) and Ni(ii) cases. *Dalton Transactions, 39*(19), 4566.

9. Bachler, V., Olbrich, G., Neese, F., & Wieghardt, K. (2002). Theoretical Evidence for the Singlet Diradical Character of Square Planar Nickel Complexes Containing Two o -Semiquinonato Type Ligands. *Inorganic Chemistry, 41*(16), 4179-4193.

10. (a) A. H. Morrish, *The Physical Principles of Magnetism*; IEEE Press: New York, 2001; p. 31. (b) O. Kahn, *Molecular Magnetism*; VCH Publishers: Cambridge, 1993; p. 9.

11. Unsymmetrical Nickel-Dithiolene Complexes Useful as Near-IR Dyes and Precursors of Sulfur-Rich Donors. *Comments on Inorganic Chemistry, 22*(6), 353-374.

12. Suzuki, K., Kobayashi, A., Kaneko, S., Takehira, K., Yoshihara, T., Ishida, H., … Tobita, S. (2009). Reevaluation of absolute luminescence quantum yields of standard solutions using a spectrometer with an integrating sphere and a back-thinned CCD detector. *Phys. Chem. Chem. Phys, 11*(42), 9850.

13. Itoh, T. (2012). Fluorescence and Phosphorescence from Higher Excited States of Organic Molecules. *Chemical Reviews, 112*(8), 4541-4568.

14. (a) Kaiwar, S. P., Vodacek, A., Blough, N. V., & Pilato, R. S. (1997). Excited State Properties of Quinoxaline-Substituted Platinum 1,2-Enedithiolates. *J. Am. Chem. Soc, 119*(14), 3311-3316. (b) Kelly A. Van Houten, Keith A. Walters, Kirk S. Schanze, Robert S. Pilato. (2000). Study of the Heterocyclic-Substituted Platinum-1,2-Enedithiolate 3ILCT Excited States by Transient Absorption Spectroscopy. *Journal of Fluorescence, 10*(1), 35-40.

15. Recatalá, D., Gushchin, A. L., Llusar, R., Galindo, F., Brylev, K. A., Ryzhikov, M. R., & Kitamura, N. (2013). Dithiolene dimetallic molybdenum(v) complexes displaying intraligand charge transfer (ILCT) emission. *Dalton Transactions, 42*(36), 12947.

16. Cummings, S. D., & Eisenberg, R. (1995). Acid-Base Behavior of the Ground and Excited States of Platinum(II) Complexes of Quinoxaline-2,3-dithiolate. *Inorganic Chemistry, 34*(13), 3396-3403.

17. Bolligarla, R., Kishore, R., Durgaprasad, G., & Das, S. K. (2010). Acid–base behavior of a simple metal bis(dithiolate) system: Synthesis, crystal structure and spectroscopy of [Bu4N]2[MII(ppdt)2] (M=Ni, Pt;

ppdt=pyrido[2,3-b]pyrazine-2,3-dithiolate). *Inorganica Chimica Acta, 363*(12), 3061-3069.

18. Frei, F., Rondi, A., Espa, D., Mercuri, M. L., Pilia, L., Serpe, A., … Cannizzo, A. (2014). Ultrafast electronic and vibrational relaxations in mixed-ligand dithione–dithiolato Ni, Pd, and Pt complexes. *Dalton Trans, 43*(47), 17666-17676.

19. *Photochemistry of Organic Compounds: From Concepts to Practice*. Klán, P. and Wirz, J. Wiley-Blackwell, 2009. p.40. ISBN 1-4051-6173-6.

20. Li, X., Sun, Y., Huo, P., Shao, M., Ji, S., Zhu, Q., & Dai, J. (2013). Metal centered oxidation or ligand centered oxidation of metal dithiolene? Spectral, electrochemical and structural studies on a nickel-4-pyridine-1,2-dithiolate system. *Phys. Chem. Chem. Phys, 15*(11), 4016.

21. Lazzaro, D. P., McGuire, R., & McMillin, D. R. (2011). Regiospecific Quenching of a Photoexcited Platinum(II) Complex at Acidic and Basic Sites. *Inorganic Chemistry, 50*(10), 4437-4444.

22. Tucker, J. W., & Stephenson, C. R. (2012). Shining Light on Photoredox Catalysis: Theory and Synthetic Applications. *The Journal of Organic Chemistry, 77*(4), 1617-1622.

23. Schultz, A. J., Wang, H. H., Soderholm, L. C., Sifter, T. L., Williams, J. M., Bechgaard, K., & Whangbo, M. H. (1987). Crystal structures of bis(5,6-dihydro-1,4-dithiin-2,3-dithiolato)gold and tetrabutylammonium bis(5,6-dihydro-1,4-dithiin-2,3-dithiolato)nickelate(1-) and the ligandlike character of the isoelectronic radicals $[Au(DDDT)_2]0$ and $[Ni(DDDT)_2]^-$. *Inorganic Chemistry, 26*(22), 3757-3761.

24. Strickler, S. J., & Berg, R. A. (1962). Relationship between Absorption Intensity and Fluorescence Lifetime of Molecules. *The Journal of Chemical Physics, 37*(4), 814.

Chapter 3
Synthesis, characterization and properties of heteroleptic complexes $[ML_1L_2]^n$, n = 0, -1 M=Ni(II), Pd(II) and Pt (II), L_1=dithioxamide L_2=dithiolate

3.1. Introduction

Square planar heteroleptic dithiolene d^8 metal complexes where the ligand, depending on the relative electron-withdrawing capability of the ligands, occurs in formally different oxidation states (dithione-dithiolato) act as intervalence compounds[1-6] (as described in Chapter 1). The dithiolate ligand acts as donor, the dithione as acceptor and the metal provides a π-bridge between them through d-orbitals involved in coordination .[1,3] A typical complex consists of Ni, Pt, or Pd bonded to N,N-substituted piperazine-dithione on one side and different 1, 2-dithiolato ligands on the other. These complexes exhibit a typical solvatochromic absorption peak in the visible region, relatable to a HOMO–LUMO transition, where the HOMO is formed by a mixture of metal and dithiolate orbitals while the dithione orbitals give a predominant contribution to the LUMO (MMLL'CT= mixed metal ligand to ligand' charge transfer). They behave as second order non-linear chromophores showing remarkably high negative molecular first hyperpolarizability. Variation of metal, the donor and the acceptor permit a tuning of second order nonlinear optical (SO-NLO) properties.

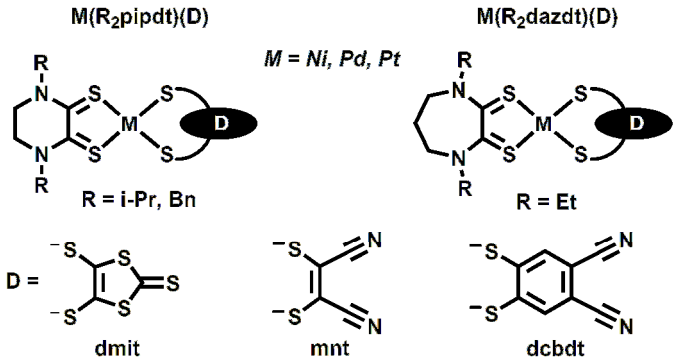

Figure3.1, General Structure of dithione-M-dithiolato complexes reported

This class of complexes has already been investigated on systematic variation of the metal, the acceptor the donor ligands to highlight their role in tuning SO-NLO properties.[1,3,5](An insight into SO-NLO phenomenon is given in the *appendix 1* of the thesis)Ni(II), Pd(II) and Pt(II) metals, dithiolate anions bearing groups with moderate to strong electron withdrawing capability (dmit, mnt, dcbdt, etc…)as donors and dithio-oxamide functionality embedded in a heterocyclic moiety as hexaatomic (R_2pipdt) or hepta-atomic (R_2dazdt) ring as acceptors were investigated to highlight their role in affecting the second-order NLO properties.(***Figure 3.1***) In general among the triads the largest SO-NLO activity was displayed by Pt derivatives followed by Pd and then Ni. Complexes containing dmit as donor ligand showed highest $\mu\beta_0$ values. (***Figure 3.2***)

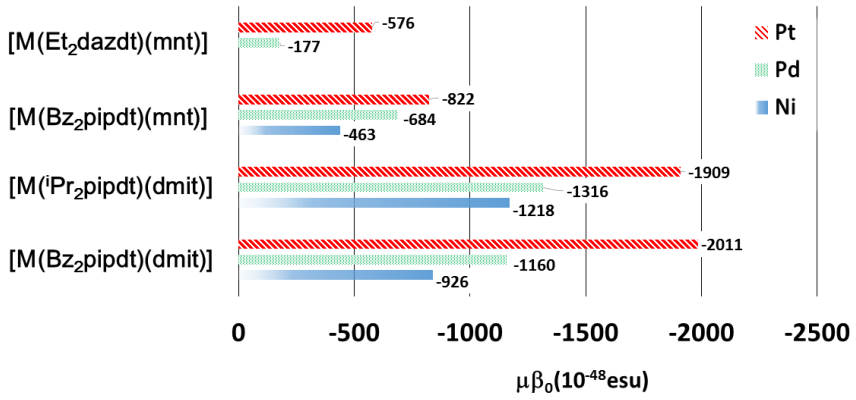

Figure3.2, Nonlinear optical data of [M(Bz2pipdt)(dmit)], [M(iPr2pipdt)(dmit)], [M(Bz2pipdt)(mnt)]and [M(Bz2dazdt)(mnt)] triad.

It was observed by computational methods that the role of the metal is important for the delocalization of the frontier orbitals. In particular the observed higher NLO activity of the platinum compounds among the triads is relatable to: i) the

most extensive mixture of the dithione/metal/dithiolato orbitals in the frontier orbitals (FOs); ii) the influence of the electric field of the solvent on the FOs that maximizes the difference in dipole moments between excited and ground state; and iii) the largest oscillator strength of the CT transition. Theoretical calculations provide further insight in understanding the properties of complexes. It was found that HOMO-LUMO gap increases with electron withdrawing capability of the dithiolate ligand and is affected by the nature of the solvent. On decreasing the polarity of the solvent, the HOMO-LUMO gap decreases with a consequent bathochromic shift of the related absorption, as predictable for a system where the ground state has higher dipolar moment than the excited one. This effect is called negative solvatochromism. This phenomenon has become a benchmark characteristic for the complex to show NLO activity in solution.

Regarding the role of the acceptor ligand, minor variations to the NLO properties were observed on changing the substituents at the N-atoms of pipdt ring. Instead, planarity of the dithione functionality plays an important role in determining the $\mu\beta_0$ response. It was proved by combined theoretical and experimental studies that lower the torsion angles (***δ1*** and ***δ2***) higher the π-delocalization and the first molecular hyperpolarizability of d^8 metal dithione-dithiolato complexes.

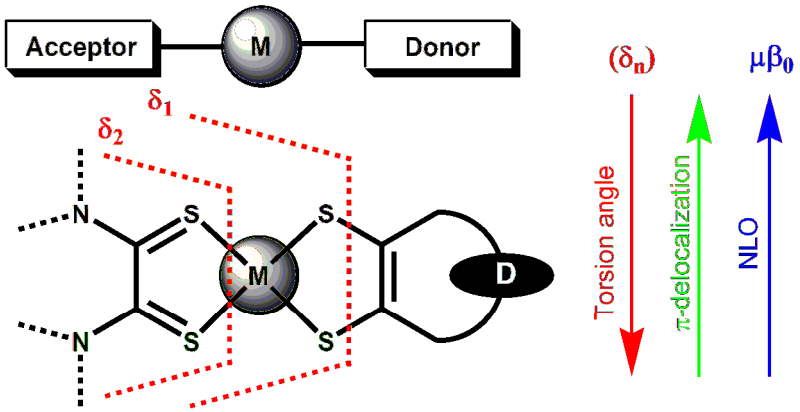

Figure 3.3, The torsion angle (*δ1 & δ2* red dots) of the dithione system inversely correlates with the oscillator strengths of the main transition of the complexes or with their beta values.

All these complexes are redox active and exhibit two reversible (or quasi-reversible) reduction waves, relatable to the acceptor ligand, and one irreversible anodic peak, relatable to the acceptor. Electrochemical properties, structural and spectroscopic data support a dithione–dithiolate description for these complexes which exhibit large negative second-order polarizabilities, amongst the highest so far reported for metal complexes. Moreover they exhibit spectroelectrochemical behavior which makes these complexes promising candidates to be investigated for redox switching of molecular first hyperpolarizabilities.

However in the bulk, the second order NLO properties are lost since these complexes crystallized in a centrosymmetric crystal system.[4] In fact to be suitable for SHG (second harmonic generation) in the bulk, non centro-symmetric crystals are required. Given the dipolar nature of the molecules, a centrosymmetric head-to-tail arrangement is the predictable one, and most often obtained. Obtaining a non-centrosymmetric arrangement of molecules is a difficult task, and even more

difficult is to get a non-centrosymmetric polar structure with specific space groups. (***Table 3.1***) A polar structure (point group) is that in which there is at least one macroscopic direction (polar axis) which is not changed in the opposite direction by symmetry transformations allowed for the material. With this reference to crystal, out of the 32 classes only 20 correspond to noncentrosymmetric crystals as shown in ***table 3.1***, which gets reduced to 11 that correspond to polar crystals, which are of particular relevance for SO-NLO. It has been shown that the highest SO-susceptibility coefficients (macroscopic nonlinearity), for a given chromophore (microscopic nonlinearity), can be reached in the (polar) crystal classes 1, 2, m and mm2 while other polar crystal classes are less favourable.[7-9]

Table 3.1, polar noncentrosymmetric point groups

Crystal system	**Polar noncentrosymmetric**	**Nonpolar noncentrosymmetric**
Triclinic	1	-
Monoclinic	2, m	-
Orthorhombic	mm2	222
Trigonal	3, 3m	32
Hexagonal	6, 6mm	6, 6m2
Tetragonal	4, 4mm	4, 422, 42m
cubic	4, 4mm	23, 43m, 432

With the view to obtain crystals with non-centrosymmetric crystal packing, hopefully in most favourable point groups (***Table 3***), the introduction of a chiral group in one of the ligands (donor or acceptor) seemed a promising strategy.[6] Accordingly, my efforts were addressed to obtain crystals of chiral dithione-

dithiolato metal complexes crystallizing in a polar noncentrosymmetric space groups.

In addition, the employed ligands have been selected with additional functionality suitable to allow a tuning of properties through redox or proton switching. Optical switching at molecular level has attracted a great attention of researchers due to their scope and importance in modern technological applications.[10-17]

3.2. Results and Discussion

3.2.1. Design and synthesis

As said in the Introduction, the strategy employed to try to obtain non-centrosymmetrical crystals in heteroleptic dithiolene d^8 metal complexes was to introduce chirality within the system. In principle, inclusion of chirality either on the dithione or on the dithiolate functionality appeared convenient strategy. However, in order to preserve the electronic features responsible of the optimal molecular NLO properties, it seemed advisable to introduce the chiral group in the periphery of the molecule, to avoid affecting the nature of the frontier orbitals, responsible of the charge transfer transition. The introduction of a chiral group as substituent at the N-atom of dithio-oxamide ligand, away from the coordination core seemed the best way to achieve the objective. Also chiral carbon in the periphery of 1, 4-piperazinyl-2,3-dithione (ex. ***A2***) can provide suitable candidates, but this synthesis is more challenging. (Using chiral enantiomerically pure ***A2,*** the Nickel complex ***C15*** coordinated to *dmit* as donor ligand, has been prepared and is included in the ***appendix 2***).

In order to obtain proton switchable 2nd order NLO materials, N^1-N^2-disubstituted dithioxamide ligands, which have shown to undergo interesting protonation equilibria, have been employed.[18-22]

Dithione-metal-dithiolato complexes, having strong π-polarization (D-π-A), proton switchable properties and crystallizing in noncentrosymmetric space group, were obtained by synthesizing complexes using enantiopure N^1-N^2-disubstituted chiral dithioxamide ligand (***A1***).

A neat reaction between solid Rubeanic acid and liquid (R)-(+)-α-Methyl benzyl amine ((R)-α-MBA) in 2:1 molar ratio produced the (R)-α-MBAdto (***A1***) ligand in good yield. Purification was carried out by column chromatography on neutral alumina followed by recrystallization in concentrated dichloromethane solutions. Intermediate [M(R)-α-MBAdt)(DMSO)Cl] was obtained by reacting ***A1*** with $M(DMSO)_2Cl_2$ where M = Pt and Pd. For Ni complexes, the reaction was carried out without isolation of the intermediate. (***Scheme 3.1***) For platinum the intermediate was obtained in good yields mostly as red powder, and as orange powder for palladium. In the second step, the 1,2-dithiolate (***D***) solution, obtained by deprotection of different ligand precursors by sodium methoxide in methanol, was reacted with chloroform solutions of intermediate Pt, Pd complex at room temperatures. Nickel complex was prepared in one pot reaction, and equimolar quantity of dithiolate solution was added to a stirred equimolar mixture of ***A1*** and $NiCl_2.6H_2O$ in a 20% methanol/chloroform mixture as solvent. Finally on treatment of all the reaction mixtures with tetrabutyl ammonium bromide and purification by crystallization in Acetonitrile/ diethyl ether or ethanol, pure complexes were obtained.

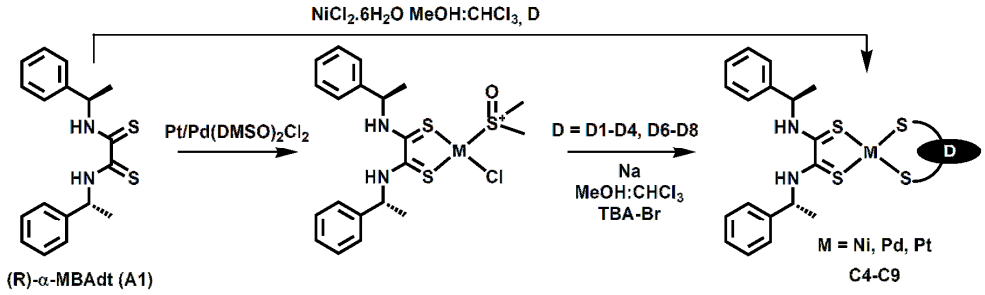

Scheme 3.1, Synthesis of chiral Heteroleptic metal dithiolenes

3.2.2. XRD studies

3.2.2.1. Crystal Structure

Crystal structures of triads **(*M-C4*)**, M = Ni, Pd and Pt, are selected for explaining the properties.(***Figure 3.4***) Well shaped crystals, suitable for X-ray crystallographic investigation, of ***Ni-C4*** complex is formed in methanol solution by slow evaporation where as ***Pd-C4*** and ***Pt-C4*** complexes were grown by diffusion method from an Acetonitrile/ether solution. Due to the enantiomerically pure (R)-α-MBAdto (***A1***) starting ligand, all the three complexes crystallize in orthorhombic system with Sohncke space groups (chiral) lacking centre of symmetry. The ***Ni-C4*** complex crystallizes in ($C222_1$) space group while ***Pd-C4*** and ***Pt-C4***complexes have same space group ($P2_12_12_1$). Crystal structures of this series of heteroleptic complexes obtained have noncentrosymmetric space groups some of which are also displayed in the ***appendix 2.***

A summary of data collection and structure refinement for triads ***M-C4*** complexes is reported in ***Table 3.2.***

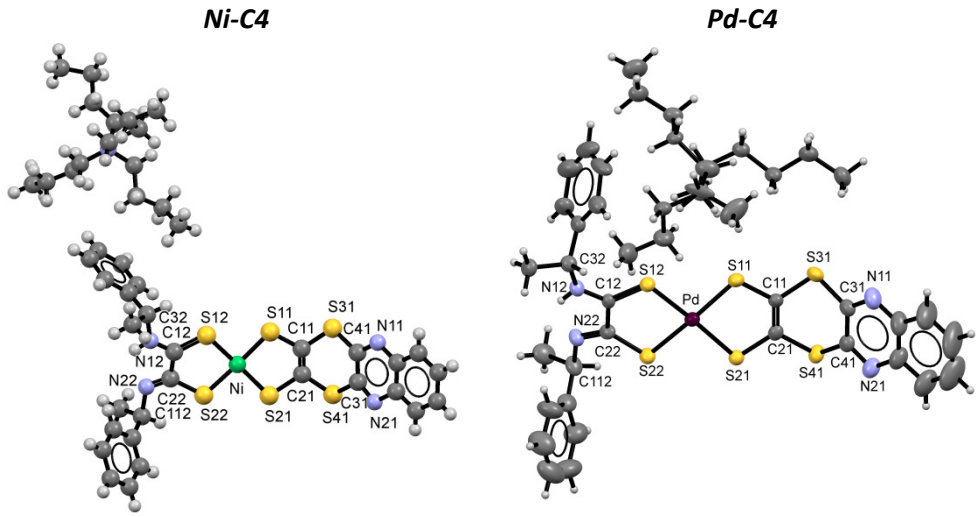

Figure 3.4, Molecular structure of ***Ni-C4***and ***Pd-C4*** with thermal ellipsoids drawn at the 40% probability level.

Table 3.2 Summary of X-ray crystallographic data for ***M-C4*** triad

	Ni	**Pd**	**Pt**
Empirical formula	C_{44} H_{59} N_5 Ni S_6	C_{44} H_{59} N_5 Pd S_6	C_{44} H_{59} N_5 Pt S_6
Formula weight	909.03	956.72	1045.41
Colour, habit	Dark purple, radiating	Apple red flakes	Dark Green
Crystal size, mm	0.200 x 0.030 x 0.020	0.41 x 0.22 x 0.03	0.21 x 0.08 x 0.02
Crystal system	Orthorhombic	Orthorhombic	Orthorhombic
Space group	C 2 22_1	$P2_12_12_1$	$P2_12_12_1$
a, Å	8.799(6)	9.165(2)	9.165(2)
b, Å	25.04(2)	18.253(3)	18.211(3)
c, Å	46.07(3)	29.053(4)	29.093(5)
α, deg.	90	90	90
β, deg.	90	90	90
γ, deg.	90	90	90
V, Å3	10150(13)	4860.2(15)	4855.7(16)

Z	8	4	4
T, K	293(2)	293(2)	293(2)
ρ (calc), Mg/m3	1.190	1.307	1.430
μ, mm−1	0.662	0.674	3.182
θ range, deg.	1.626 to 15.497	1.40 to 24.95	1.32 to 24.77
No.of rflcn/obsv	16745 / 2253	52201 / 8469	51410 / 8260
GooF	1.054	1.007	1.008
R1	0.0891	0.0575	0.0493
wR2	0.1994	0.1001	0.0756

R1 = Σ||Fo|-|Fc||/Σ|Fo|, wR2 = [Σ[w(Fo2-Fc2)2]/Σ[w(Fo2)2]]½ , w = 1/[σ2(Fo2) + (aP)2 + bP], where P = [max(Fo2,0) + 2Fc2]/3

The crystal structure of ***M-C4*** complexes consists in a square planar arrangement where the metal is coordinated by four sulfur atoms, two from bidentate S, S dithiolate ligand and other two sulfur from dithioxamide ligand. The chiral carbons of α-MBAdt ligand in the complex show a (R,R)-configuration. The bent 1, 4-dithiane ring makes a chair like conformation for all ***M-C4*** complexes. In the lattice tetrabutyl ammonium cation is included as a counterion per single molecule of monoanionic complex. In the triads of ***M-C4*** complexes the M-S (thiolate) single bonds fall in a relatively narrow range of 2.146(12)-2.309(19) Å and their lengths vary due to the asymmetric complexation. The ***M-S*** bond lengths follow the order ***Pd-C4***>***Pt-C4***>***Ni-C4,*** as predictable. The C(12)-S(12) distances are fall in the range of thione lengths. The different thiolate C-S bond distances (1.718(10)- 1.83(4) Å.) are in agreement with the different nature of the ligands. In ***Table 3.3*** the more significant bond distances are reported.

The bond angles between opposite sulfur atoms connected diagonally through the metal in S(11)-M-S(22) and S(12)-M-S(21) fall in the range of 173.4(5) to 175.68(10) which is approximately 5-8° far from 180° (complete planarity). The torsion angles, calculated as ***δ1*** between S(11)-C(11)-C(21)-S(21) and ***δ2*** between S(12)-C(12)-C(22)-S(22) are shown and listed in ***Figure 3.5.*** It can be pointed out that in general for complexes ***M-C4*** the dihedral angle for dithioxamide is greater than the dithiolate **(*δ2*>*δ1*)** and ***δ2*** is high when central metal is Pd or Pt.

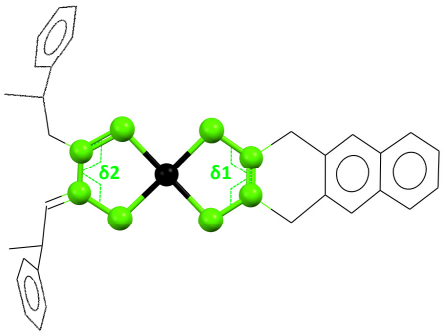

	Ni-C4	***Pd-C4***	***Pt-C4***
δ1	-4.28	1.41	4.23
δ2	7.27	11.5	11.44

Figure 3.5, Dihedral angle**(*δ1*)** and (***δ2***) in the metal complex and respective values for ***M-C4***

Table 3.3, Selected bond lengths and angles

Bonds	***Ni-C4***	***Pd-C4***	***Pt-C4***
M-S(11)	2.177(12)	2.279(2)	2.275(3)
M-S(12)	2.146(12)	2.3098(19)	2.293(2)
M-S(21)	2.162(12)	2.285(2)	2.278(3)
M-S(22)	2.189(11)	2.2991(19)	2.300(2)
C(11)-S(11)	1.73(4)	1.744(8)	1.742(10)
C(12)-S(12)	1.70(4)	1.683(6)	1.674(8)
C(21)-S(21)	1.83(4)	1.739(7)	1.718(10)
C(22)-S(22)	1.81(4)	1.735(7)	1.731(10)
C(11)-C(21)	1.27(4)	1.327(9)	1.356(12)

C(12)-C(22)	1.43(4)	1.497(9)	1.518(12)
N(22)-C(22)	1.22(4)	1.274(9)	1.276(11)
		Angles	
S(11)-M-S(21)	92.2(4)	89.87(7)	89.78(9)
S(12)-M-S(22)	91.9(4)	89.05(7)	88.54(9)
S(11)-M-S(12)	87.8(4)	90.74(7)	90.91(9)
S(21)-M-S(22)	88.7(4)	90.83(7)	91.13(9)
S(11)-M-S(22)	174.9(5)	175.33(8)	175.68(10)
S(12)-M-S(21)	173.4(5)	173.93(7)	175.13(9)
C(11)-S(11)-M	103.3(15)	102.1(2)	102.4(3)
C(12)-S(12)-M	105.6(18)	103.7(2)	105.7(3)
C(21)-S(21)-M	101.5(14)	101.7(2)	102.5(3)

3.2.2.2. Crystal packing:

These complexes crystallise in noncentrosymmetric space groups as expected due to the presence of the chiral dithioxamide ligand (***A1***). ***Figure 3.6a***&***b*** shows the crystal packing diagram of ***Ni-C4*** and ***Pd-C4*** complexes approximately along the crystallographic a-axis. The red arrows show the versus of dipolar moments in the molecules. The unit cell in ***Ni-C4*** contains eight molecules of complex (orthorhombic, $C222_1$) and their corresponding counterions. The complexes are arranged as A-M-D....D-M-A with a partial π-stacking (distance 3.52 Å) interaction between peripheral aromatic carbon atoms of donor ligand. The unit cell in ***Pd*** and ***Pt-C4*** contains four molecules of complex and their counterions. (Orthorhombic, $P2_12_12_1$) (***Figure 3.6b***)

Ni-C4 crystal packing (***Figure 3.6a***) shows most interactions between tetrabutyl ammonium and the complex at distances smaller than *van der Waal's* radii, as shown in the ***Figure 3.6*** The layers interact with each other by means of the

aromatic rings through partial π-stacking interaction between C(71) carbons of two complex molecules with inter stacking distance of 3.252 Å.

Since ***Pd-C4*** and ***Pt-C4*** complexes crystallize with same space groups (P_{212121}) only ***Pd-C4*** packing is briefly discussed. Contacts smaller than *van der Waal's* radii occur between complexes and counter ion, namely, central S11-H13D, 2.696 Å, dithione ring S41-H93A 2.899Å, C82-H53A 2.785Å.

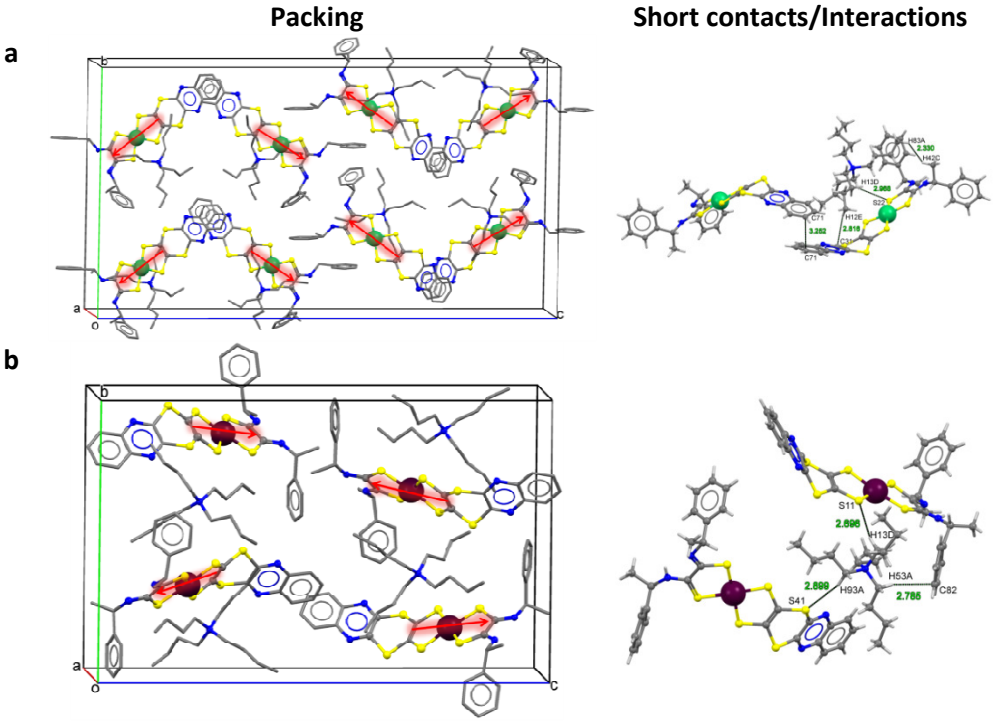

Figure 3.6, Crystal packing of (a)***Ni-C4***and (b) ***Pd-C4*** showing interactions at distances shorter than the *Van der Waal* radii, arranged approximately along a-axis showing bc-plane. Red arrows indicate the dipolar moment, Hydrogen atoms are omitted for clarity)

3.2.3. Electrochemical properties

Cyclic Voltammetric Data of [M(X)(Y)] X= α-MBAdt, Y=quinoxdtcomplexes, ***Pd-C4*** and ***Pt-C4*** are presented in ***Table 3.4.*** Cyclic voltammetric experiments performed on DMF solutions of the complexes show that ***M-C4*** exhibits one *quasi*-reversible oxidation wave.(***Figure 3.7***)

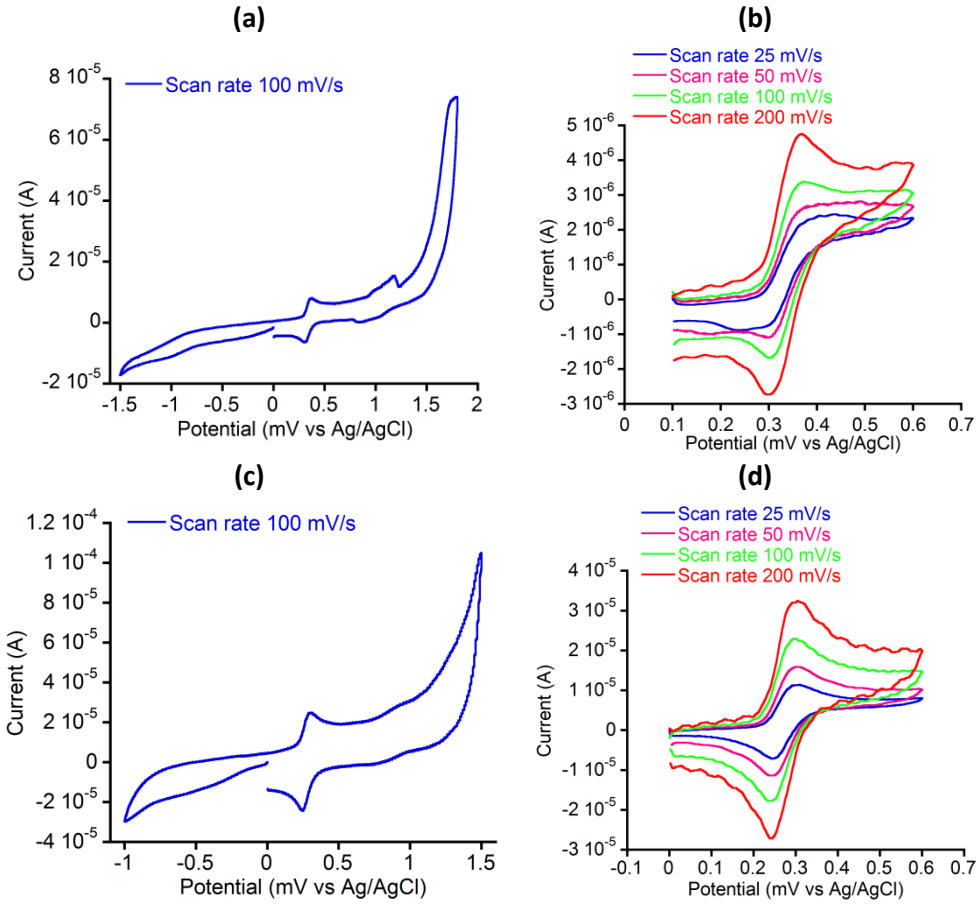

Figure 3.7, Cyclic voltammetry in 0.2 M $TBAClO_4$/Acetonitrile(a)&(c) full scan (b) (d) at different scan rates of ***Pd-C4&Pt-C4***respectivelymeasuring current (I), in response to an applied potential (E)

Table 3.4,Cyclic Voltammetric Data of [M(X)(Y)] (X= α-MBAdt, Y=quinoxdt) complexes

	Pd-C4	***Pt-C4***
$\mathbf{E_a\ (V)_a}$ $\mathbf{M(X)(Y)^{-1} - e^- \leftrightarrow M(X)(Y)^0}$	0.25 (mV)	0.27 (mV)

3.2.4. Optical properties

3.2.4.1. Absorption spectroscopy

The absorption spectrum of the ***Pt-C4*** complex in acetonitrile solution is reported in ***Figure 3.8,*** where the calculated spectrum in the same solvent (TD-DFT (B3LYP/6-31+G(d)-SDD, 20 states) is also reported. Absorption is dominated by a broad medium intense band (ε = $5.5x10^3$ M^{-1} cm^{-1}) centred at 595 nm with a shoulder at higher energy (~500 nm), and a quite intense (ε = $10.3x10^3$ M^{-1} cm^{-1}) absorption band at 375 nm.

The calculated energies and compositions of the lowest lying singlet electronic transitions of ***Pt-C4*** in acetonitrile solution are reported in ***Table 3.5.*** According to TD-DFT calculations, the lowest absorption band can be assigned to a HOMO → LUMO transition from π-orbitals of the dithiolato ligand with metal contribution to π-orbitals of the dithioxamide ligand ***A1***, of considerable CT character from the ***D1*** to the ***A1*** ligand. This attribution is supported by the significant negative solvatochromism of this band upon changing the solvent (*i.e.* bathochromic shift on decrease of solvent polarity) (see ***Figure 3.10a***).

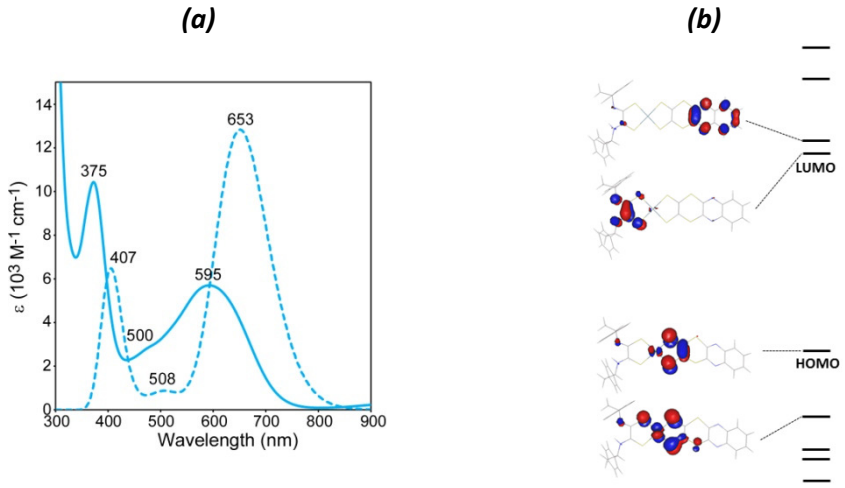

Figure 3.8, (a) Experimental (solid line) and calculated (dashed line) absorption spectra for ***Pt-C4*** in acetonitrile solution. (b) TD-DFT Calculated MOs involved in the absorption transitions.

Table 3.5,TD-DFT calculated energies and compositions of the lowest lying singlet electronic transitions of ***Pt-C4*** in the solution phase, acetonitrile, (B3LYP/6-31+G(d)-SDD). The principal singlet transition responsible for the main absorption band in the visible region is shown in bold.

State	Composition[a]	ΔE(eV/nm)[b]	*f*[c]	Character
1	HOMO → LUMO, 97%	1.90 / 653	0.1543	Quinox/Pt → MBA
2	HOMO → L+1, 98%	1.96 / 632	0.0082	Quinox/Pt → Quinox
3	HOMO→ L+2, 96%	2.19 / 565	0.0001	Quinox/Pt → PtS_4
4	H-1→ LUMO, 97%	2.44 / 508	0.0106	Quinox/Pt/MBA → MBA
5	H-1 → L+2, 77%	2.78 / 446	0.0001	
6	H-1 → L+1, 93%	2.80 / 444	0.0050	
7	H-3 → LUMO, 93%	2.81 / 441	0.0006	
8	HOMO → L+3, 64% H-3 → L+2, 28%	3.03 / 409	0.0021	
9	H -2 → LUMO, 68%	3.05 / 407	0.0506	Quinox/Pt/MBA → MBA
10	H-3 → L+2, 52% H-2 → LUMO, 22%	3.09 / 402	0.0287	Pt → PtS_4, Quinox/Pt/MBA → MBA

[a]Compositions of electronic transitions are expressed in terms of contributing excitations between ground-state Kohn–Sham molecular orbitals.[b]Transition energy from the ground state in eV. [c] Oscillator strength.

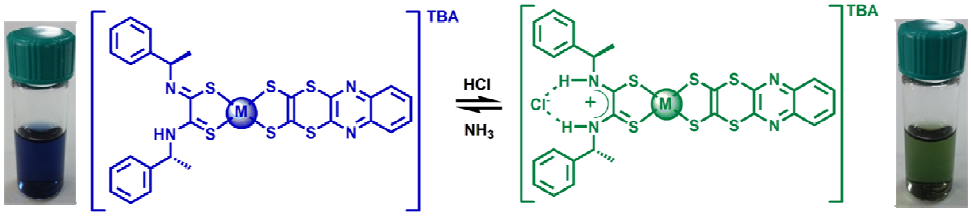

Figure 3.9 HCl uptake and release and related colour change for ***Pt-C4***

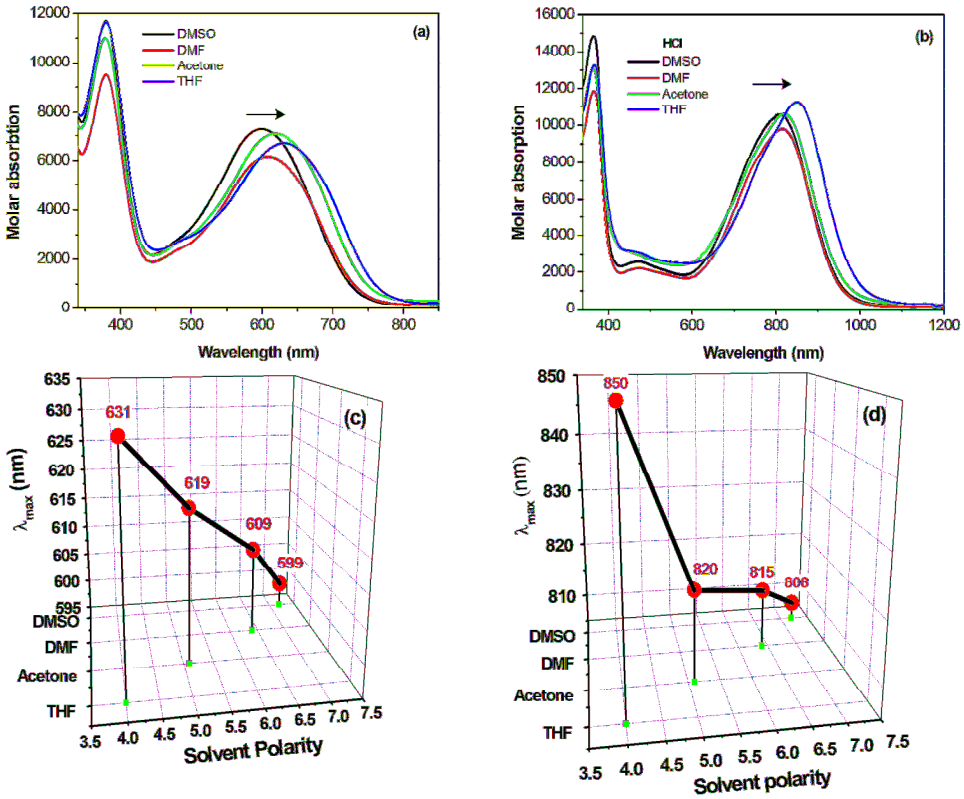

Figure 3.10, (a) Absorption spectra of ***Pt-C4*** in different solvents. (b) Absorption spectra of ***Pt-C4. HCl***in different solvents and their respective negative solvatochromism of the lowest absorption bands of ***Pt-C4***as (c) ***Pt-C4. HCl*** (d) in different solvents with corresponding solvent polarity

On the other hand, the attribution of the two higher energy bands on the basis of computational calculations (***Table 3.5***) may be questionable, as some

discrepancies can be evidenced with experimental and literature data and considerations already made for the symmetrical ***Pt-C1*** complex (in ***Chapter 2***), as will be discussed later.

On addition of HCl the colour of the solution changes from deep blue to green, suggesting an acid uptake by the complex most likely through the peripheral dithioxamide part of the complex, ***Pt-C4.HCl***, as depicted in ***Figure 3.9***.[19] A related substantial change in the absorption profile is observed (***Figure 3.11***) as the lowest absorption band disappears whereas a new one is formed at higher wavelengths (800 nm for the ***Pt-C4.HCl)***, and the presence of a well defined Isosbestic points suggests that an equilibrium between two absorbing species occurs. Also the two higher energy bands (the near-UV bad at 375 nm and the less intense shoulder at 500 nm) are quite sensitive to HCl addition and a hypsochromic shift is observed.

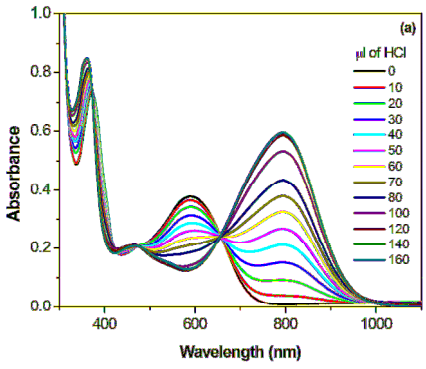

Figure 3.11, UV-visible spectral changes of (a) TBA [Pt((R)-α-MBAdto)(quinoxdt)] and (b) TBA [Pd((R)-α-MBAdto)(quinoxdt)] on addition of Stoichiometric quantities of Aq. HCl

It must be pointed out that the change of the optical properties of the complex is fully reversible upon addition of NH_3 to the acidic form. The protonated form of

the complex still displays significant negative solvatochromism upon solvent polarity change, hinting at a preserved dominant LL'CT (ligand to ligand charge transfer) character of the transition, as shown in ***Figure 3.10b***.

It is worth to mention that in solid crystalline state, the crystals of ***Pt-C4*** apparently (under microscope) change the colour on exposure to HCl vapours reversibly (on heating), however, our attempts to characterize the apparent HCl-incorporated crystal failed because the sample did not show any X-diffraction (after exposure to HCl).

Homoleptic platinum complexes coordinated to similar dithioxamide ligands have been extensively investigated by *Santo Lanza* and *Sebastiano Campagna* group.[19-21] It was observed that when solid or solutions of such complexes were treated with HCl vapour or Aq. HCl a change in colour was clearly visible. This change was also reversible on treatment with NH_3 gas or Aq. NH_3 respectively.[22] The change in colour was rationalized, by NMR spectroscopic evidences, as formation of "*contact ion pairs*" by protonation of C=N group while Cl^- anions lying in the periphery through interaction with N-H. Absorption spectroscopy showed a very large bathochromic shift (~200-300nm) in absorption maxima between the initial complex and its contact ion pair with acid. It was suggested that contact ion pair formation had a strong effect on frontier molecular orbital in the complexation core. It was also observed that contact ion pair formation was not observed in pure ligand but occur only in metal complexes. It must be emphasized that till date there is no crystallographic evidence for the formation of contact ion pairs however it has only been explained by NMR spectroscopy.[22] The two NH protons come at δ 12-13ppm as a broad singlet at room temperature which slowly

changes to two sharp singlet signals of N-H protons on recording NMR spectra at subsequently lower temperatures. This result clearly indicates that at high temperatures a rapid exchange of the amidic proton does occur; however, this process is characterised by high activation energy, so that hydrogen atoms have a fixed arrangement in the molecule also at room temperature. In addition, the values of the frequencies of the two N-H signals indicate that both N-H protons are engaged in a strong hydrogen bond[23] of the type 'N-H...Cl^{-}.

This peculiar capability of this kind of N^1, N^2-disubstituted dithioxamide complexes to form contact ion pairs suggests to check the capability of chiral heteroleptic complexes with potential proton switchable SO-NLO property, to crystallize in noncentrosymmetric space group.

No "contact ion pairs" are expected and found in complexes based on piperazinyl or diazepanyl dithiones. Instead by employing acyclic N^1-N^2-disubstituted dithioxamide, the mono-deprotonated dithioxamide binds the metal in the form of thiol-thione tautomeric form which appears to be most stable form in basic conditions. The coordination of M(II) to thione-thiolate ligand on one side and dithiolate ligand on the other makes the complex monoanionic (-1). (***Figure 3.12***) Complexes based on piperazinyl dithiones showed redox switchability by spectroelectrochemistry[1] whereas this property has not yet been evaluated for the complexes under discussion here.

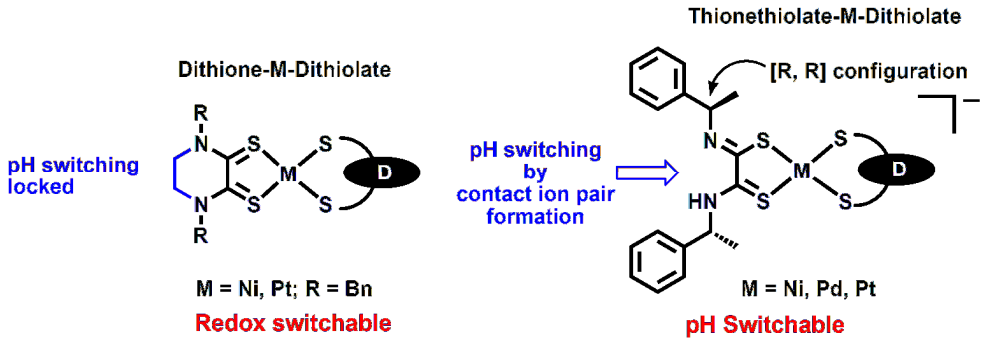

Figure 3.12, Comparison between metal complexes of dithioxamide fused in piperazine heterocycles (left) and N^1-N^2-disubstituted dithioxamide complex (right)

3.2.4.1.1. Photoluminescence properties

Upon irradiation in the visible region at 450nm the complex shows photoluminescence in acetonitrile solution at room temperature in the deep red at 750 nm (***Figure 3.13a***). The excitation spectrum correspondent to this emission seems to overlap with the absorption band appearing as a shoulder at 500 nm in the absorption spectrum. A clear dependence on the excitation wavelength is observed, as no emission is detected when irradiating the sample at 600 nm, where the lowest absorption band lies. This apparent anti-Kasha behaviour is similar to that observed in the case of the homoleptic ***Pt-C1*** complex (see ***Chapter 2*** and related discussion), where the lowest excited state only involves orbitals of the dithiolene core and emission likely originates from ligand centred transitions of the quinoxaline moiety.

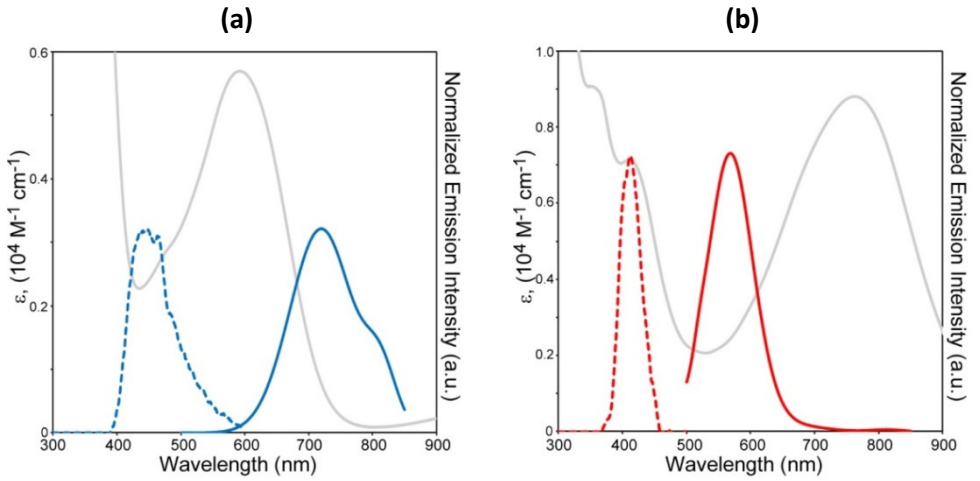

Figure 3.13, (a) Emission (solid blue line), excitation (dashed blue line) and absorption (grey solid line)spectra of ***Pt-C4***in acetonitrile solution, Excitation wavelength was 450 nm. Excitation spectrum was collected by monitoring emission at 750 nm. (b) Emission (solid red line), excitation (dashed red line) and absorption (grey solid line) spectra of ***Pt-C4.HCl*** in acetonitrile solution. Excitation wavelength was 420 nm. Excitation spectrum was collected by monitoring emission at 550 nm.

The ***Pt-C4.HCl***species (contact ion pair) preserves the emissive properties but luminescence switches from deep red to green, with the emission maximum shifting from 750 to 550 nm (***Figure 3.13b***). In this case, the anti-Kasha behaviour is immediately evident, as emission is detected well above the lowest absorption band at 780 nm. The excitation spectrum for this emission shows a hypsochromic shifts with respect to the non-protonated form, and is peaked around 420 nm. This spectral change is in good accordance with that observed in the absorbance spectra for the two forms of the complex, as depicted in ***Figure 3.14.*** No emission is detected upon irradiation at 500 nm.

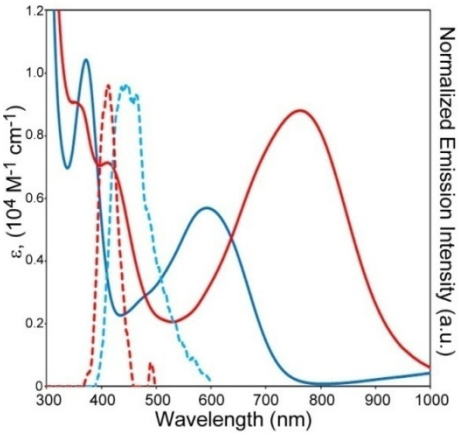

Figure 3.14, Absorption (solid lines) and excitation (dashed lines) spectra for ***Pt-C4*** (blue) and ***Pt-C4.HCl*** complex (red) in acetonitrile solution.

Moreover, it has to be pointed out that no photoluminescence response is observed in the region above 850 nm at any wavelength throughout the absorption profile for both species. This observation confirms the unusual anti-Kasha behaviour of this compound as already observed for the homoleptic ***Pt-C1*** complex (see ***Chapter 2*** and related discussion). In principle, similar considerations may then be drawn also in this case, by ascribing the observed emission as originating from ligand-centred transitions from excited states not involving orbitals from the dithiolene core, and invoking a poor wavefunctions' overlap between the superior excited state and the lower one, slowing down the rate of non radiative internal conversion. However, in this heteroleptic complex, where both ligands are known to display emissive properties[24] (***Figure 2.13b***), a proper explanation for this peculiar behaviour seems more complicated with respect to the case of the homoleptic complex bearing only the quinoxdt ligand. TD-DFT calculations at 20 states seem not sufficient to this purpose as some

discrepancies, in comparison to ***Pt-C1***, concerning the expected sequence of frontier molecular orbitals involved in the electronic transitions, are noticed. In fact, when comparing literature reports on homoleptic complexes of similar dithioxamide ligands[24]and our own observations on ***Pt-C1***,and taking into account the positions of emission maxima, it is at a first sight possible to assign emission at 750 nm as originating from the ***A1*** ligand and the one at 550 nm to the quinoxdt moiety. However, these attributions are not fully supported by TD-DFT calculations and seem to be in contrast with the observed behaviour as a function of acid/base addition, as only the protonated form of the dithioxamide ligand is expected to be emissive[24] whereas luminescence from quinoxdt should be quenched by proton. As a matter of fact, an opposite response to the acidic conditions is observed in this case.

Therefore, a deeper theoretical and experimental (time-resolved photophysical measurements, including excited state absorption) study is in this case mandatory to achieve a complete picture of the photocycle taking place in this complex.

Anyway, it must be underlined that this heteroleptic complex behaves as a very effective luminescent molecular switch, turning emission colour from deep red to green upon HCl addition and showing full reversibility of the optical properties after subsequent addition of NH_3, as shown in ***Figure 3.15.***

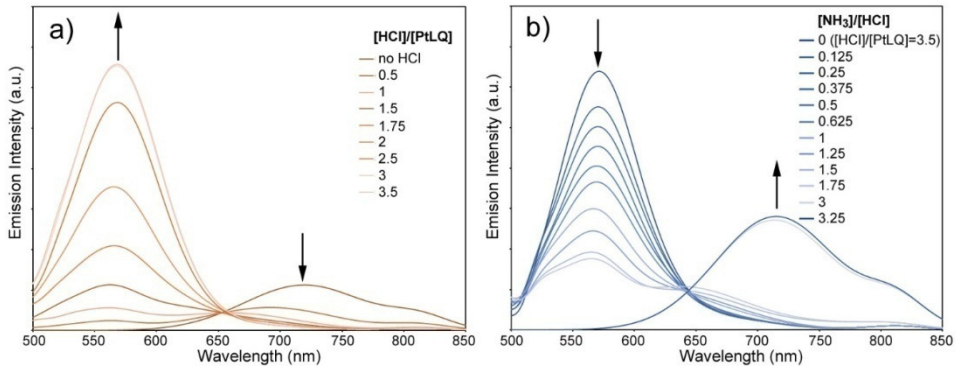

Figure 3.15, a) Emission spectra of ***Pt-C4*** in acetonitrile solution as a function of added HCl. b) Emission spectra of ***Pt-C4.HCl*** in acetonitrile solution as a function of added NH_3. Excitation wavelength was kept at 450 nm for both experiments corresponding to a region where no substantial change in absorption is detected.

3.2.4.2. Luminescent doped sol-gel glasses

To explore the potential of this complex for application purposes as a luminescent molecular sensor for HCl/NH_3, preliminary studies on its incorporation into porous silica sol-gel glasses have been performed. This strategy is useful to overcome limitations of poor thermal stability and low mechanical strength of organic compounds and afford suitable materials for use in the fabrication of optical devices, being doped silica glasses highly transparent and homogeneous and having good mechanical properties. Moreover, the silica matrix hardly influences the energy levels of the doping emissive complex and has also a negligible absorption coefficient at the excitation wavelengths used in photoluminescence experiments.

The silica matrix was prepared from a mixture of the two precursors shown in ***Figure 3.16,*** tetramethoxysilane (TMOS) and the organically-modified silicon alkoxide (ORMOSIL), glycidoxypropyltrimethoxysilane (GLYMO). ORMOSILs are

formed by a silicate backbone in which alkoxide –OR groups are replaced by organic –R groups. The GLYMO precursor has been selected in view of the improved mechanical properties of the glass (lower shrinkage) due to the filling of the pores by bulky organic groups and ability to ensure a good dispersion of the dopant complex into the matrix with respect to the commonly used tetraalkoxysilanes such as TMOS and TEOS (tetraethoxysilane) alone.

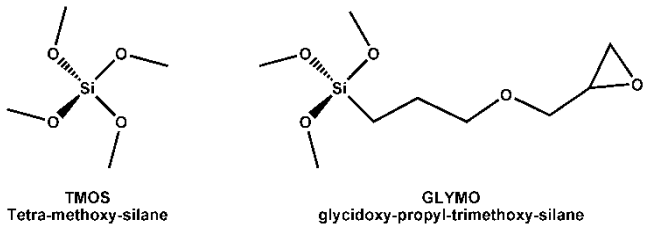

Figure 3.16, Structure of alkoxysilane precursors.

The preparation of the doped sol–gel glass was performed through a one-step process in which a solution of the complex in CH_3CN–CH_3CH_2OH (1 : 1 v/v) solvent mixture was mixed with the liquid sol matrix (ethanolic mixture of TMOS and GLYMO precursors where the hydrolysis reaction was already started) at 50 °C and at neutral pH. Hydrolysis and condensation reactions in the sol–gel process were carried out without acidic or basic catalysis in order to avoid interferences with the dopant complex. For this reason, TMOS, which hydrolyses easily under neutral conditions, was preferred to the more commonly used TEOS (tetraethoxysilane).

The resulting doped sol solution was then dropped into a Teflonvial and allowed to age at room temperature. Slow solvent evaporation led to the formation of a

homogeneous and transparent glass, showing intense luminescence under UV light illumination, as shown in ***Figure 3.18.***

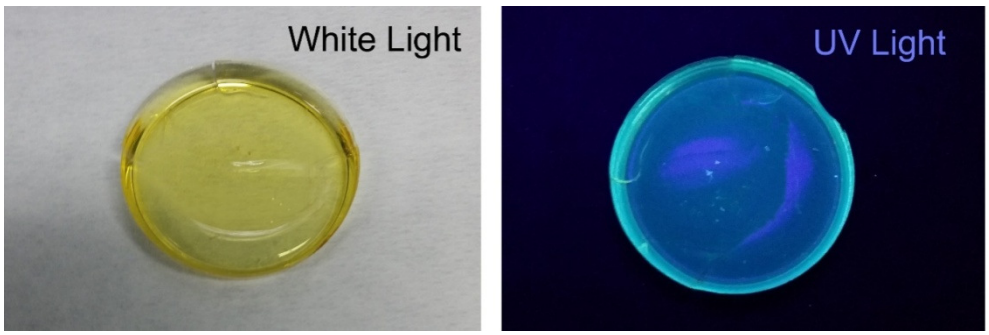

Figure 3.17. Silica sol-gel glass doped with ***Pt-C4*** under white light (left) and UV light (right) illumination.

However, despite carrying the synthesis under neutral or slightly basic (by addition of small amounts NH_3 or urea) conditions, the color of the obtained glass and of the emitted light resembles that of the protonated form of the complex. This may be due to an interaction of the complex with the residual Si-OH groups present in the silica matrix even in the absence of chloride ions, or to a molecular rearrangement responsible for the shift of the emission. Further photophysical studies and investigation of synthetic conditions (nature of silica precursors, pH…) are currently being carried out to optimize procedures to obtain an optical material suitable to be used as HCl or NH_3 sensor or luminescent switch.

3.2.5. SO-NLO properties

The efficiency of second harmonic generation (SHG) was measured using the Kurtz powder method on crystalline samples of ***Pd***&***Pt-C4, C5***, ***C7*** and ***Ni-C15***. Out of the tested complexes only ***M-C7*** complexes showed significant activity. (***Table 3.6***)

Table 3.6, Evaluation of SHG for compounds

Complex code	SHG value[a]
Pd-C4	till background noise limit
Pt-C4	till background noise limit
Pd-C5	till background noise limit
Pt-C5	till background noise limit
Pd-C7	0.2
Pt-C7	0.5
Ni-C15	till background noise limit

[a]Second harmonic intensity measured at 1064nm fundamental radiation, relative to urea.

The best values of SHG are found for compounds possessing strong electron withdrawing diester (R) groups (**M-C7)**. If we relate the solid state SO-NLO activity of complexes with respect to the arrangement of complexes and their dipoles (D-M-A transition plane) in crystal packing, ***Pt*** and ***Pd-C7*** complexes crystallize in triclinic system (see ***Appendix 2***, ***Figure S2.4*** and ***Table S2.1***) with chiral P1 space group. The SO-NLO activity displayed by the M-C7 complexes is due to the bulk arrangement with polar noncentrosymmetric space group P1, while the other complexes crystallize in non-polar $P2_12_12_1$space groups (see ***Table 3.1***)

Kurtz powder technique are very difficult to interpret in terms of molecular structure–property relationships, since they depend not only on the molecular hyperpolarisability β, but also very strongly on the crystal packing structure, grain size, phase-matching properties, etc.

SHG measurements on HCl-incorporated solid form of the complexes and solution state SO-NLO properties are in course.

3.3. Experimental

[Pt((R)-α-MBAdt)(DMSO)Cl]

A solution of (0.321 g, 0.76 mmol) $Pt(DMSO)_2Cl_2$ in 30mL $CHCl_3$ was added portion wise to a solution of (0.25 g, 0.76 mmol) N^1,N^2-bis((R)-1-phenylethyl)ethanebis(thioamide) (***A1***), (R)-α-MBAdto, in 130mL $CHCl_3$ and stirred for 5h at room temperature. The obtained apple red solution was then concentrated under vacuum, re-dissolved in 15mL dichloromethane filtered through tight cotton plug and reprecipitated by petroleum ether. An apple red powder of (0.41g, 84%) [Pt((R)-α-MBAdto)(DMSO)Cl] was obtained by centrifugation. The product was used for next step without further purification.

FT–IR (KBr): vcm−1 : 3193 (s); 3090 (s); 2980 (m); 2925 (m); 1568 (vs); 1529 (m); 1494 (w); 1447 (m); 1430 (vs); 1384 (s); 1347 (w); 1326 (w); 1214 (w); 1188 (m); 1087 (m); 1022 (w); 980 (vw); 915 (vw); 840 (vw); 760 (m); 698 (s), 540 (w)

TBA[Pt((R)-α-MBAdt)(quinoxdt)]

A solution of Na (8 mg, 0.35 mmol) in 10 mL of methanol was added drop wise to a stirred suspension of [1,3]dithiolo[5,6][1,4]dithiino[2,3-b]quinoxaline-2-one (***D1***) (48.4 mg, 0.16 mmol) in methanol/$CHCl_3$. The mixture was stirred for 30 min at room temperature to obtain a reddish-brown dithiolate solution. The dithiolate solution was then added drop wise to an apple red solution of [Pt((R)-α-MBAdt)(DMSO)Cl] (100 mg, 0.16 mmol) in 120mL 20% MeOH/$CHCl_3$ at room temperature. The reaction mixture was stirred overnight and the solution turned to violet-purple. The obtained mixture was filtered, and the solvent evaporated to

a 1/4th of the initial volume. Afterwards, a solution of Bu_4NBr (101.2 mg, 0.31 mmol) in MeOH was added drop wise and the resulting mixture was roto-evaporated to dryness. The solid product was dissolved in ca. 15 mL of CH_3CN and filtered through a cotton plug directly into a crystallization vessel. Dark green crystals (69,6 mg, 0.066 mmol; yield 41.3%) were obtained by recrystallization in CH_3CN/diethyl ether. Analytical results are in accordance with the formula $(Bu_4N)[Pt((R)$-α-MBAdt)(quinoxdt)]. Elemental Analysis: calculated for $C_{44}H_{59}N_5PtS_6$ (1045.45): C 50.55, H 5.69, N 6.70, S 18.40; found: C 50.59, H 5.5, N 6.5, S 18.38 UV-vis (DMF solution): λ (nm) ε ($molcm^{-1}dm^{-3}$): 298 (2.25×10^4); 379 (1.25×10^4); 475sh (3.12×10^3); 604 ($7.80\times\cdot10^3$).FT–IR (KBr): vmax/cm−13233 (w); 3059 (vw); 3026 (vw); 2964 (s); 2926 (m); 2869 (m); 1497 (vs); 1470 (s); 1451 (s); 1383 (s); 1306 (m); 1256 (s); 1211 (w); 1171 (s); 1127 (m); 1110 (s); 1088 (m); 1018 (w); 975 (w); 874 (w); 775 (s); 737 (w); 689 (s); 645 (w); 598 (w); 547 (m); 533 (w); 486 (vw); 443 (vw).

[Pd((R)-α-MBAdt)(DMSO)Cl]

A solution of $Pd(DMSO)_2Cl_2$ (250 mg, 0.75 mmol) in 20 mL methanol was added portion wise to a solution of (R)-α-MBAdto (***A1***), (246.1mg, 0.75 mmol) in 130mL $CHCl_3$. Orange-Yellow solution obtained was then stirred for overnight at room temperature. Orange-Yellow powder of [Pd((R)-α-MBAdt))(DMSO)Cl] (392 mg, 95%) was collected by centrifugation. The product was used for next step without further purification.FT–IR (KBr): ν_{max} cm^{-1}:3193 (s); 3090 (s); 2980 (m); 2925 (m); 1568 (vs); 1529 (m); 1494 (w); 1447 (m); 1430 (vs); 1384 (s); 1347 (w); 1326 (w); 1214 (w); 1188 (m); 1087 (m); 1022 (w); 980 (vw); 915 (vw); 840 (vw); 760 (m); 698 (s), 540 (w)

Bu_4N[Pd((R)-α-MBAdto)(quinoxdt)]

A solution of Na (9.2 mg, 0.4mmol) in 15 mL of methanol was added drop wise to a stirred suspension of [1,3]dithiolo[5,6][1,4]dithiino[2,3-b]quinoxaline-2-one (***D1***) (59.1 mg, 0.18 mmol) in 50mL 50% methanol/$CHCl_3$. The mixture was stirred for 30 min at room temperature to obtain a reddish-brown dithiolate solution. The dithiolate solution was then added drop wise to an yellow solution of [Pd(R)-α-MBAdt)(DMSO)Cl] (100 mg, 0.18 mmol) in 120mL 20% MeOH/$CHCl_3$ at room temperature. The reaction mixture was stirred overnight and the solution turned to red-purple. The obtained mixture was filtered, and the solvent evaporated to a 1/4th of the initial volume. Afterwards, a solution of Bu_4NBr (117.5 mg, 0.37 mmol) in MeOH was added drop wise and the resulting mixture was roto-evaporated to dryness. The solid product was dissolved in ca. 15 mL of CH_3CN and filtered through a cotton plug directly into a crystallization vessel. Dark apple red crystals (93 mg, 0.097 mmol; yield 54 %) were obtained by recrystallization in CH_3CN/diethyl ether.

Analytical results are in accordance with the formula (Bu_4N)[Pd((R)-α-MBAdt)(quinoxdt)].Elemental Analysis: calculated for $C_{44}H_{59}N_5PdS_6$: C 55.23; H 6.22; N 7.32; S 20.11 found:UV-vis (DMF solution): λ (nm) ε ($molcm^{-1}dm^{-3}$):373 (1.58×10^4); 550 (5.47×10^3)FT–IR (KBr): ν_{max} cm^{-1}:3204 (w); 3060 (vw); 3026 (vw); 2961 (m); 2927 (m); 2873 (w); 1508 (vs); 1495 (s); 1479 (s); 1450 (s);1382 (s); 1327 (w); 1303 (w); 1257 (s); 1174 (s); 1111 (s); 1015 (m); 909 (w); 865 (m); 758 (s); 699 (s); 658 (m); 597 (w); 550 (vw).

Bu_4N[Ni((R)-α-MBAdt)(Quinoxdt)]

A solution of $NiCl_2.6H_2O$ (100 mg, 0.304 mmol) in 20 mL methanol was added drop wise to a solution of N1,N2-bis((R)-1-phenylethyl)ethanebis(thioamide), (R)-α-MBAdto, (100 mg, 0.304 mmol) in 130mL 50% MeOH:$CHCl_3$. Orange-Yellow solution was obtained after stirring for 30min. In a separate flask a sodium dithiolate solution of Quinoxdto (98.78 mg, 0.304 mmol) and sodium (15.59mg, 0.68 mmol) obtained by above method was added drop wise to reaction mixture. A purple-pink solution was obtained after stirring the reaction mixture for overnight. The reaction mixture was concentrated to 1/4th volume during which blue microcrystalline solid separated was filtered. To the purple-pink filtrate was added a solution of Bu_4NBr (100 mg, 0.304 mmol) in Methanol. After slow evaporation of filtrate crystals of (Bu_4N)[Ni((R)-α-MBAdt)(quinoxdt)] formed were collected by decantation (40 mg, 0.044 mmol, 15%).

Elemental Analysis: calculated for $C_{44}H_{59}N_5NiS_6$: C 58.13; H 6.54; N, 7.70; S, 21.16FT–IR (KBr): ν_{max} cm^{-1}:3230 (w); 3057 (vw); 3049 (vw); 2961 (m); 2929 (m); 2872 (w); 1520 (vs); 1451 (m); 1383 (m); 1364 (m);1323 (m); 1253 (m); 1171 (s); 1121 (s); 1022 (vw); 1011 (vw); 908 (vw); 795 (vw); 754 (m); 741 (m); 700 (w); 671 (w); 619 (w); 600 (w); 562 (w); 549 (w); 423 (vw).

Doped sol-gel glass

Preparation of the precursor solution (*sol*): 8 mL of absolute ethanol, 8 mL of TMOS, 8 mL of GLYMO and 4 mL H_2O were mixed in a round-bottom flask. This mixture was maintained 1 day under stirring at room temperature (~22°C). Preparation of doped sol-gel glass: 2 mL of a $1{\cdot}10^{-3}$ M solution of the Pt-C4 complex in CH_3CN/EtOH 1:1 were added to 3 mL of the sol solution and the

mixture wass maintained under stirring at 50°C for 1 h. The mixture was then transferred into a cylindrical Teflon vial and let cool down at room temperature. Afterward, the vial was covered with Parafilm pierced with a needle to let the solvent evaporate slowly. After few days, depending on the viscosity of the sol-gel, 2 or 3 more holes were made into the Parafilm and the sample was allowed to stand at room temperature (~22°C) until the glass is formed (> 1 month).

Instrumentation details

Elemental analyses were performed by means of a Perkin Elmer CHNS/O PE2400 Series II.

FTIR. spectra (4000–400 cm^{-1}) were recorded with a Bruker IFS55 FT–IR Spectrometer on KBr pellets.

Electronic spectra were recorded with a Agilent Cary 5000 spectro-photometer. Solvent contribution was subtracted for all absorbance/emission spectra.

Emission and excitation spectra were collected with a Horiba-Jobin Yvon Fluoromax-4 spectrofluorimeter using a DC Xenon lamp. All spectra were spectrally corrected for detector response and solvent contribution was subtracted. Appropriate optical filters were used (475 longpass filter) and a smooth function was applied to data. Bandpass for emission spectra was set as 10 nm slit width for each measurement.

Electrochemical studies were performed with a Princeton Applied Research potentiostat/galvanostat model 263A equipped with a General Purpose

Electrochemical System (GPES) in one-compartment three electrode cell, consisting of a platinum wire as the working electrode, a platinum wire as the counter-electrode and Ag/AgCl (saturated KCl) as the reference electrode. The cyclic voltammograms were performed at room temperature (25 °C) in anhydrous and argon-degassed DMF containing 0.2 M tetrabutylammonium perchlorate ($TBAClO_4$)at 100 mV/s; the ferrocenium/ferrocene couple presented $E_{1/2}$ = 459 mV with an anodic to cathodic peak separation of 70 mV under the above conditions.

X-ray crystallography:

Single crystal data were collected with a Bruker Smart APEXII area detector diffractometer, Mo Kα: λ = 0.71073 Å. The unit cell parameters were obtained using 60 ω-frames of 0.5° width and scanned from three different zone of reciprocal lattice. The intensity data were integrated from several series of exposures frames (0.3° width) covering the sphere of reciprocal space.[25] An absorption correction was applied using the program SADABS[26] with min. and max. transmission factors of: 0.622-1.000. The structure was solved by direct methods (SIR2004) [27] and refined on F^2 with full-matrix least squares (SHELXL-14) [28], using the WinGX software package[29]. Non hydrogen atoms were refined anisotropically and the hydrogen atoms were placed at their calculated positions. Graphical material was prepared with the Mercury 3.0[30] program.

Computational studies: The electronic properties of *M-C4* were investigated by means of DFT methods using the spin unrestricted formalism.[31] All the calculations were performed with the Gaussian 03 program suite.[32] The molecular structures of the complex was optimized starting from the X-ray experimental geometry of ***M-C4*** without symmetry

constraints. The Becke three-parameters exchange functional with Lee-Yang-Parr correlation functional (B3LYP)17,[33] was employed together with the 6-31+G(d) basis set[34,35] for the C, H, N, and S atoms. The Pt atom was treated with the SDD valence basis set[36-39] and with the MWB60 (Pt) effective core potentials. Single point calculations were performed using the B3LYP density functional and the triple-ζ quality basis set def2-TZVP[40] for the metal atoms and with pseudo potentials for Pt,[41] whereas the C, H, N, S atoms were treated with the 6-311+G(d) basis set.[42] TD-DFT calculations were performed for 30 excited states using the same level of theory of the single point calculations. Natural population analysis (NAO) was performed with the NBO 3.1 program[43] incorporated in the Gaussian03 package. Molecular orbital diagrams were generated with the Gabedit program.[44]

3.4. References

1. Espa, D., Pilia, L., Marchiò, L., Mercuri, M. L., Serpe, A., Barsella, A., … Deplano, P. (2011). Redox-Switchable Chromophores Based on Metal (Ni, Pd, Pt) Mixed-Ligand Dithiolene Complexes Showing Molecular Second-Order Nonlinear-Optical Activity. *Inorganic Chemistry, 50*(6), 2058-2060.
2. Espa, D., Pilia, L., Makedonas, C., Marchiò, L., Mercuri, M. L., Serpe, A., … Deplano, P. (2014). Role of the Acceptor in Tuning the Properties of Metal [M(II) = Ni, Pd, Pt] Dithiolato/Dithione (Donor/Acceptor) Second-Order Nonlinear Chromophores: Combined Experimental and Theoretical Studies. *Inorganic Chemistry, 53*(2), 1170-1183
3. Pilia, L., Espa, D., Barsella, A., Fort, A., Makedonas, C., Marchiò, L., … Deplano, P. (2011). Combined Experimental and Theoretical Study on Redox-Active d 8 Metal Dithione–Dithiolato Complexes Showing Molecular Second-Order Nonlinear Optical Activity. *Inorganic Chemistry, 50*(20), 10015-10027.
4. Espa, D., Pilia, L., Marchiò, L., Attar, S. S., Barsella, A., Fort, A., … Deplano, P. (2015). Structural changes in M II dithione/dithiolato complexes (M = Ni, Pd, Pt) on varying the dithione functionalization. CrystEngComm, 17(22), 4161-4171.
5. Frei, F., Rondi, A., Espa, D., Mercuri, M. L., Pilia, L., Serpe, A., … Cannizzo, A. (2014). Ultrafast electronic and vibrational relaxations in mixed-ligand dithione–dithiolato Ni, Pd, and Pt complexes. *Dalton Trans, 43*(47), 17666-17676.
6. "Introduction to Organic Electronic and Optoelectronic Materials and Devices" Edited by Sam-Shajing Sun, Larry R. Dalton, Authors Mojca jazbinsek and Peter Gunter *Chapter 15*, p.451
7. Pidcock, E. (2005). Achiral molecules in non-centrosymmetric space groups. *Chemical Communications*, (27), 3457.
8. Advances in Macromolecules: Perspectives and Applications editor: edited by Maria Vittoria Russo, Authors Paolo Prosposito, Fabio De Matteis

Chapter 2 Macromolecular Systems with Nonlinear Optical Properties: Optical Characterization and Devices p.95

9. (a) Handbook of Electronic and Photonic Materials editor: Safa Kasap, Peter Capper chapter 27 Ferroelectric materials p. 597 (b) "Introduction to Organic Electronic and Optoelectronic Materials and Devices" Edited by Sam-Shajing Sun, Larry R. Dalton, Authors Sei-Hum jang, Alex K.Y. Jen *Chapter 16*, p.469
10. Feringa, B. L. (2001). *Molecular switches.* Weinheim: Wiley-VCH.
11. Irie, M. (2000). Photochromism: Memories and SwitchesIntroduction. *Chemical Reviews, 100*(5), 1683-1684.
12. De Silva, A. P., Gunaratne, H. Q., Gunnlaugsson, T., Huxley, A. J., McCoy, C. P., Rademacher, J. T., & Rice, T. E. (1997). Signaling Recognition Events with Fluorescent Sensors and Switches. *Chemical Reviews, 97*(5), 1515-1566.
13. Sato, O. (2003). Optically Switchable Molecular Solids: Photoinduced Spin-Crossover, Photochromism, and Photoinduced Magnetization. Accounts of *Chemical Research, 36*(9), 692-700.
14. Coe, B. J. (1999). Molecular Materials Possessing Switchable Quadratic Nonlinear Optical Properties. *Chemistry - A European Journal, 5*(9), 2464-2471.
15. Asselberghs, I., Clays, K., Persoons, A., Ward, M. D., & McCleverty, J. (2004). Switching of molecular second-order polarisability in solution. *Journal of Materials Chemistry, 14*(19), 2831.
16. Coe, B. J. (2006). Switchable Nonlinear Optical Metallochromophores with Pyridinium Electron Acceptor Groups. *Accounts of Chemical Research, 39*(6), 383-393.
17. Green, K. A., Cifuentes, M. P., Samoc, M., & Humphrey, M. G. (2011). Metal alkynyl complexes as switchable NLO systems. *Coordination Chemistry Reviews, 255*(21-22), 2530-2541.

18. Rosace, G., Giuffrida, G., Saitta, M., Guglielmo, G., Campagna, S., & Lanza, S. (1996). Luminescence Properties of Platinum(II) Dithiooxamide Compounds. *Inorganic Chemistry, 35*(23), 6816-6822.
19. Giannetto, A., Puntoriero, F., Barattucci, A., Lanza, S., & Campagna, S. (2009). Tight-Contact Ion Pairs Involving Pt(II) Dithiooxamide Complexes: the Acid−Base Reactions between Hydrohalogenated Ion-Paired Complexes and Pyridine. *Inorganic Chemistry, 48*(21), 10397-10404.
20. Lanza, S., Nicolò, F., Cafeo, G., Rudbari, H. A., & Bruno, G. (2010). The Absolute Configuration of Palladium(II) and Ruthenium(II) Pseudochiral Centers in either Chiral or Achiral Environments. *Inorganic Chemistry, 49*(20), 9236-9246.
21. Giannetto, A., Lanza, S., Puntoriero, F., Cordaro, M., & Campagna, S. (2013). Fast transport of HCl across a hydrophobic layer over macroscopic distances by using a Pt(II) compound as the transporter. *Chemical Communications, 49*(69), 7611.
22. Lanza, S., Monsù Scolaro, L., & Rosace, G. (1994). Organoplatinum(II) complexes containing disubstituted dithioxamides: Evidence for an S,S' Pt coordinated neutral dithioxamide acting as an anion binding agent. *Inorganica Chimica Acta, 227*(1), 63-69
23. Emsley, J. (1980). Very strong hydrogen bonding. *Chemical Society Reviews, 9*(1), 91.
24. Nastasi, F., Puntoriero, F., Palmeri, N., Cavallaro, S., Campagna, S., & Lanza, S. (2007). Solid-state luminescence switching of platinum(ii) dithiooxamide complexes in the presence of hydrogen halide and amine gases. *Chemical Communications,* (45), 4740.
25. Brouwer, A. M. (2011). Standards for photoluminescence quantum yield measurements in solution (IUPAC Technical Report). *Pure and Applied Chemistry, 83*(12). 2213–2228.
26. SMART (control) and SAINT (integration) software for CCD systems; Bruker AXS: Madison, WI, 1994.

27. Area-Detector Absorption Correction; Siemens Industrial Automation, Inc.: Madison, WI, 1996.
28. Burla, M. C., Caliandro, R., Camalli, M., Carrozzini, B., Cascarano, G. L., De Caro, L., … Spagna, R. (2005). SIR2004 : an improved tool for crystal structure determination and refinement. *J Appl Cryst, 38*(2), 381-388.
29. Sheldrick, G. M. (2007). A short history of SHELX. *Acta Cryst Sect A, 64*(1), 112-122.
30. Farrugia, L. J. (1999). WinGX suite for small-molecule single-crystal crystallography. *J Appl Cryst, 32*(4), 837-838.
31. Parr, R. G.; Yang, W. *Density-Functional Theory of Atoms and Molecules*; Oxford University Press: New York, **1989**.
32. Gaussian 03, Revision C.02, Frisch, M. J.; Trucks, G. W.; Schlegel, H. B.; Scuseria, G. E.; Robb, M. A.; Cheeseman, J. R.; Montgomery, Jr., J. A.; Vreven, T.; Kudin, K. N.; Burant, J. C.; Millam, J. M.; Iyengar, S. S.; Tomasi, J.; Barone, V.; Mennucci, B.; Cossi, M.; Scalmani, G.; Rega, N.; Petersson, G. A.; Nakatsuji, H.; Hada, M.; Ehara, M.; Toyota, K.; Fukuda, R.; Hasegawa, J.; Ishida, M.; Nakajima, T.; Honda, Y.; Kitao, O.; Nakai, H.; Klene, M.; Li, X.; Knox, J. E.; Hratchian, H. P.; Cross, J. B.; Bakken, V.; Adamo, C.; Jaramillo, J.; Gomperts, R.; Stratmann, R. E.; Yazyev, O.; Austin, A. J.; Cammi, R.; Pomelli, C.; Ochterski, J. W.; Ayala, P. Y.; Morokuma, K.; Voth, G. A.; Salvador, P.; Dannenberg, J. J.; Zakrzewski, V. G.; Dapprich, S.; Daniels, A. D.; Strain, M. C.; Farkas, O.; Malick, D. K.; Rabuck, A. D.; Raghavachari, K.; Foresman, J. B.; Ortiz, J. V.; Cui, Q.; Baboul, A. G.; Clifford, S.; Cioslowski, J.; Stefanov, B. B.; Liu, G.; Liashenko, A.; Piskorz, P.; Komaromi, I.; Martin, R. L.; Fox, D. J.; Keith, T.; Al-Laham, M. A.; Peng, C.

Y.; Nanayakkara, A.; Challacombe, M.; Gill, P. M. W.; Johnson, B.; Chen, W.; Wong, M. W.; Gonzalez, C.; and Pople, J. A. *Gaussian, Inc.,* Wallingford CT, 2004.

33. Becke, A. D. (1988). Density-functional exchange-energy approximation with correct asymptotic behavior. *Phys. Rev. A, 38*(6), 3098-3100.
34. Becke, A. D. (1993). Density-functional thermochemistry. III. The role of exact exchange. *The Journal of Chemical Physics, 98*(7), 5648.
35. Ditchfield, R. (1971). Self-Consistent Molecular-Orbital Methods. IX. An Extended Gaussian-Type Basis for Molecular-Orbital Studies of Organic Molecules. *The Journal of Chemical Physics, 54*(2), 724.
36. Rassolov, V. A., Ratner, M. A., Pople, J. A., Redfern, P. C., & Curtiss, L. A. (2001). 6-31G* basis set for third-row atoms. *J. Comput. Chem, 22*(9), 976-984.
37. Fuentealba, P., Preuss, H., Stoll, H., & Von Szentpály, L. (1982). A proper account of core-polarization with pseudopotentials: single valence-electron alkali compounds. *Chemical Physics Letters, 89*(5), 418-422.
38. Cao, X., & Dolg, M. (2002). Segmented contraction scheme for small-core lanthanide pseudopotential basis sets. Journal of Molecular Structure: THEOCHEM, 581(1-3), 139-147.
39. Schwerdtfeger, P., Dolg, M., Schwarz, W. H., Bowmaker, G. A., & Boyd, P. D. (1989). Relativistic effects in gold chemistry. I. Diatomic gold compounds. *The Journal of Chemical Physics, 91*(3), 1762.
40. Weigend, F., & Ahlrichs, R. (2005). Balanced basis sets of split valence, triple zeta valence and quadruple zeta valence quality for H to Rn: Design and assessment of accuracy. Phys. Chem. Chem. Phys, 7(18), 3297.

41. Andrae, D., Haussermann, U., Dolg, M., Stoll, H., & Preuss, H. (1990). Energy-adjustedab initio pseudopotentials for the second and third row transition elements. *Theoretica Chimica Acta, 77*(2), 123-141.
42. Krishnan, R., Binkley, J. S., Seeger, R., & Pople, J. A. (1980). Self-consistent molecular orbital methods. XX. A basis set for correlated wave functions. *The Journal of Chemical Physics, 72*(1), 650.
43. Glendening, E.D., Reed, A.E.; Carpenter, J.E, Weinhold, F. *NBO version 3.1*, **1998**.
44. Allouche, A. (2010). Gabedit-A graphical user interface for computational chemistry softwares. *J. Comput. Chem, 32*(1), 174-182.

Chapter 4 Conclusion, Perspectives and Appendices

4.1. Conclusions

d^8metal homoleptic and heteroleptic dithiolene complexes have designed & obtained.

The homoleptic complexes have the following features:

- ✓ Exhibit a radical monoanionic form as most accessible redox status.
- ✓ When containing a quinoxalinato moiety in the periphery of the molecule, show room temperature, proton dependent luminescence with anti-Kasha behaviour.
- ✓ Work as photo/electrocatalyst for hydrogen production from aqueous solvents.

The heteroleptic complexes have the following features:

- ✓ Behave as second order NLO-chromophores
- ✓ Form crystals with non centrosymmetric space group when chiral groups are introduced in the periphery of the ligands.
- ✓ When containing as acceptor ligand secondary dithioxamides capable to undergo acid/base equilibria, are potential proton switchable NLO-chromophores

- ✓ When containing as acceptor ligand secondary dithioxamides and a quinoxalinato moiety in the periphery of the donor molecule, exhibit proton dependent dual-wavelength response with different colors and dual luminescence with unusual anti-Kasha behaviour resulting as multi-stimuli responsive molecule.

4.2. Perspectives

Hydrogen Evolution Reaction

- Investigation of Photocatalytic hydrogen production using Pt-C3 ligand and its comparison with the corresponding Ni-derivative.
- Developing Noble metal free system for photo catalytic hydrogen generation using ***Ni-C3*** as a photo catalyst and organic dyes or quantum dots as PS.
- Investigation of Electrocatalytic activity of the ***M-C3*** complexes
- Complete investigation of hydrogen evolving redox reaction of radical anionic complexes with acids by using a suitable SED.

Photophysical studies

Further investigation by means of advanced photophysical techniques and theoretical studies are planned to fully elucidate the luminescent properties described here.

2nd Order NLO properties

- Development of thin films of chiral complexes and their NLO activity evaluation are in progress
- Synthesis of Bimetallic complexes using N-complexation from rear site of dithioxamide complexes M-C4-C9 as starting materials and suitable acceptor ligands to achieve ***D-M-dithioxamide-M'-A*** kind of systems is a challenging new research work planned for future.

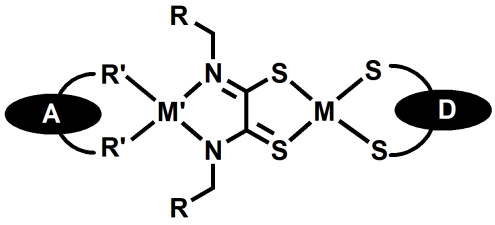

R' =S or N

Appendix 1 Non linear Optics theory

A1.1. Insight into second order Non linear Optics (NLO)

Non-linear optics represents the optical phenomenon, by which, after the interaction of an oscillating electromagnetic field (light) with specific molecules or bulk materials, a new electromagnetic wave (new light) is generated, which differs from the incident one not only in the frequency, but also in the phase or other optical properties[12]

The interaction of an electromagnetic field with matter induces a polarization in the matter. In linear optics there is an instantaneous displacement (polarization) of the electron density of an atom by the electric field E of the light wave. The displacement of the electron density away from nucleus results in a charge separation (an induced dipole), with moment, μ [1-4].

With small fields, the strength of the applied fields is proportional to the displacement of charge from equilibrium position, and leads to the relation:

$$Polarization = \vec{\mu} + \alpha\vec{E} \qquad \text{...}\textbf{\textit{Eq. A1.1}}$$

Where α is the linear polarizability of the molecular atom.

When the applied electromagnetic field is interacting with a single molecule, the molecule's polarizability can change and be driven beyond the linear regime. Therefore, the now nonlinear molecular polarization is expressed by (***Eq. A1.2***):

$$\vec{P} = \mu_0 + \alpha\vec{E} + \beta\vec{E}^2 + \gamma\vec{E}^3 + \ldots \qquad \textbf{...Eq. A1.2}$$

Where μ_0 is the molecular ground state electric dipole moment, α the linear polarizability, β and γ the quadratic and cubic hyperpolarizabilities, respectively. The intensity of the emission decreases by increasing the order; usually above the third-order it is too low to observe a significant effect. In conclusion, non-linearity is a secondary process of emission of light related to the intensity of the incident light and to the electronic properties controlling the polarizability of molecules or of bulk materials.

Second order nonlinear optical effects occur when two incident waves, with ω frequency interact with the molecule or the bulk material, characterized by a given value of quadratic hyperpolarizability (β), a new wave or Second Harmonic (SHG), with doubled frequency (2ω) is produced (see ***Figure A 1.1***)[2].

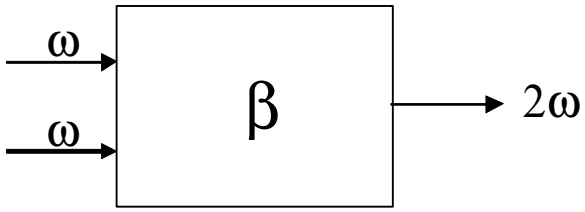

Figure A1.1, Second Harmonic Generation (SHG).

To obtain molecular materials displaying significant second order NLO effects it is necessary to have high values of the molecular quadratic hyperpolarizability β.

In 1977, Oudar[45] produced a theoretical interpretation of the electronic origin of and therefore of the main electronic factors acting on SHG, thus providing a simple model for the design of second-order NLO molecular materials. Since NLO properties are related to the polarizability of the electrons under the effect of the electric field of the light, second-order NLO properties are dependent on electronic transitions with high charge-transfer character. Oudar assumed that in asymmetric NLO chromophores the second-order NLO response is dominated mainly by one major charge-transfer process, so that it is possible to infer that:

$$\beta_{zzz} = \frac{3}{2h^2c^2} \frac{\nu_{eg}^2 r_{eg}^2 \Delta\mu_{eg}}{\left(\nu_{eg}^2 - \nu_L^2\right)\left(\nu_{eg}^2 - 4\nu_L^2\right)} \qquad \text{...}\textbf{\textit{Eq. A1.3}}$$

where *z* is the direction of the charge-transfer, (cm−1) the frequency of the charge-transfer transition, its transition dipole moment, is the difference between the excited state and ground state molecular dipole moment and is the frequency of the incident radiation.

The (***Eq. A1.3***) is based on the so-called "two state" model, a simple way to estimate from spectroscopic data the frequency dependent quadratic hyperpolarizability or, when a single charge-transfer dominates the NLO response.

Extrapolation to zero frequency allows estimation of the static quadratic hyperpolarizability, useful figure of merit to evaluate the basic second-order NLO properties of a molecular material, according to ***Eq. A1.4***:

$$\beta_0 = \beta_\lambda \left[1 - \left(\frac{2\lambda_{max}}{\lambda}\right)^2\right]\left[1 - \left(\frac{\lambda_{max}}{\lambda}\right)^2\right] \quad \text{...Eq. A1.4}$$

where β_λ is the quadratic hyperpolarizability value at incident wavelength and is the absorption wavelength of the considered charge-transfer transition .

According to the two state model, molecules that possess large β values contain an electron Donor group connected to an electron Acceptor through a π-bridging moiety (see scheme ***Figure A1.2***)[1].

Figure A 1.2 Scheme of a D-π-A chromophore

Such polarizable molecules are characterized by low-energy Donor/Acceptor intramoleculer Charge-Transfer transition. This kind of arrangement will give rise to a non-centrosymmetric molecule. In addition large $\Delta\mu_{eg}$ and r_{eg} are required in order that large β-values are produced.

A1.2. Techniques for Measuring SHG in molecular materials

A variety of experimental techniques have been used for investigating the second-order NLO activity of molecular materials. The molecular first hyperpolarisability can be obtained by the electric field induced second harmonic generation (EFISH) technique and is useful for neutral, dipolar molecules. This technique allows the determination of the μβ dot product when an electric field is applied to a solution of an NLO-active species. The μβ value, i.e., the vector component of the βijk tensor along the dipole moment direction, can be thus extracted if the ground-state dipole moment, μ_g, is known[6]. The schematic diagram of the setup for an EFISH experiment is reported ***Figure A1.3***.

Alternatively, the hyper-Rayleigh scattering (HRS) technique involves detecting the incoherently scattered second harmonic generated from an isotropic solution and allows the determination of the 'whole' β tensor, or more exactly, the mean value of the β X β tensor product. Analysis of the polarisation dependence of the second harmonic signal can provide information about single tensor βijk components. This method has the advantage that it can be used even for non-dipolar or charged molecules. Frequency dependent β (EFISH) or β (HRS) values are eventually extrapolated to static β_0 ones by means of the two-level model discussed above [Eqns. ***A1.3*** and ***A1.4***]. In fact, the static hyperpolarisability represents the most important feature when comparing the molecular second-order NLO response of different chromophores. However, these estimated β_0 data are generally approximate, especially when dynamic β data are resonantly enhanced or when the two-level model breaks down, that is, when many states, instead of one, contribute to NLO response. The above SOS method and the

related two-state simplification represent, however, the most useful approaches for chemists to understand structure–hyperpolarisability relationships, in order to design new, highly efficient second-order NLO molecular materials[7].

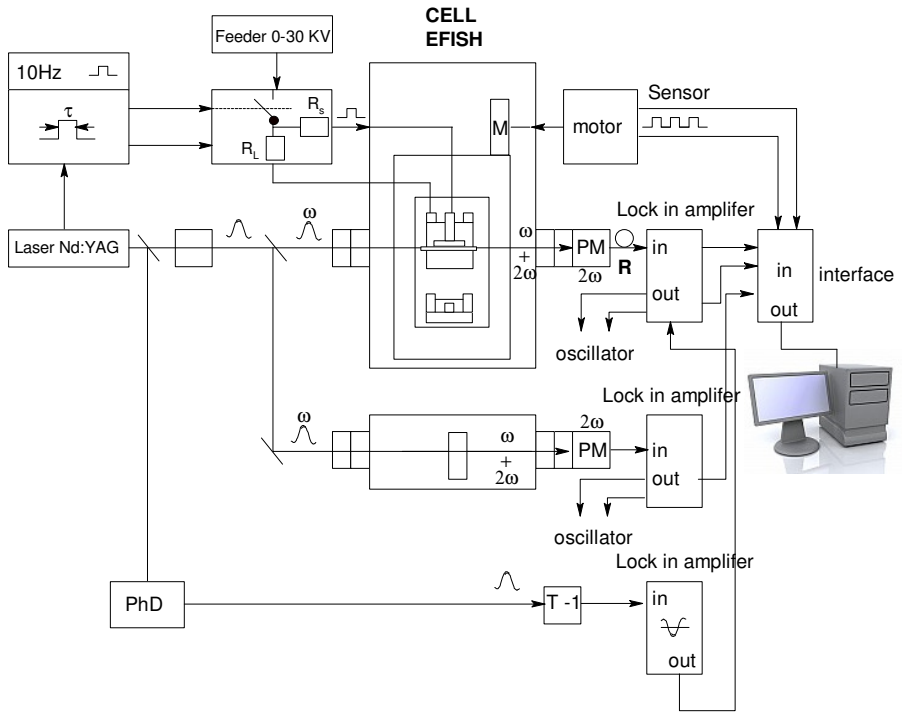

Figure A1.1, Schematic diagram of the setup for an Electric field induced second harmonic generation (EFISH) experiment

Appendix 2 Supplementary material

A2.1. Chapter 1

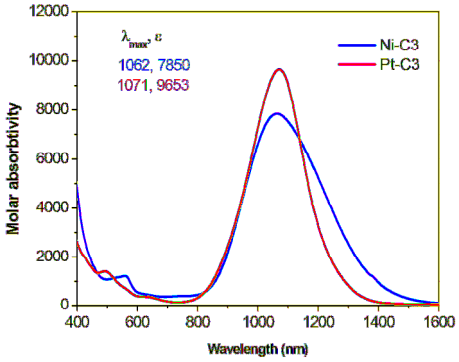

Figure S1.1, Vis-NIR spectra of M-C3 in DMF

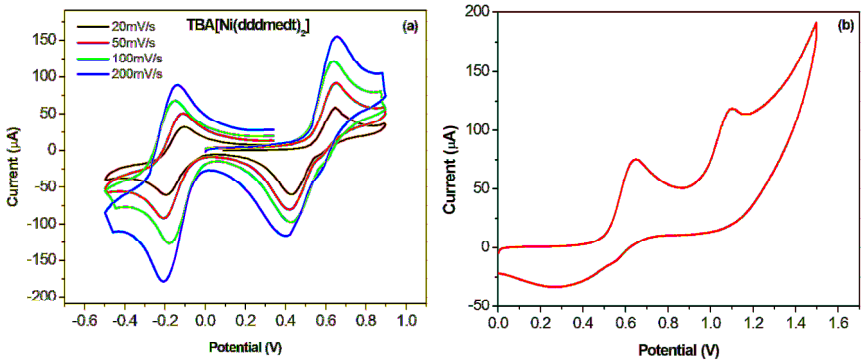

Figure S1.2, CV at different scan rates for Ni-C3 in acetonitrile

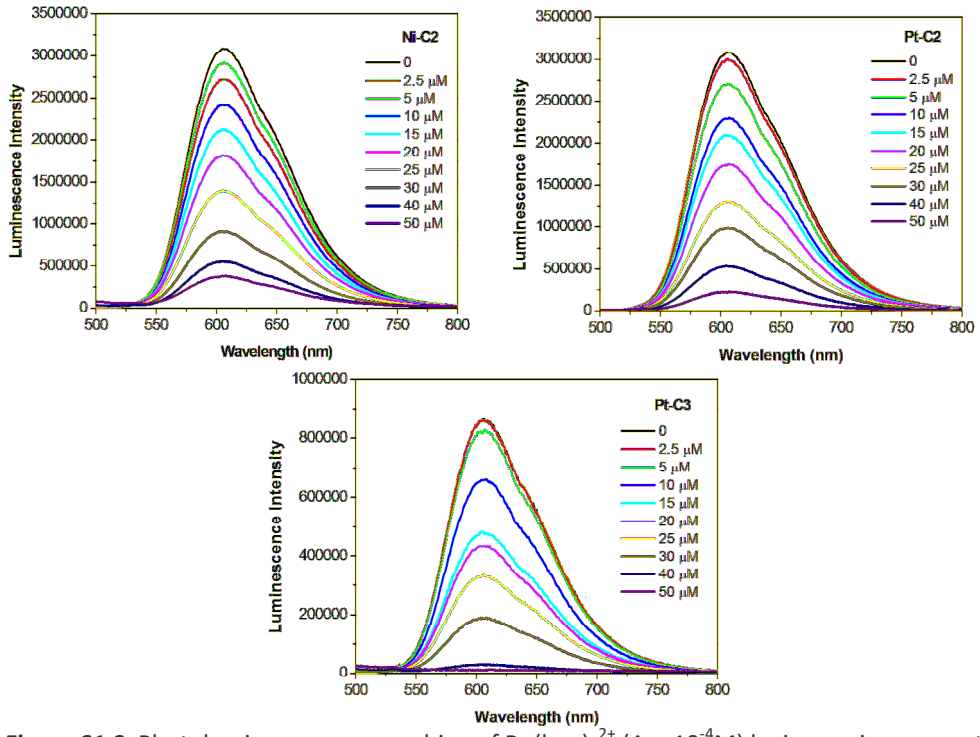

Figure S1.3, Photoluminescence quenching of $Ru(bpy)_3^{2+}$ (Aq. 10^{-4}M) by increasing amount of ***M-C2,*** and ***C3*** complexes.

A2.2. Chapter 2

Electronic Spectroscopy

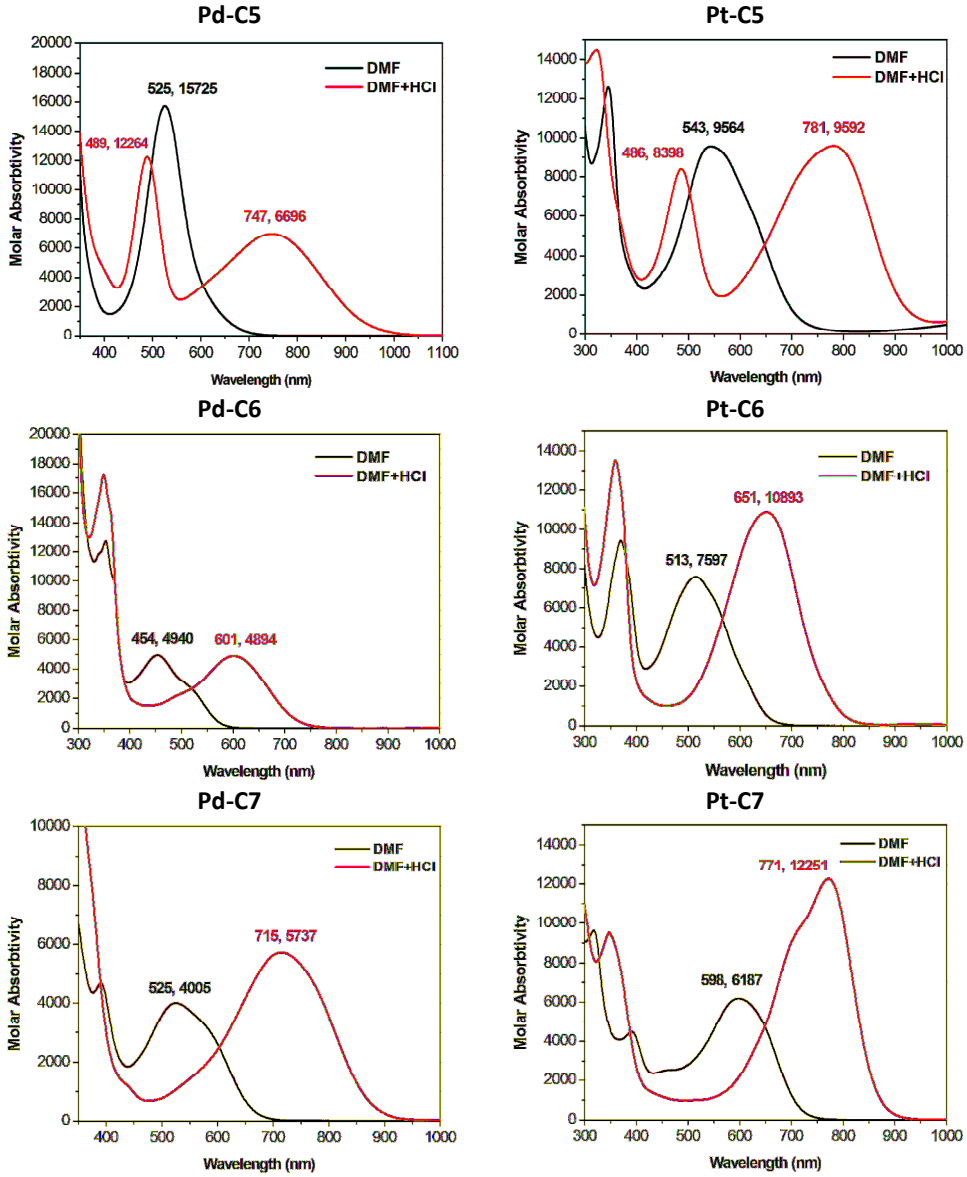

Figure S2.1, Change in absorption spectra for DMF solutions and M-C5-C7 with HCl treatment

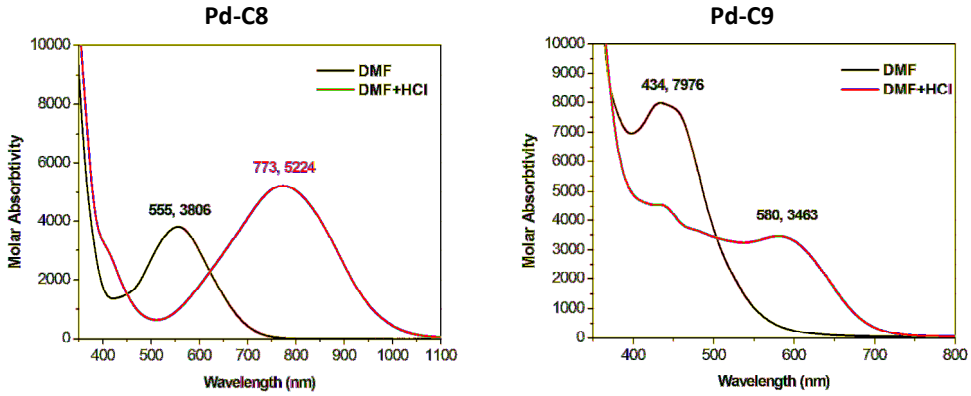

Figure S2.2, Change in Absorption spectra for ***Pd-C8*** & ***Pd-C9*** on treatment with HCl in DMF

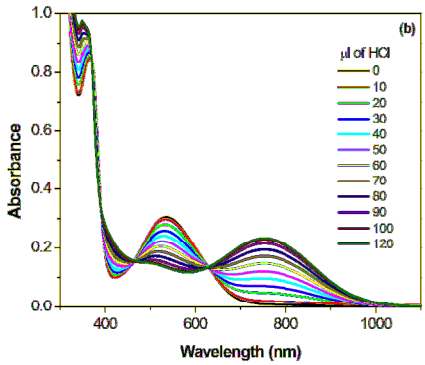

Figure S2.3 UV-visible spectral changes of ***Pd-C4*** on addition of Stoichiometric quantities of Aq. HCl

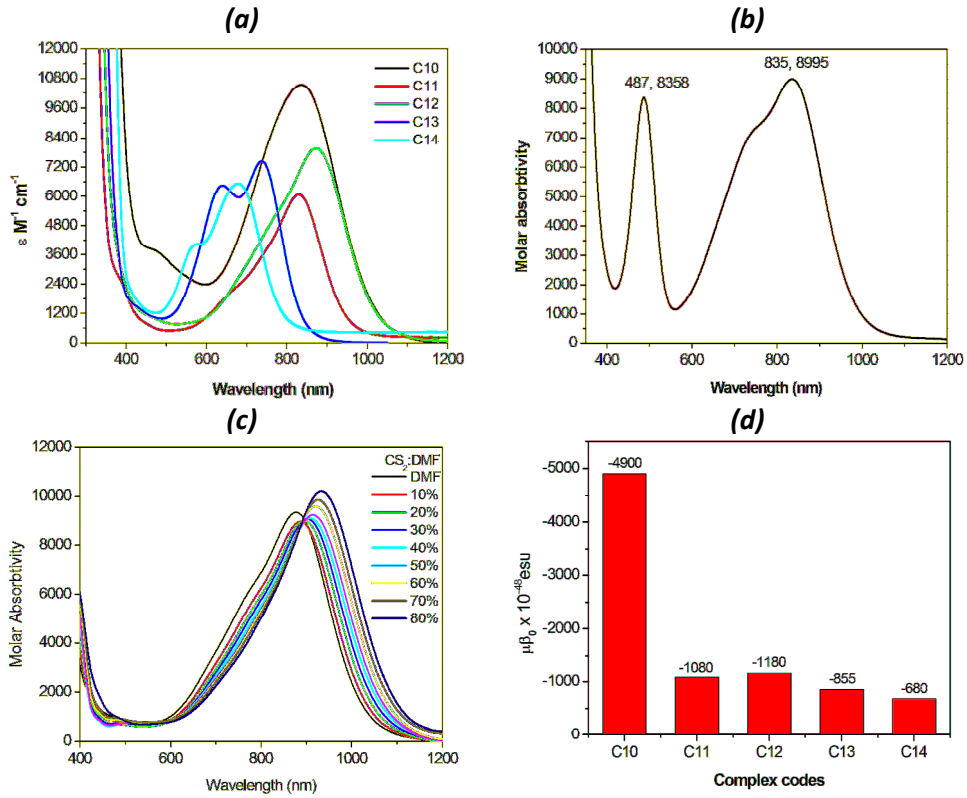

Figure S2.3, Absorption spectra of (a) ***Ni-C15 in DMF*** and (b) ***M-C10-C14 in DMF*** (c) solvatochromism in DMF:CS_2 system (d) Relative comparison of NLO activity among the neutral complexes ***C10-C14***

Table S2.1, NLO activity and corresponding absorption spectral parameters

Complex	λ_{max} (nm)	$\varepsilon \times 10^3$ ($M^{-1}cm^{-1}$)	$\mu\beta(10^{-48})$ esu
C10	836	10.54	-4900
C11	830	6.06	-1080
C12	872	7.96	-1180
C13	737, 639	7.44, 6.44	-855
C14	678, 565	6.52, 3.94	-680

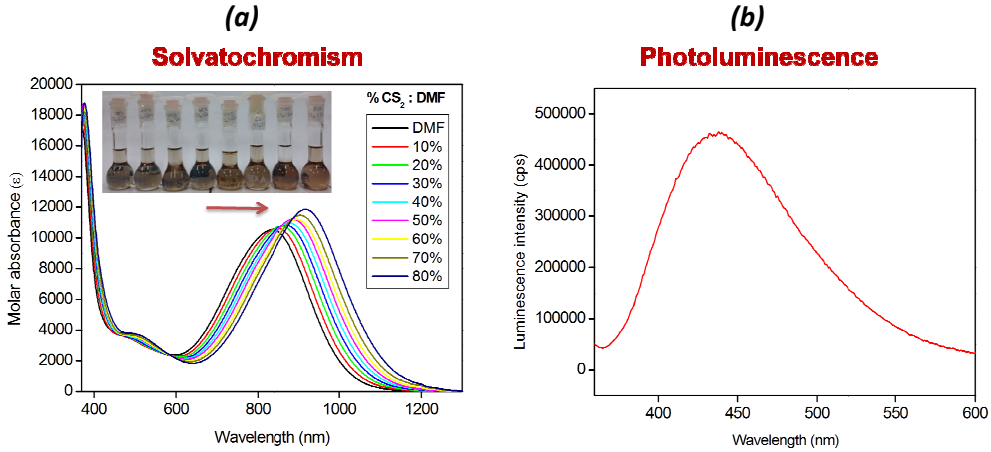

Figure S2.4, solvatochromic behaviour of ***Pt-C10*** DMF: CS_2 system, (b) emission spectrum collected by excitation at λ_{Ex} = 320nm (λ_{Em} = 436nm) c = 10^{-4}M in DMF

Cyclic voltammetry:

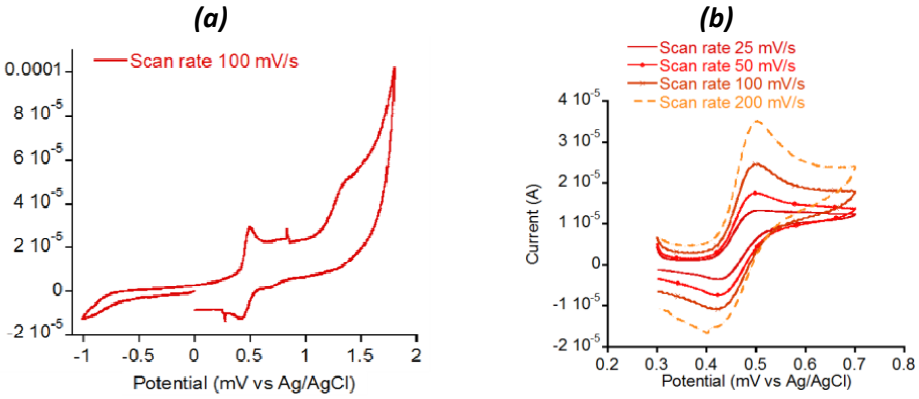

Figure S2.5, Cyclic voltammogram of 0.2MTBAClO_4 solutions of ***Pd-C7*** in Acetonitrile

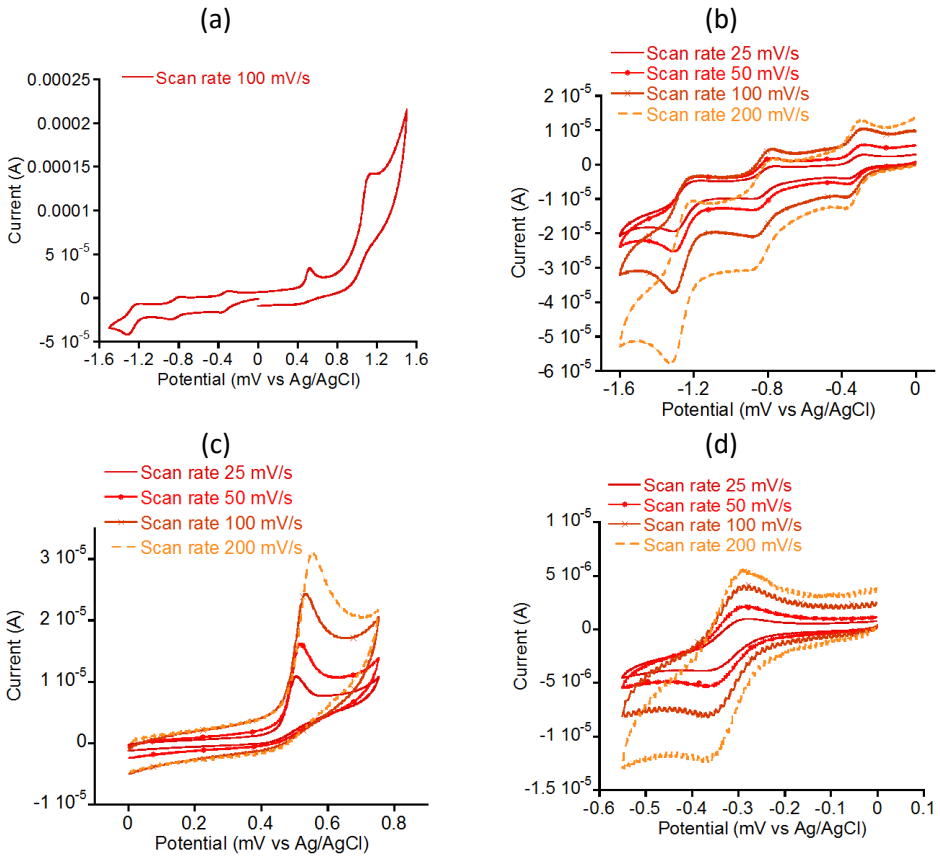

Figure S2.6, Cyclic voltammogram of 0.2MTBAClO_4 solutions of ***Ni-C14*** in Acetonitrile

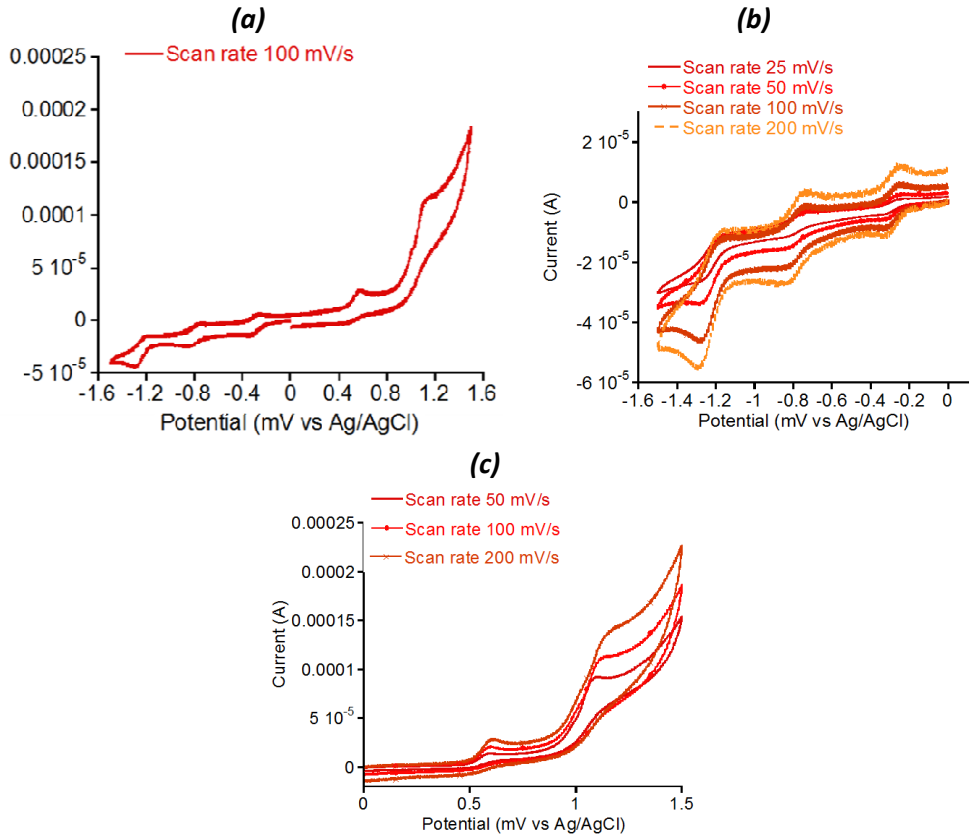

Figure S2.7, Cyclic voltammogram of 0.2MTBAClO_4 solutions of ***Ni-C13*** in Acetonitrile

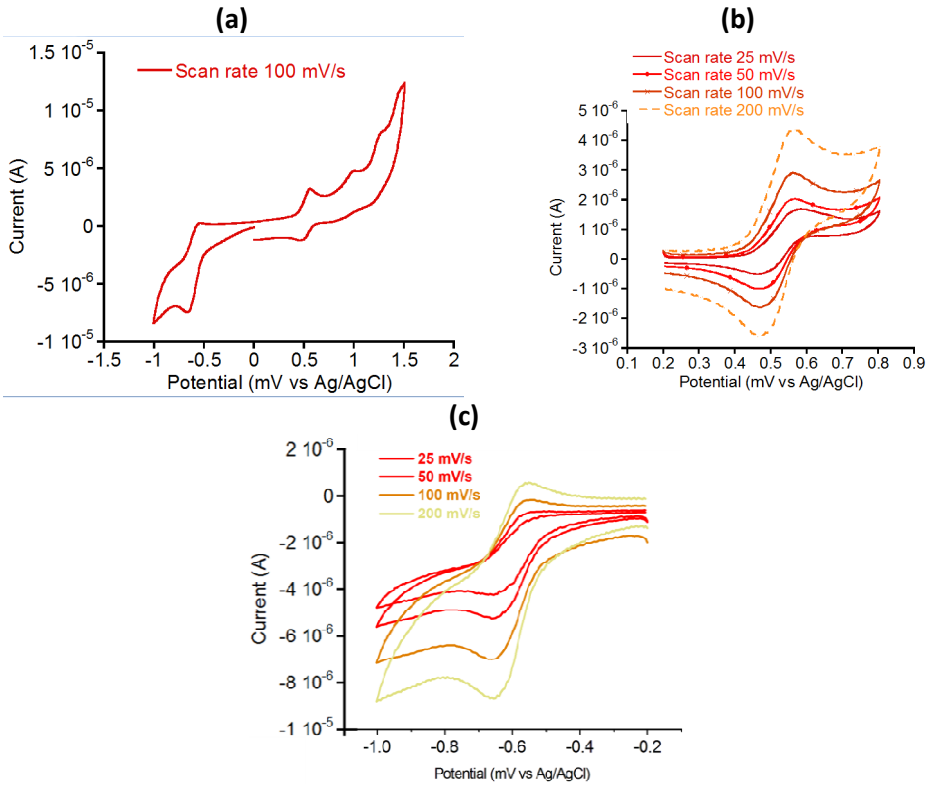

Figure S2.8 Cyclic voltammogram of 0.2MTBAClO_4 solutions of ***Pt-C10*** in Acetonitrile

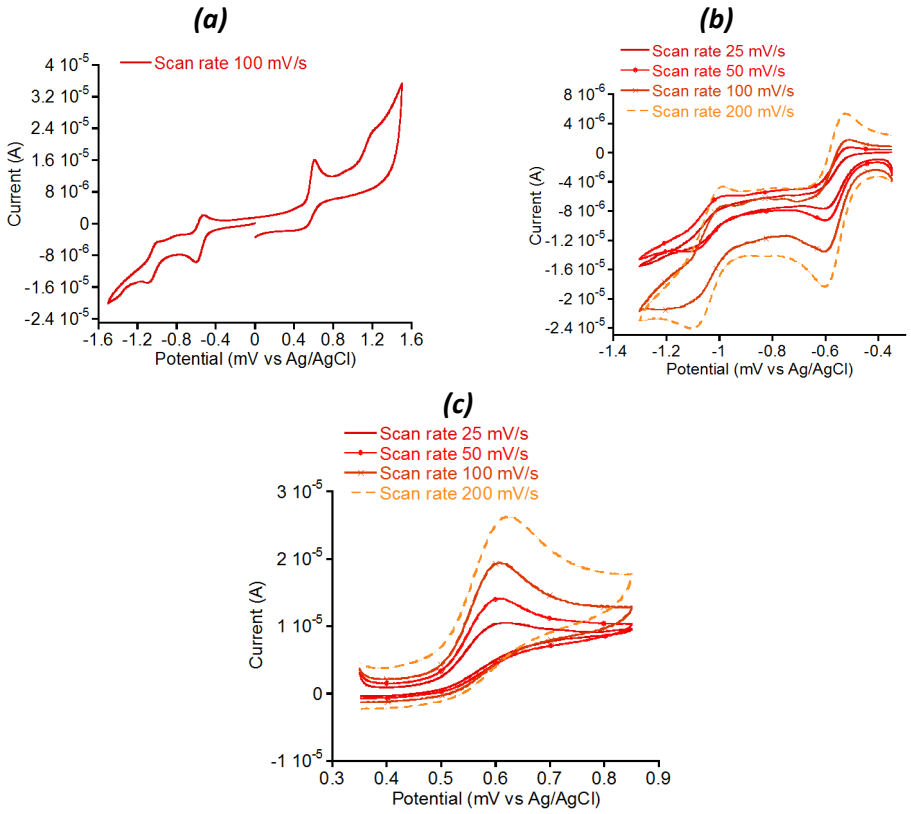

Figure S2.9, Cyclic voltammogram of 0.2MTBAClO4 solutions of ***Ni-C15*** in Acetonitrile

XRD Crystallographic analysis

Pd-C7

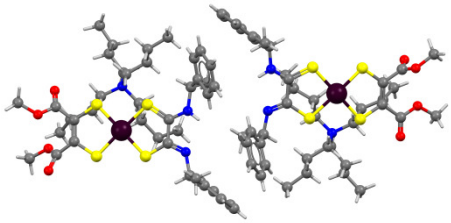

Figure S2.10, Crystal structures ***M-C7***

Table S2.2, Summary of X-ray crystallographic data for ***M-C7***

	Pd-C7	***PtC7***
Empirical formula	$C_{80}\ H_{124}\ N_6\ O_9\ Pd_2\ S_8$	$C_{80}\ H_{122}\ N_6\ O_9\ Pt_2\ S_8$
Formula weight	1783.12	1958.49
Colour, habit	Purple, flakes	Reddish-brown, needles
Crystal size, mm	0.20 x 0.03 x 0.03	0.20 x 0.14 x 0.03
Crystal system	Triclinic	Triclinic
Space group	P 1	P 1
***a*, Å**	8.943(6)	8.940(9)
***b*, Å**	13.375(9)	13.345(13)
***c*, Å**	20.680(10)	20.805(18)
α, deg.	102.61(3)	102.072(15)
β, deg.	91.98(2)	91.462(14)
γ, deg.	107.96(1)	108.272(12)
***V*, Å^3**	2282(2)	2294(4)
Z	1	1
***T*, K**	296(2)	296(2)
***ρ* (calc), Mg/m^3**	1.297	1.418
***μ*, mm^{-1}**	0.630	3.281

θ range, deg.	1.015 to 20.992	1.006 to 22.155
No.of rflcn/obsv	4818	12769
GooF	1.022	1.049
***R*1**	0.0865	0.1071
***wR*2**	0.1982	0.2510

$R1 = \Sigma||F_O|-|F_C||/\Sigma|F_O|$, $wR2 = [\Sigma[w(F_O^2-F_C^2)^2]/\Sigma[w(F_O^2)^2]]^{½}$, $w = 1/[\sigma^2(F_O^2) + (aP)^2 + bP]$, where $P = [\max(F_O^2,0) + 2F_C^2]/3$

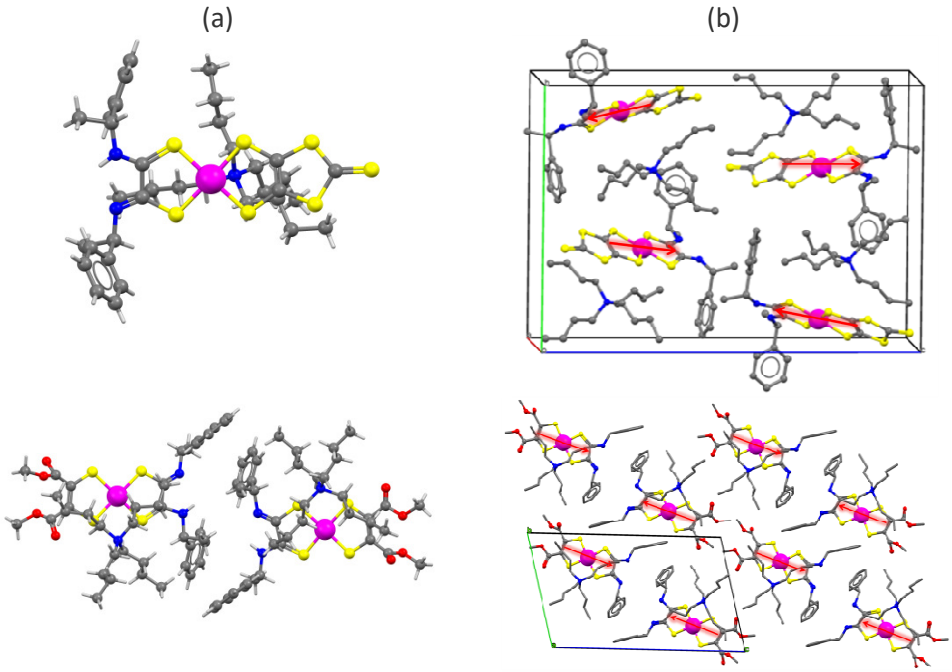

Figure 2.11, Crystal structure and packing of (a) ***Pt-C5*** and (b) ***Pt-C7*** approximately along a-axis (H-atoms omitted for clarity) showing direction of *D-M-A.*

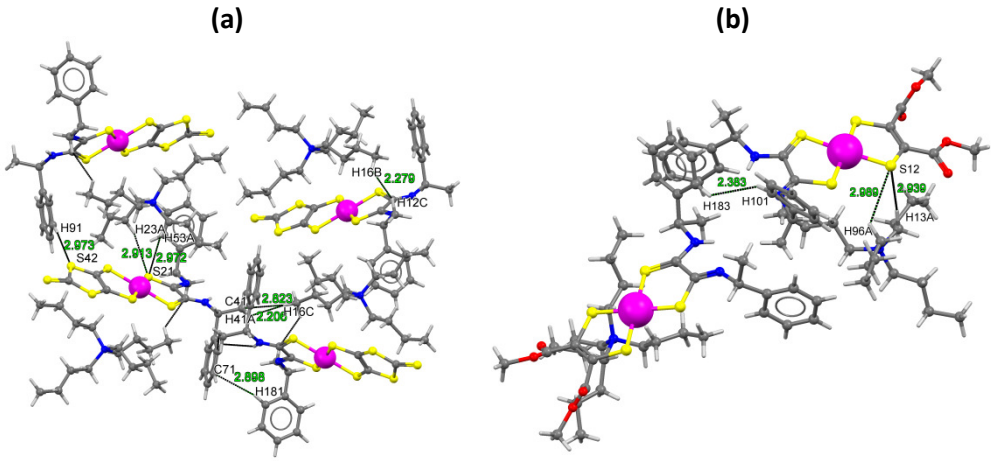

Figure S2.12, Crystal packing of (a) ***Pt-C5*** and (b) ***Pt-C7*** showing short contacts and corresponding distances.

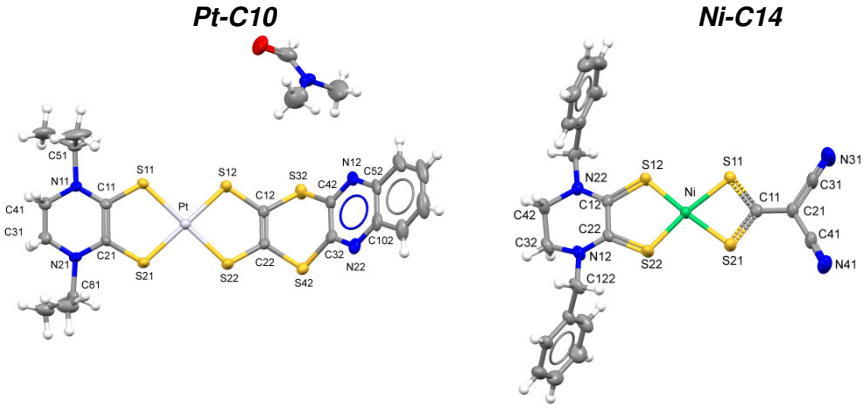

Figure S2.13, Crystal structures of ***Pt-C10*** and ***Ni-C14*** with thermal ellipsoids at 30 % probability level

Table S2.3, Crystal structure parameters of ***C10*** and ***C14***

	Pt-C10	***Ni-C14***
Empirical formula	C23 H29 N5 O Pt S6	C21 H18 N5 Ni S4
Formula weight	778.96	527.35
Colour, habit	Green, plates	Green, needles
Crystal size, mm	0.18 x 0.11 x 0.05	0.19 x 0.09 x 0.05
Crystal system	Triclinic	Triclinic
Space group	P -1	P -1
a, Å	9.017(1)	9.040(3)
b, Å	9.237(1)	11.556(3)
c, Å	18.037(2)	12.136(4)
α, deg.	79.282(2)	73.582(4)
β, deg.	86.132(2)	70.444(5)
γ, deg.	72.614(2)	83.313(5)
V, Å^3	1408.5(3)	1145.6(6)
Z	2	2
T, K	240(2)	296(2)
ρ (calc), Mg/m^3	1.837	1.529
μ, mm^{-1}	5.453	1.231
θ range, deg.	2.30 to 25.36	1.838 to 24.825
No.of rflcn/obsv	15616 / 5144	12122 / 3935
GooF	1.003	1.008
*R*1	0.0422	0.0357
*wR*2	0.0783	0.0947

Synthesis and Analytical results

Bu_4N[Pd((R)- α -MBAdt)(dmit)] ***Pd-C5***

Elemental Analysis: calculated for $C_{37}H_{55}N_3PdS_7$ (872.73) C, 50.92; H, 6.35; N, 4.81; Pd, 12.19; S, 25.72 UV-vis (DMF solution): λ (nm) ε ($molcm^{-1}dm^{-3}$): 525, $1.57x10^4$; FT–IR (KBr): ν_{max} cm^{-1}: 3190 (m); 3022 (vw); 2962 (m); 2869 (w); 1636 (m); 1516 (s); 1454 (s); 1377 (m); 1342 (w); 1300 (w); 1205 (vw); 1163 (w); 1130 (w); 1051 (vs); 1026 (m); 898 (w); 761 (m); 700 (m); 659 (vw); 554 (w); 516 (vw); 485 (vw)

Bu_4N[Pt((R)- α -MBAdt)(dmit)] ***Pt-C5***

Elemental Analysis: calculated for $C_{37}H_{55}N_3PtS_7$ (961.39) C, 46.22; H, 5.77; N, 4.37; Pt, 20.29; S, 23.35 UV-vis (DMF solution): λ (nm) ε ($molcm^{-1}dm^{-3}$): 543, $9.56x10^3$; FT–IR (KBr): ν_{max} cm^{-1}: 3209 (m); 3051 (vw); 2960 (m); 2869 (w); 1649 (m); 1500 (vs); 1452 (s); 1378 (w); 1343 (m); 1173 (w); 1131 (vw); 1053 (vs); 1027 (s); 906 (w); 759 (w) 699 (m); 549 (vw); 515 (vw); 467 (vw)

Bu_4N[Pd((R)-α-MBAdt)(tdas)] ***Pd-C6***

Elemental Analysis: calculated for $C_{36}H_{55}N_5PdS_5$ (824.6); C, 52.44; H, 6.72; N, 8.49; Pd, 12.91; S, 19.44 found: C, 52.25; H, 6.62; N, 8.56; Pd, 12.99; S, 19.12 UV-vis (DMF solution): λ (nm) ε ($molcm^{-1}dm^{-3}$): 454, $4.94x10^3$

Bu_4N[Pt((R)- α -MBAdt)(TDAS)] ***Pt-C6***

Elemental Analysis: calculated for $C_{36}H_{55}N_5PtS_5$ (913.26); C, 47.35; H, 6.07; N, 7.67; Pt, 21.36; S, 17.56 UV-vis (DMF solution): λ (nm) ε ($molcm^{-1}dm^{-3}$): 513, $7.6x10^3$ FT–IR (KBr): ν_{max} cm^{-1}: 3250 (w); 3031 (vw); 2962 (m); 2932 (m); 2871 (w);

1632 (w) 1504 (vs); 1470 (m); 1376 (w); 1311 (m); 1225 (m); 1171 (w); 1132 (w); 1023 (vw); 885 (vw); 772 (m); 743 (m); 700 (m); 654 (w); 546 (w); 492 (vw).

Bu_4N[Pd((R)- α -MBAdt)(ddmedt)] ***Pd-C7***

Elemental Analysis: calculated for $C_{40}H61N_3O_4PdS_4$ (882.61); C, 54.43; H, 6.97; N, 4.76; O, 7.25; Pd, 12.06; S, 14.53 UV-vis (DMF solution): λ (nm) ε ($molcm^{-1}dm^{-3}$): 525, $4.0x10^3$; FT–IR (KBr): ν_{max} cm^{-1}: 3210 (m) 3025 (vw); 2961 (m); 2871 (w); 1720 (s); 1698 (s); 1681 (s); 1650 (m); 1514 (vs); 1454 (m); 1429 (w); 1379 (w); 1322 (w); 1228 (vs); 1162 (w); 1102 (vw); 1073 (w); 1034 (m); 883 (vw); 745 (m); 710 (m); 491 (vw)

Bu_4N[Pt((R)- α -MBAdt) (ddmedt)] ***Pt-C7***

Elemental Analysis: calculated for $C_{40}H_{61}N_3O_4PtS_4$ (971.27); C, 49.46; H, 6.33; N, 4.33; O, 6.59; S, 13.21 found : UV-vis (DMF solution): λ (nm) ε ($molcm^{-1}dm^{-3}$): 513, $7.6x10^3$; FT–IR (KBr): ν_{max} cm^{-1}: 3208 (m);3028 (vw); 2964 (m); 2872 (w); 2834 (vw); 1691 (s); 1633 (s); 1522 (vs); 1454 (vs); 1378 (w); 1323 (w); 1226 (vs); 1182 (m); 1132 (m); 1086 (m); 1024 (m); 908 (vw); 797 (vw); 743 (m); 697 (m); 565 (w)

Bu_4N[Pd((R)- α -MBAdt)(dddmedt)] ***Pd-C8***

Elemental Analysis: calculated for $C_{42}H_{61}N_3O_4PdS_6$ (970.76) C, 51.96; H, 6.33; N, 4.33; O, 6.59; Pd, 10.96; S, 19.82 UV-vis (DMF solution): λ (nm) ε ($molcm^{-1}dm^{-3}$): 555, 3.8×10^3; FT–IR (KBr): ν_{max} cm^{-1}: 3211 (m); 3024 (vw); 2962 (m); 2870 (w); 1718 (vs); 1650 (w); 1505 (vs); 1452 (m); 1377 (w); 1346 (w); 1246 (vs); 1170 (w); 1129 (w); 1070 (w); 1021 (m); 865 (w); 757 (m); 698 (m); 548 (w)

Bu_4N[Pd((R)- α -MBAdt)(sqdt)] ***Pd-C9***

Elemental Analysis: calculated for $C_{38}H_{55}N_3O_2PdS_4$ (820.54) C, 55.62; H, 6.76; N, 5.12; O, 3.90; Pd, 12.97; S, 15.63 UV-vis (DMF solution): λ (nm) ε ($molcm^{-1}dm^{-3}$): 434, $7.97x10^3$; FT–IR (KBr): ν_{max} cm^{-1}: 3147 (m); 3054 (vw); 2963 (m); 2871 (w); 1742 (vs); 1701 (s); 1598 (m); 1534 (s); 1427 (s); 1208 (m); 1157 (w); 1130 (vw); 1108 (vw); 1022 (w); 912 (w); 877 (vw); 739 (w); 700 (w); 661 (vw); 528 (vw);

Synthesis of neutral complexes

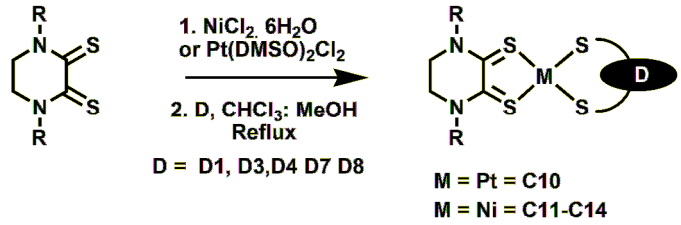

Scheme S2.1, General synthetic scheme for neutral complexes

Experimental:

[Pt(iPr$_2$pipdt)Cl$_2$]

A solution of $Pt(DMSO)Cl_2$ (75 mg, 0.177mmol) in chloroform was added to a solution of 1,4-diisopropylpiperazine-2,3-dithione (i-Pr_2-Pipdt) (41mg, 0.177 mmol) in 20% MeOH:$CHCl_3$ at room temperature and then refluxed for overnight. The reaction mixture was concentrated to half of initial quantity and the reddish pink precipitate was collected by centrifugation. (78 mg, 88 %)

FT–IR (KBr): ν_{max} cm^{-1} 2979 (w); 1604 (vw); 1513 (vs); 1461 (w); 1426 (w); 1367 (vs); 1281 (w); 1249(vw); 1190 (m); 1120 (s); 1027 (vw); 973 (vw); 902 (vw); 728 (vw); 674 (vw); 589 (m)

[Pt(iPr$_2$pipdt)(Quinoxdt)] ***Pt-C10***

A solution of (7.9 mg, 345 mmol) of sodium in 10mL of methanol was added to a suspension of [1,3]dithiolo[5,6][1,4]dithiino[2,3-*b*]quinoxaline-2-one (Quinoxdto) (48.5 mg, 0.157 mmol) in methanol and stirred at room temperature for 30 min. The solution of dithiolate formed was added drop wise to a suspension of Pt (i-Pr$_2$Pipdt)Cl$_2$ (78 mg, 0.157 mmol) in 200mL of 15% MeOH:CHCl$_3$. The reaction mixture was then refluxed for overnight to obtain green microcrystalline [Pt(i-Pr$_2$Pipdt)(Quinoxdt)] (96mg, 86 %) was collected by centrifugation. Crystallization DMF: Diethyl Ether by diffusion. Elemental Analysis: calculated for $C_{20}H_{22}N_4PtS_6$ (705.88) : C 34.03, H 3.14, N 7.94, S 27.25; found: C 34.08, H 3.11, N 8.01, S 27.21; UV-vis (DMF solution): λ (nm) ε (molcm^{-1}dm^{-3}): 369 (1.73×10^4); 465sh (3.8×10^3); 836 (1.05×10^4). FT–IR (KBr): ν_{max} cm^{-1}: 2925 (m); 2854 (w); 1734 (vw); 1613(s); 1458 (w); 1403 (vw); 1254 (w); 1206(vw); 1176 (w); 1112 (s); 1017 (w); 875 (vw); 762 (w); 668 (vw); 598 (vw); 552 (vw).

[Ni(Bn2pipdt)(dt)] ***(Ni-C11-C14)***

To a stirred solution of 1,4-dibenzylpiperazine-2,3-dithione (100 mg, 306.29 mmol) in 150mL chloroform was added drop wise a solution of nickel chloride hexahydrate (72.8 mg, 306.29 mmol) in 25mL methanol. The reaction mixture was then refluxed for 3h to obtain a green solution of Ni(1,4-dibenzylpiperazine-2,3-dithione)dichloride]. A solution of different sodium dithiolates (***D3, D4, D7*** and ***D8***) (306.29 mmol) in 15mL Methanol were added drop wise to the reaction mixture and further refluxed for overnight to obtain a green microcrystalline complexes, collected by centrifugation.

[Ni(Bn2pipdt)(ddmedt)] Ni-C11

Anal. Cal. for $C_{24}H_{24}N_2NiO_4S_4$ (591.41) : C, 48.74; H, 4.09; N, 4.74; S, 21.69; found: C, 48.78; H, 4.16; N, 4.79; S, 21.72; UV-vis (DMF solution): λ (nm) ε

($molcm^{-1}dm^{-3}$): 262 (1.28×10^4) ; 314 (1.97×10^4); 830 (6.06×10^3); FT–IR (KBr): ν_{max} cm^{-1}: 3060 (vw); 2962 (m); 2954 (w) 1714 (s); 1557 (s); 1520 (m); 1453 (w); 1432 (m); 1357 (m); 1234 (vs); 1118 (vw); 1081 (w); 1028 (m) 766 (vw);738 (w) 695 (w); 667 (vw); 620 (vw).

[Ni(Bn2pipdt)(dddmedt)] ***Ni-C12***

Anal. Cal. for $C_{26}H_{24}N_2NiO_4S_6$ (679.56) : C, 45.95; H, 3.56; N, 4.12; S, 28.31; found: C, 45.79; H, 3.51; N, 4.16; S, 28.35; UV-vis (DMF solution): λ (nm) ε ($molcm^{-1}dm^{-3}$): 262 (1.12×10^4); 321 (2.97×10^4); 872 (7.96×10^3); FT–IR (KBr): ν_{max} cm^{-1}: 3030 (vw); 2950 (w); 2917 (vw) 1729 (s); 1566 (m); 1516 (s); 1431 (m); 1357 (s); 1249 (vs); 1074 (m); 1110 (m); 899 (vw); 737 (m); 698 (w); 460 (vw).

[Ni(Bn2pipdt)(sqadt)] ***Ni-C13***

Anal. Cal. for $C_{22}H_{18}N_2NiO_2S_4$ (529.34) : C, 49.92; H, 3.43; N, 5.29; S, 24.23; found: C, 49.98; H, 3.42; N, 5.3; S, 24.28; UV-vis (DMF solution): λ (nm) ε ($molcm^{-1}dm^{-3}$): 259 (2.76×10^4); 319 (4.64×10^4); 635sh (6.42×10^3); 737 (7.44×10^3); FT–IR (KBr): ν_{max} cm^{-1}: 3032 (vw); 2927 (w); 1817 (vw); 1742 (vs); 1705 (s); 1652 (m); 1524 (s); 1428 (s); 1359 (s); 1256 (m); 1160 (m); 1113 (w) 937 (vw); 875 (vw);739 (m) 698 (m) 668 (vw) 525 (w)

[Ni(Bn2pipdt)(i-mnt)] ***Ni-C14***

Anal. Cal. for $C_{22}H_{18}N_4NiS_4$ (525.36): C, 50.30; H, 3.45; N, 10.66; S, 24.41; found: C, 50.66; H, 3.35; N, 10.68; S, 24.52; UV-vis (DMF solution): λ (nm) ε ($molcm^{-1}dm^{-3}$): 257 (1.52×10^4); 327 (4.7×10^4); 350sh (2.23×10^4); 582sh (4.03×10^3); 678 (6.52×10^3); FT–IR (KBr): ν_{max} cm^{-1}: 3031 (vw); 2867 (w); 2195 (s) 1533 (s); 1428 (s); 1398 (s); 1375 (s); 1361 (s); 1259 (w); 1184 (m); 1110 (w); 1029 (vw); 939 (w) 893 (w); 738 (m); 698 (m) 604 (vw) 547 (w) 476 (w)

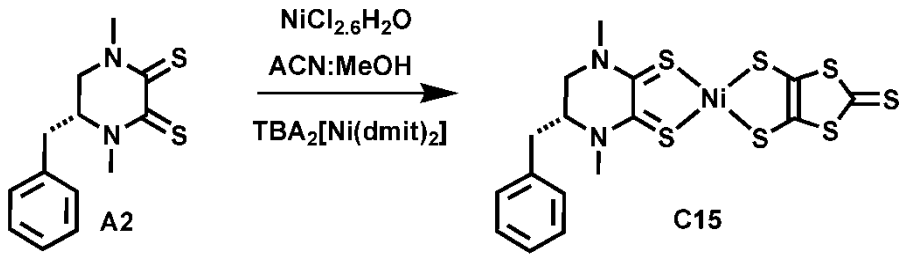

Figure S2.7, Scheme for preparation of *Ni-C15*

The ligand A2 was synthesized according to the reported procedure[8]

Ni [((5R)-BnMe$_2$Pipdt)(dmit)] (C15)

To a solution of (0.15g, 0.567 mmol) (5*R*)-5-benzyl-1,4-dimethylpiperazine-2,3-dithione in 50mL Acetonitrile was added drop wise a solution (0.135 g, 0.567 mmol) Nickel chloride hexahydrate in 10mL Methanol. The reaction mixture was stirred for overnight at room temperature during which a green-blue coloured solution was obtained. A solution of $TBA_2[Ni(dmit)_2]$ (0.53 g, 0.567mmol) in methanol was added drop wise to the reaction mixture and refluxed for 2h to obtain green microcrystalline complex (0.186 g, 0.578mmol, 63.16 %) isolated by centrifugation.

Elemental Analysis: calculated for $C_{16}H_{16}N_2NiS_7$ C 36.99, H 3.10, N 5.39, Ni 11.30, S 43.21 Found: C 36.55, H 3.19, N 5.85, Ni 11.31, S 43.25 UV-vis (DMF solution) λ (nm) ε ($molcm^{-1}dm^{-3}$): 835, $8.9x10^3$, 487, $8.36x10^3$; *FT-IR v* max (KBr)/cm^{-1} : 3022 (vw), 2905 (vw), 1735 (vw), 1650 (w), 1511 (vs), 1439 (w), 1397 (m), 1340 (s), 1252 (w), 1218 (w), 1142 (w), 1102 (vw), 1061 (vs), 916 (vw), 740 (w), 698 (w), 509 (w)

References

1. S. Di Bella, Chem. Soc. Rev. 30 (2001) 355.
2. Cariati, E.; Pizzotti M.; Roberto D.; Tessore F.; Ugo R.; *Coord. Chem. Rev.* 2006, 250, 1210-1233.
3. (a) H.S. Nalwa, Appl. Organomet. Chem. 5 (1991) 349; (b) J. Zyss, Molecular Nonlinear Optics, Academic Press, New York, 1994; (c) N.J. Long, Angew. Chem. 107 (1995) 1, 37-56; (d) J. Heck, S. Dabek, T. Meyer-Friedrichsen, H. Wong, Coord. Chem. Rev. 190–192 (1999) 1217; (e) D.M. Roundhill, J.P. Fackler, Optoelectronic Properties of Inorganic Compounds, Plenum Press, New York, 1999; (f) J. Heck, S. Dabek, T. Meyer-Friedrichsen, H. Wong, Coord. Chem. Rev. 190–192 (1999) 1217;(g) H. Le Bozec, T. Renouard, Eur. J. Inorg. Chem. (2000) 229; (h) P.G. Lacroix, Eur. J. Inorg. Chem. (2001) 339; (i) B.J. Coe, in: J.A. McCleverty, T.J. Meyer (Eds.), Comprehensive Coordination Chemistry II, vol. 9, Elsevier Pergamon, Oxford, UK, 2004, pp. 621–687; (k) B.J. Coe, N.R.M. Curati, Comments Inorg. Chem. 25 (2004) 147.
4. a) S. Curreli, P. Deplano, C. Faulmann, A. Ienco, C. Mealli, M.L. Mercuri, L. Pilia, G. Pintus, A. Serpe & E.F. Trogu. Electronic factors a ecting second-order NLO properties: case study of four di erent push-pull bis-dithiolene nickel complexes. Inorg. Chem., vol. 43, no. 16, pages 5069-5079, 2004; b) P. Deplano, L. Pilia, D. Espa, M.L. Mercuri & A. Serpe. Square-planar d^8 metal mixed-ligand dithiolene complexes as second order nonlinear optical chromophores: structure/property relationship. Coord. Chem. Rev., vol. 254, pages 1434-1447, 2010.
5. (a) J.L. Oudar, D.S. Chemla, J. Chem. Phys. 66 (1977) 2664;(b) J.L. Oudar, J. Chem. Phys. 67 (1977) 446; (c) J.L. Oudar, H. Le Person, Opt. Commun. 15 (1975) 258.
6. (a) B.F. Levine, C.G. Bethea, Appl. Phys. Lett. 24 (1974) 445; (b) K.D. Singer, A.F. Garito, J. Chem. Phys. 75 (1981) 3572; (c) I. Ledoux, J. Zyss, Chem. Phys. 73 (1982) 203.
7. (a) J. Zyss, I. Ledoux, Chem. Rev. 94 (1994) 77; (b) R.W. Terhune, P.D. Maker, C.M. Savage, Phys. Rev. Lett. 14 (1965) 681; (c) P.D. Maker, Phys. Rev. 1 (1970) 923; (d) K. Clays, A. Pearson, Phys. Rev. Lett. 66 (1991) 2980.
8. Barbara Piotrkowska Małgorzata Myślińska Maria Gdaniec Aleksander Herman Tadeusz Połoński J. Org. Chem., 2008, 73 (7), pp 2852–2861

Acknowledgements

This work has required multidisciplinary skills involving multi technique characterization, including specific investigation of the materials performance by EFISH (Electric Field Induced Second Harmonic generation), light promoted photocatalytic hydrogen generation reactions, These skills were available through collaborative work inside local, national or international research Centers through COST ACTION *1202* as acknowledged below:

At UNICA

- *Prof. Paola Deplano*
- *Dr. Davide Espa, Dr. Luca Pilia, Dr. Flavia Artizzu, Dr. Elisa Sessini, Dr. Francesco Secci, Dr. Flaminia Cesare Marincola and Dr Angela Serpe*
- *Prof. Mariano Casu*

Other

- *Dr. Luciano Marchiò, Università di Parma*
- *Prof. Santo Lanza University of Messina*
- *Prof. Maddalena Pizzotti and Dr. Francesca Tessore Università di Milano*
- *Prof. Benjamin Dietzek and Dr. Martin Schulz (Friedrich Schiller University Jena)*

Funding

- *COST action 1202 for funding*
- *Università di Cagliari and Fondazione Banco di Sardegna*